USE OF WIND POWER MAPS TO ESTABLISH FATIGUE DESIGN CRITERIA FOR TRAFFIC SIGNAL AND HIGH-MAST STRUCTURES

Richard L. Price
Jay A. Puckett
Michael G. Barker

Department of Civil and Architectural Engineering
University of Wyoming

in cooperation with

U.S. Department of Transportation
Federal Highway Administration
Mountain-Plains Consortium

December 2008

Acknowledgements

The funding from the Mountain-Plains Consortium, United States Department of Transportation and the University of Wyoming are appreciated. Special thanks needs to be given to Mr. Chris Meyer from Kansas Department of Transportation for all his help accessing and interpreting the inspection records for Kansas' traffic structures.

Disclaimer

ABSTRACT

Recent design requirements for traffic signal and sign structures incorporated fatigue load criteria related to wind that are producing significant increases in size and cost. The Fourth Edition of the AASHTO Luminaire and Traffic Signal Specification (2002 with interims) specification is a significant change to past practice and often results in much larger and more costly structures. Here conservative principles (envelope wind demands and infinite fatigue life) for design at increased cost even for those regions not adversely affected by wind-induced fatigue. The states that do not have steady, sustained winds and have not experienced significant fatigue failures have concerns with the larger and more costly structures. A rationale basis for lowering the fatigue design loads may be appropriate.

This study compares fatigue failures with respect to wind power (expressed as a function of average wind velocity). Inspection reports for approximate 2500 cantilevered traffic structures and 700 high-mast luminaires were collected and analyzed for suspected fatigue cracking. Each structure was located spatially and the associated wind power classification for that location was noted. (Wind power classifications are used to site wind generators.) This paper is limited to traffic signal structures.

The inspected structures were classified as cracked or non-crack and then categorized by their wind power classification and ambient average wind velocity. The probability of a structure having fatigue cracks increases with greater wind power classifications. Structure orientation, pole diameter, mast-arm length, in-service age, along with other details were also studied for their roles in in-service fatigue performance. Structures in low wind power classes have a lower probability of having fatigue developing cracks. The converse is true.

TABLE OF CONTENTS

LIST OF FIGURES

LIST OF TABLES

1. INTRODUCTION

1.1 Problem Statement

Recent design improvements for traffic signal and sign structures incorporated fatigue load criteria related to wind that are producing significant increases in size and cost. This current design specification is the Fourth Edition of the AASHTO Luminaire and Traffic Signal Specification (2001 with interims). The specification is based upon limited wind loading and fatigue resistance data and analysis provided by NCHRP Report 411 and NCHRP 469. Based on these reports, a generalized fatigue load criteria was developed and implemented. This AASHTO specification is a significant change to past practice and typically results in much larger and more costly structures. Thus, states have been hesitant to adopt the changes. The fatigue failures have been prominent only in certain areas of the country. The revised specification applies conservative principles (envelope wind demands and infinite fatigue life) for design in these critical regions; hence, the more costly structures for all regions. Thus, the states that do not have highly sustained winds and have not experienced significant fatigue cracking have concerns with the larger and more costly structures. States are searching for justification before accepting the new fatigue design requirements. This study examines and compares fatigue failures with respect to wind demands that create fatigue cycles. Sustained wind velocity is one of the keys to fatigue cracking; higher average wind velocity produces a higher probability of fatigue cracking. This report includes traffic signal structures (mast-arms) and high-mast poles.

1.2 Background

The fatigue loads considered by AASHTO are broken into four types: Galloping, Vortex Shedding, Natural Wind Gusts and Truck Gusts. The purpose of these loads are to predict the loads that a structure may experience due to naturally occurring winds, wind pressure load by large trucks and flow phenomena around the pole and then compare the effects with the pole's design resistance. The design should resist these loads with a reasonable factor of safety, but if it does not, fatigue cracks can develop. These different types of loads are further discussed in the literature review, but typically Galloping and Natural Gusts control fatigue design for traffic signal structures.

Fatigue cracking depends on the size of a load and how many times that structure has been repeatedly loaded. Typically fatigue cracks initiate in the base metal near the welds of structure connections. These cracks increase in length over time and will eventually lead to a failure in the structure if not detected and remediated (e.g., Figure 1.1).

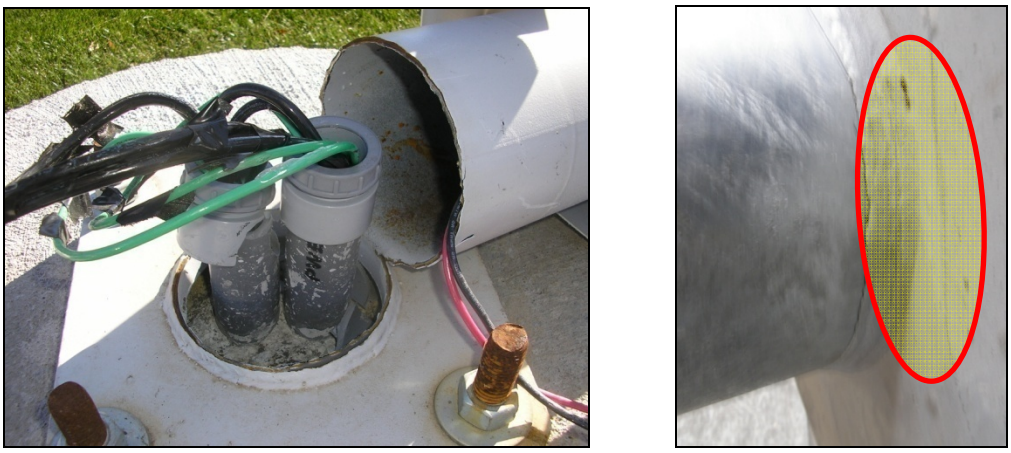

Figure 1.1 Fatigue Cracking in Traffic Structures (Courtesy John Peiffer)

Figure 1.2 Cantilever Traffic Signal and High-Mast Luminaire

Because fatigue cracking depends on the number of load cycles experienced, wind-caused cyclic loads are important. Wind loads cause stress throughout the structure, but the stress is magnified due to stress concentrations near the welds. Additionally, the connection welds are typically the weak details for fatigue. A structure located in areas with nearly constant wind will accumulate load cycles more quickly than a structure in areas with less frequent winds, thus developing fatigue cracks more quickly. Herein, inspections of in-service structures for fatigue cracks were compared with applicable wind data. The resulting data provides an added benefit as it is historical data to empirically evaluate the need for the current broad-based fatigue specification.

1.3 Research Objectives

The primary study objective is to validate the use of wind power (the measure of energy available in the wind) to predict fatigue damage in cantilever traffic structures. To accomplish this, inspection data for in-service traffic structures was gathered and studied for evidence of fatigue cracking. The wind power for

each structure location was also determined. Finally, a statistical model was developed to study the relationship between fatigue cracking and wind power.

A secondary objective was to determine if other in-service elements played a vital role in fatigue cracking. Structure age, length, orientation, diameter, and various other aspects were investigated to examine what affects they had on fatigue cracking performance.

The final objective is to provide recommendations for future AASHTO fatigue load criteria changes based on the findings. The suggested modifications will hopefully lead to a less conservative specification that allows structures in areas with no historical problems to allow more reasonable and less costly designs than dictated by the current fatigue design provisions in AASHTO.

1.4 Organization of Report

This report is divided into seven chapters. A short literature review related to wind-induced vibration, wind power theory, and binary logistic regression modeling is presented in Section 2. Section 3 discusses the methods used in this study. Section 4 presents the results of the various analyzes performed and Section 5 discusses the implications of these results. Study conclusions are presented in Section 6. Section 6 also provides the recommendations for future work and AASHTO modifications based on this study. Finally, the references are provided in Section 7.

2. LITERATURE REVIEW

This section provides a broad overview into the general principles that underlay this project. However, no similar research correlating wind power and fatigue cracking has been conducted.

2.1 AASHTO Specifications and NCHRP Reports

The fatigue criteria in the Fourth Edition of the AASHTO (2001) Luminaire and Traffic Signal Specification (2002 with interims) are based on NCHRP Report 412 (Dexter, Kaczinski, and Van Dien 1998), NCHRP Report 469 (Dexter and Ricker 2002) and NCHRP 494 (Fouad, et al. 2003). These fatigue design criteria attempt to model various aspects of wind-induced vibration reactions of typical traffic structures. The Specification and these reports separate these vibrations into four types: Galloping, Vortex Shedding, Natural Wind Gusts, and Truck Gusts. NCHRP Report 412 addresses research into each of these areas and suggests a new approach to the AASHTO specifications for fatigue. Wind tunnel testing used in the research showed examples of luminaire vibration. The report showed that these structures have low natural frequencies and almost no damping, so they are susceptible to vibration and cyclic loading. NCHRP Report 469 furthered the research presented in NCHRP Report 412, but with special emphasis placed on vibration mitigation, increased inspections and awareness, and anchor rod testing. The authors also suggested that the vortex shedding fatigue design needed further testing and refinement. Wind speed map refinement, treatment of gusts, and the differences in design loads were the main issues addressed in NCHRP Report 494.

The Fourth Edition of the AASHTO Luminaire and Traffic Signal Specification (2001 with interims) covers fatigue design in Section 11. Five types of structures are considered: overhead cantilevered sign structures, overhead cantilevered signal structures, high-level high-mast lighting structures, overhead non-cantilevered sign structures, and overhead non-cantilevered traffic signal structures. Here, only the cantilevered structures are considered. Another important aspect of the Specifications is the fatigue importance factors (three categories) derived from NCHRP Reports 469 and 494 (AASHTO 2001, 11-6). Category I are structures with mitigation devices, structures on roadways with speed above 35 mph, and/or structures with average daily traffic volume in excess of 10,000. This category allows for no reduction in predicted loads and the design specification is based on an infinite fatigue life. Category III structures are any structure on roadways with speed limits of less than 35 mph and the design has been calibrated to past practice with the associated limited fatigue life. Category II is any structure that does not fit into I or III and the design is based on the midway point between a Category I and III design. These categories make a large difference (up to 70%) in the amount of expected load. The overall intent of the importance factors are to make Category III be a minimal change (small or no increase in diameter, connection types) and Category I be a significant redesigning change (much larger diameters and heavier duty connections) (Dexter and Ricker, Fatigue-Resistant Design of Cantilevered Signal, Sign, and Light Supports 2002, 61).

2.2 Aeroelastic Behavior

This project does not directly address research into specifics of aerodynamic phenomena related to cantilever structures like vortex shedding, galloping, wind gusts, or truck gusts. These phenomena are known to cause fatigue cracking and exist for in-service structures. For these reasons, a short review of the subject follows.

Natural Wind gusts are simply modeled as equivalent static pressures, and typically cause other wind phenomena like galloping or vortex shedding. Vortex Shedding occurs when vortices are shed on alternate sides of a symmetric member (i.e. no attachments). This results in a varying load which creates

vibrations perpendicular to the wind direction (Phares, et al. 2007, 8). If these vibrations reach resonance with the structure, large displacements can occur. These displacements translate into stress which is resisted by the structure, connections, and welds. Typically only luminaire support structures have problems with vortex shedding because the other traffic structures have irregular geometry with attached signs and signals. Vortex shedding tends to occur with steady continuous winds between 5 and 15 m/s or 11 and 34 mph (U.S. Department of Transportation Federal Highway Administration n.d., 10-11). A more in-depth explanation of vortex shedding can be seen in Phares, et al.

Galloping is a phenomena that occurs in structures with asymmetric members. This is usually found in mast arms with signals or signs attached. Typically a strong wind gust will cause initial vibration. Then steady winds keep the vibration going and may amplify it. Eventually, if the vibrations reach critical frequency of the structure, the vibrations lock-in and grow in magnitude, causing large displacements. These vibrations typically lock into the first mode (approximately 1 Hz) and make mast arms sway in the vertical direction (Hamilton, et al. 2004, 5). Galloping needs uniform steady winds to occur, not gusty winds (U.S. Department of Transportation Federal Highway Administration n.d., 12). Another key element to galloping is that the structure needs to be able to twist as well as move vertically, which implies flexible mono-tubes are especially susceptible to this type of wind phenomena. Fatigue cracking from this type of loading typically takes several years to develop and these cracks tend to be found in the mast-arm-to-pole or base connections. Interestingly, galloping in structures can be decreased by adding a damper of some sort to the end of the mast arms. This has been proven to be an effective way to reduce fatigue due to galloping (Dexter and Ricker, Fatigue-Resistant Design of Cantilevered Signal, Sign, and Light Supports 2002, 25).

Truck Gusts are generally just modeled as equivalent static pressures. These pressures are not constant, but repeated loads from truck passages create a fatigue loading situation. Truck Gusts are created by a truck passing below a structure. The air displaced by the truck pushes upward as it approaches the structure, then pulls air back down as it pass the structure (Hamilton, et al. 2004, 5). These pressures are affected by the speed of the truck and the distance the bottom of the mast arm is from the top of the truck. The closer the truck is to the mast arm, the more pressure created. There are no known failures due to truck gust fatigue cracking for cantilever sign and signal structures, but there are suspected failures in variable message sign structures due to their large horizontally projected areas (Dexter, Kaczinski, and Van Dien 1998, 14).

2.3 Fatigue Cracking

Fatigue cracks develop from cyclic loading that causes stress ranges. The variable stress ranges can be modeled as constant amplitude loading. The difference in applied stress (stress range) causes fatigue cracking, not the magnitude of the load. Given this, dead loads may not be relevant to fatigue cracking. This means stress fluctuation, not the overall stress magnitude, controls fatigue cracking (U.S. Department of Transportation Federal Highway Administration n.d., 13). Additionally, the limit strength (i.e. yield stress) and type of steel has negligible effects on the fatigue resistance of a structure. Different materials will have different fatigue resistance, likely aluminum will have less resistance than steel, but different alloys of the same type of materials will have little difference in fatigue resistance. Additionally, different types of welding processes have little effect on resistance.

> "The welding process and minor deviations in weld quality from AWS D1.1 standards, while important, also do not typically have a significant effect on the fatigue resistance." (U.S. Department of Transportation Federal Highway Administration n.d., 13)

The exception to the above statement is when welds are not tied into each other at weld terminations. Fatigue cracks typically initiate at the weld toe of mast-arm or base plate connection; the crack occurs because the welds and connections create stress concentrations at high-stress regions. Chen, et al. (2003, 53) showed the weld profile does not change cracking significantly. Their research also concluded that weld quality was important and, if a weld has undercutting at the toe, it is much more likely to develop fatigue cracking.

Fatigue cracks typically form in structures that are subjected to stress ranges greater than the fatigue thresholds at its critical details. Basically, fatigue cracking typically comes from under-designed connections, and the lack of knowledge of applicable loads. This means structures should not designed uniformly throughout the country, but should be designed on a region-specific manner. For instance, fatigue cracking and fatigue failures have been found in areas of high wind velocity in Missouri (Chen, et al. 2003, 3), Wyoming (Hamilton, et al. 2004), Iowa (Phares, et al. 2007), Pennsylvania, Illinois and many other states, but fatigue cracking in the lower average wind velocity areas is less common.

2.4 Wind Power

Wind power is the measure of energy available in the wind at a specific location. The term comes from the energy-producing industry for wind turbines. The wind power quantity depends on the wind velocity, air density, and the area of sweep by a wind generator blade. Equations 1 through Equation 4 are all ways to express wind power. The air density and wind generator area are not overly important factors for this research because they do not vary much, or can be assumed to be constant throughout an area of interest. The wind velocity is the key component and because wind velocity is a cubed term, it has the potential to increase wind power greatly with small increases in wind velocity.

$$W = \frac{1}{2}\rho A v^3$$ Equation 1 (Iowa Energy Center 2006)

$$\rho = 1.323\frac{P}{T}$$ Equation 2 (Iowa Energy Center 2006)

$$W = 0.0052 A v^3 \text{(U.S. Std.)}$$ Equation 3 (Iowa Energy Center 2006)

$$W = 0.625 A v^3 \text{(Metric)}$$ Equation 4 (Iowa Energy Center 2006)

$$v_2 = v_1\left(\frac{Z_2}{Z_1}\right)^N$$ Equation 5 (Iowa Energy Center 2006)

$$v_2 = v_1\left(\frac{Z_2}{Z_1}\right)^\alpha$$ Equation 6 (AWS Scientific Inc. 1997)

where:

W = Wind Power
ρ = Air Density
A = Rotor Area
v = Wind Velocity
T = Temperature in Rankine
P = Pressure in Inches of Mercury Adjusted for Elevation
v_2 = Wind Velocity at Height 2
v_1 = Wind Velocity at Height 1
z_2 = Height of Wind Velocity of Interest
z_1 = Height of Wind Velocity Measurement Device (Reference Height)
N = Roughness Coefficient
α = Wind Shear Coefficient

Wind power as a source of energy has been on the rise throughout the United States (AWS Scientific Inc. 1997, 3-2). Due to this, wind power maps have been published for each state as a guide for locating wind power generators. These maps were originally generated by the U.S. Department of Energy by using pre-1979 wind velocity measurements along with topography and landform characteristics to create the Wind Energy Resource Atlas of the United States (National Renewable Energy Laboratory 1982). These maps were then verified using 270 post-1979 measurement sites. These maps have recently been updated using computer simulations and historical data from the National Climatic Data Center to create wind power maps for 50 meters (164 feet) above the ground surface (U.S. Department of Energy n.d.). Both of these maps use variations of Equation 5 and Equation 6 to convert wind velocities measured at station and to wind velocities at 50 meters. The values of alpha or N used for Equation 5 and Equation 6 can be seen in Table 2.1. Figure 2.1 shows the effect of the different values of N. As the value of N increases, the ratio of the velocity will increase. Figure 2.2 shows different wind velocities graphed used Equation 5 and an N of 0.143.

To generate site-specific wind power data, the following are required: station location and height, local topography, anemometer height and exposure, type of observation (instant, average), and duration of data record (AWS Scientific Inc. 1997). Wind power maps express the energy in the wind; this wind impacts a structure causing it to vibrate, which creates load cycles that can create cracks. Additionally, wind power maps are standardized and the methods used to create them are thoroughly calibrated. They are readily available, hence convenient and economical for the AASHTO community.

Table 2.1 Roughness Coefficients N - (Iowa Energy Center 2006)
and α - (AWS Scientific Inc. 1997)

Ground Cover Description	**α**	**N**
Smooth Surface: Oceans, Sands	0.10	0.10
Low Grass Land or Fallow Grounds	0.143	0.16
High Grass Land or Low Row Crops	N.A.	0.18
Tall Row Crops or Low Woods	N.A.	0.20
High Woods or Small Towns	N.A.	0.30

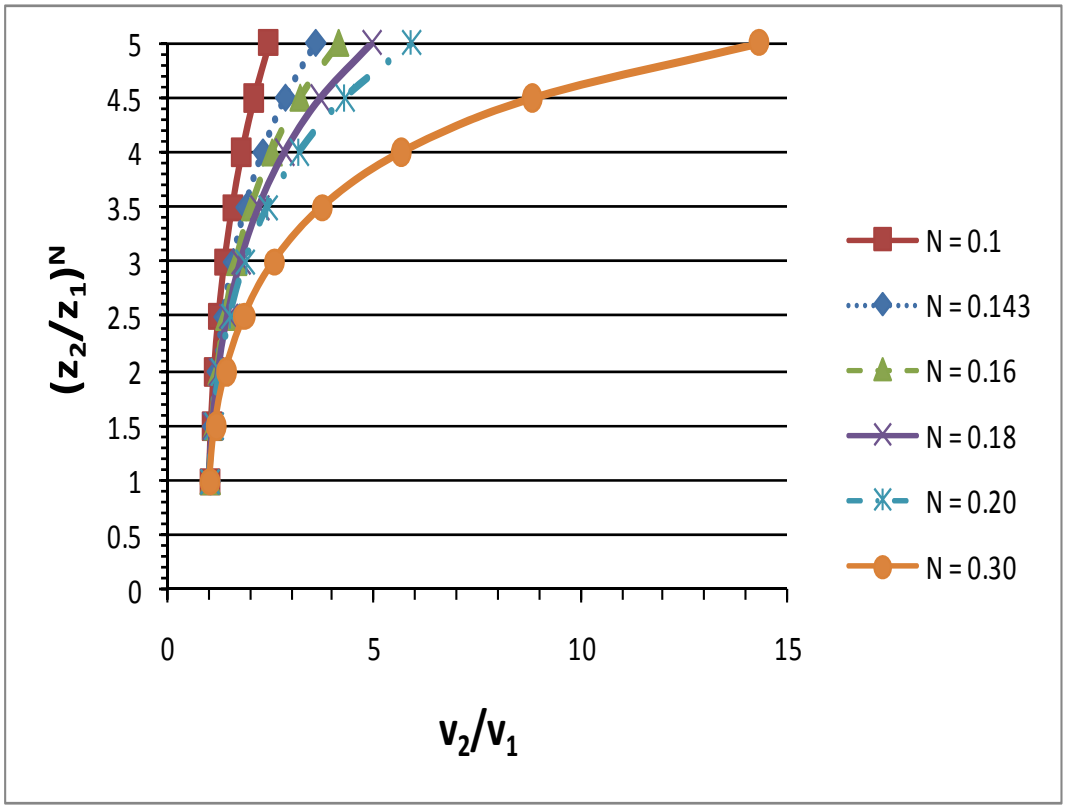

Figure 2.1 Ground Roughness Effects

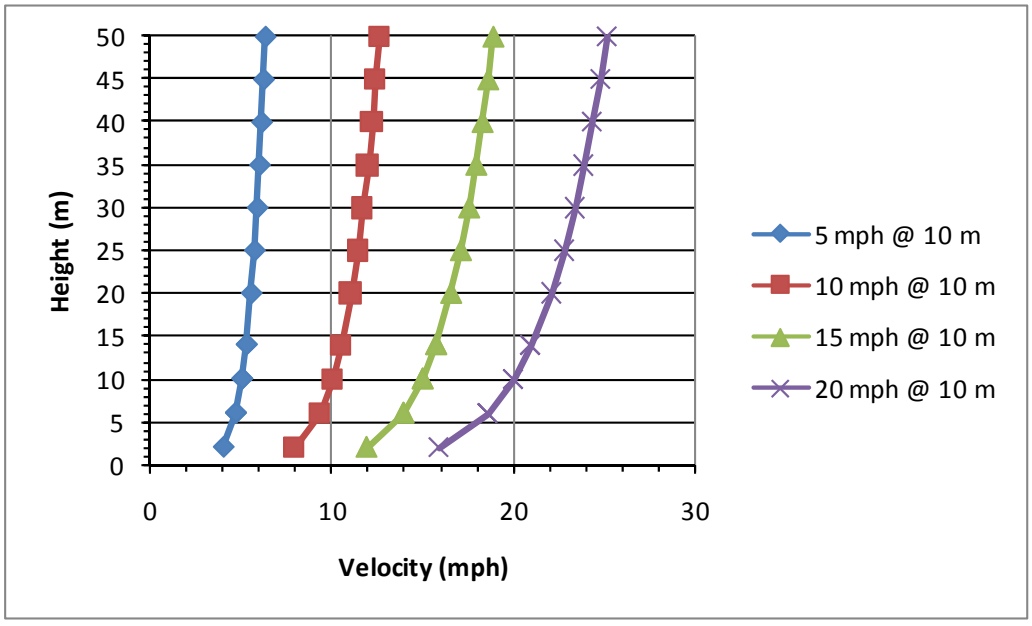

Figure 2.2 Effects of Height on Velocity (N = 0.143)

2.5 Binomial Logistic Regression

The relationship of wind demand (wind power) to fatigue cracking was studied using a logistic regression model. Poles were considered either cracked or not cracked, which is a binary response. Binary data are common and models are available for a wide variety of applications ranging from engineering to medical sciences (Hadjicostas 2006, 629).

Binary logistic regressions employ three scales: (log(odds) (also called logits), odds, and probability (Equations 7, 8, and 9 respectively). Here, a cracked pole is assigned a value of one and an uncracked pole is assigned a value of zero. To create a BLR for this type of response, a line is fitted so that all responses are between 0 and 1 (e.g., see Figure 2.5). A model (line) is created using Equation 7 through Equation 9 (Perkins, et al. 2007, 93). An example of the equation results using an α = +/-10 and a β = -/+0.2 are shown in Figure 2.3 through Figure 2.5.

Models may be validated several ways. Probably one of the oldest validation methods is to create the model using a training sample and testing the model using a holdout sample (Oral 2006). This method tests the predictability of the model, but it is potentially flawed by not using all the known data to create the model. Other types of tests include goodness-of-fit tests (GOF). The most common type of GOF tests are the Pearson x^2 test, the deviance test and the Homer-Lemeshow statistic. A more complete description of these tests along with a few others are described by Lin and Myers (2006). If the null hypothesis of a zero slope ($\beta = 0$) is true, then the proportion of poles that crack does not change in association with changes in a putative predictor variable.

$$Logit = \propto + \beta x \qquad \text{Equation 7}$$

$$Odds\ Ratio\ (OR) = e^{\propto + \beta x} \qquad \text{Equation 8}$$

$$\text{Probability } (P) = \frac{OR}{1 - OR} \qquad \text{Equation 9}$$

where:

α = Binary Regression Model Intercept
β = Predictor Coefficient
x = Predictor Value

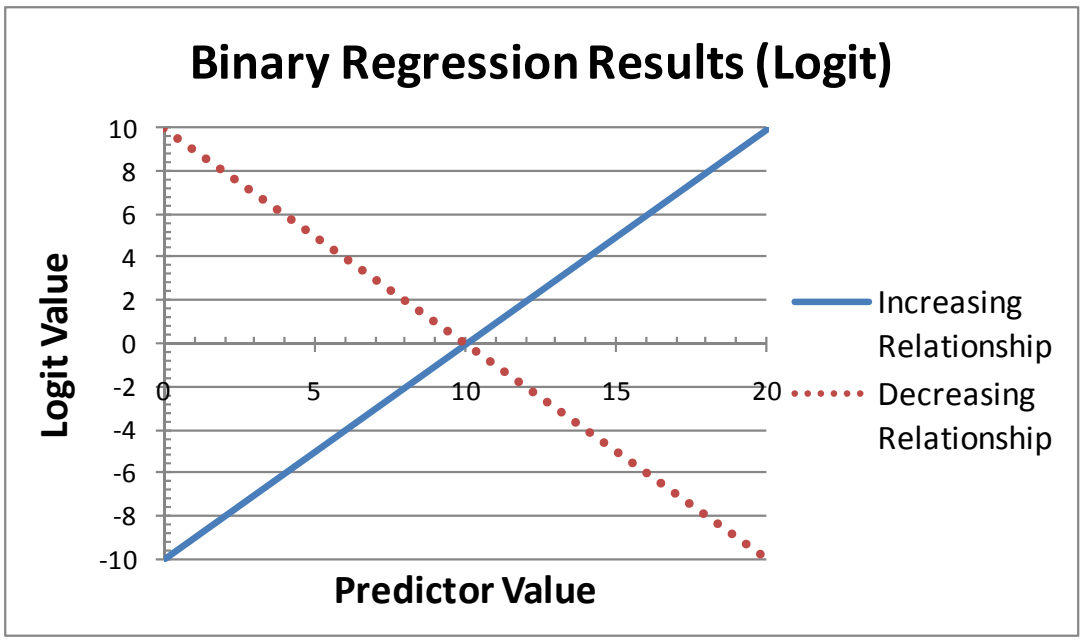

Figure 2.3 Example of Binary Regression Results: Logit Scale

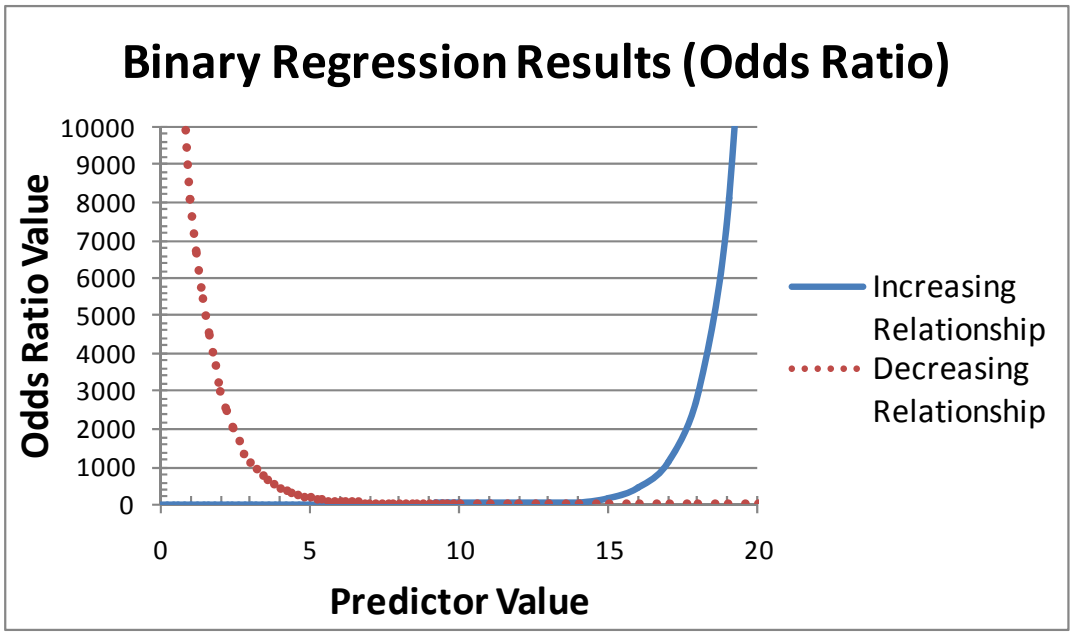

Figure 2.4 Example of Binary Regression Results: Odds Ratio Scale

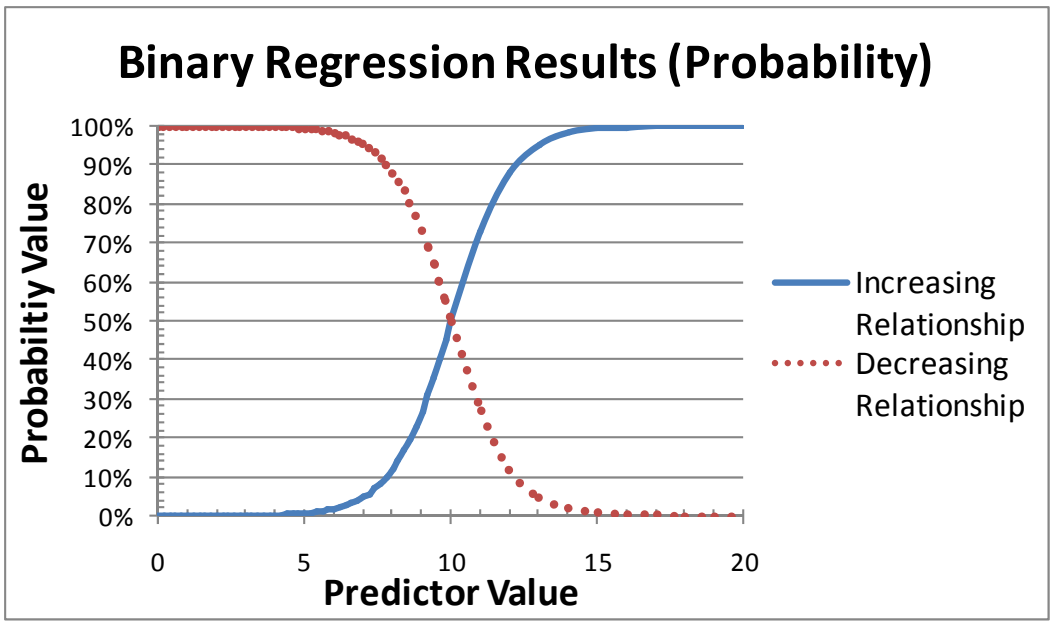

Figure 2.5 Example of Binary Regression Results: Probability Scale

3. METHODOLOGY

3.1 Introduction

The *2001 Standard Specifications for Structural Supports for Highway Signs, Luminaires and Traffic Signals* states that fatigue should be considered for overhead cantilevered sign structures, overhead cantilevered traffic signal structures, high-level high-mast lighting structures, overhead non-cantilevered sign structures, and overhead non-cantilevered traffic signal structures (AASHTO 2001). While many sources support this specification (see Literature Review), there is resistance from states for adoption due to the impact in structure size and cost for the conservative requirements. Many states do not have sustained winds and they have not experienced significant fatigue cracking. This study examines the relation between wind demand and fatigue failures. A simple way of predicting the magnitude of fatigue load is by getting the average annual wind velocity. The wind velocity can be computed by relating wind power to wind velocity (Equation 3). This is achieved by comparing the location of each structure to existing wind power maps. Finally, the results of structure cracking and average annual wind velocity are examined to determine if a correlation exists between the wind power classes (WPCs) (ranges of average annual wind velocity) and fatigue cracking. The following sections describe the methods used to complete these goals.

3.2 Data Collection

Inspection data were collected to relate observed in-service performance with the ambient winds, specifically wind power and average wind velocity. With adequate data, the effect of wind on fatigue cracking within cantilever traffic structures in different WPCs was statistically correlated. State departments of transportation (DOTs) own and maintain a significant number of these types of structures, and likely have the best inspection records. A significant portion of these structures are also owned by local agencies such as municipalities, counties, and other roadway authorities.

An initial (brief) survey was distributed to 50 state bridge engineer offices. The initial survey inquired about the existence and completeness of inspection data on cantilever traffic signal poles and high-mast luminaires. The survey polled for failures for cantilever traffic structures or high-mast luminaires and associated details. The survey concluded with contact information for the person with whom to follow up for a subsequent, more comprehensive survey. Twenty responses were received as illustrated in Figure 3.1. Few states have comprehensive inspection and several are just beginning formal programs.

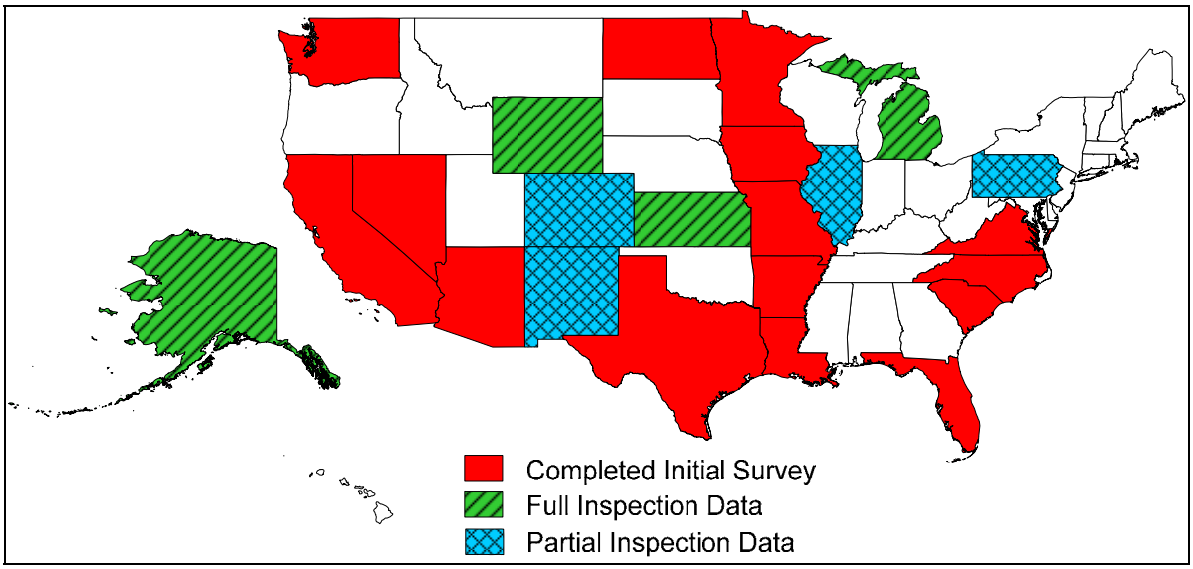

Figure 3.1 Survey Response

Based upon the review of the initial surveys, Wyoming, Kansas, Alaska, Michigan, Colorado, New Mexico, Pennsylvania, Iowa, and North Dakota were contacted to share their inspection data. Wyoming, Kansas, Alaska, Michigan, and New Mexico sent their current inspection data. Iowa provided a report about high-mast luminaires and Pennsylvania had some failures in the Lake Erie region, but no inspection program statewide. New Mexico was in the process of converting its inspection reports into a database format. Of the structures it had converted, they had no significant cracking related to fatigue. Colorado is in the process of conducting inspections and plans to have full inspection data in the future. North Dakota just inspects high-mast luminaires and had only a list of structures, their location and general condition.

Wyoming, Alaska, Kansas, and Michigan provided the most complete set of inspection records. These records included the structure condition, year the structure was erected, arm lengths, orientation, and many more items. Wyoming and Alaska also had partial records of type of connections. Kansas provided information on base-plate thickness and Michigan's inspections focused toward the bolts and base condition.

3.3 Data Organization

The inspection data provided by the different states came in two general formats. Wyoming and Michigan provided inspection data as Microsoft Excel sheets, and Kansas' and Alaska's data were in a Microsoft Access database format. To organize the data, a template Excel sheet was used. The template held data fields that were most common for all the inspection files. The most common fields included: structure identification, inspection data, year built, structure type, structure sub type, location, damage, structure orientation, shape, arm length, connection type, manufacturer, and base-plate thickness. However, not all data were known for each structure. Using Microsoft Access, Kansas' and Alaska's data were transferred into the template Excel sheet, and Michigan and Wyoming's data were reorganized to match. Once the data were contained in a consistent format, the WPC was determined based upon each structure location.

3.4 Wind Power Classification

The next step was to gather wind power information for the location of each pole. Originally, the power class was gathered from the 1980's *Wind Energy Resource Atlas of the United States* (Figure 3.2), however after more research, maps were used from the *Department of Energy's Wind Program and the National Renewable Energy Laboratory (NREL)* (Figure 3.3). The NREL maps are more current than the Atlas and provide more classifications that are specific. This project uses wind power maps generated by estimating the average wind speeds at 50 meters (164 ft) above the ground. The average wind is determined using a combination of GPS mapping tools, satellites, weather balloons, and meteorological tower data. NREL, along with some private companies, are generating these maps in an effort to make investing in wind power generation more predictable and, therefore, more economically feasible. Herein, these maps were used to classify the wind power associated with each structure's location. To classify each, the GPS coordinates provided by inspection records were plotted using ArcGIS and overlaid over county maps. The county location is then added to the Excel sheet for each structure. Next, the county maps are compared to the wind power classification maps. If a county is in one type of classification, all structures in that county are given that wind power classification. However, if a county holds multiple classifications, then each structure inside the county is compared to the wind power map. The process originally planned was to associate the GIS data to recreate the wind power maps using ArcGIS and then overlay the structures. Due to the proprietary nature of some of the data, the wind power maps were never recreated using ArcGIS. The wind maps were printed and using a backlight the hard-to-place structures were classified. This restriction leads to a less automated, more labor-intensive process.

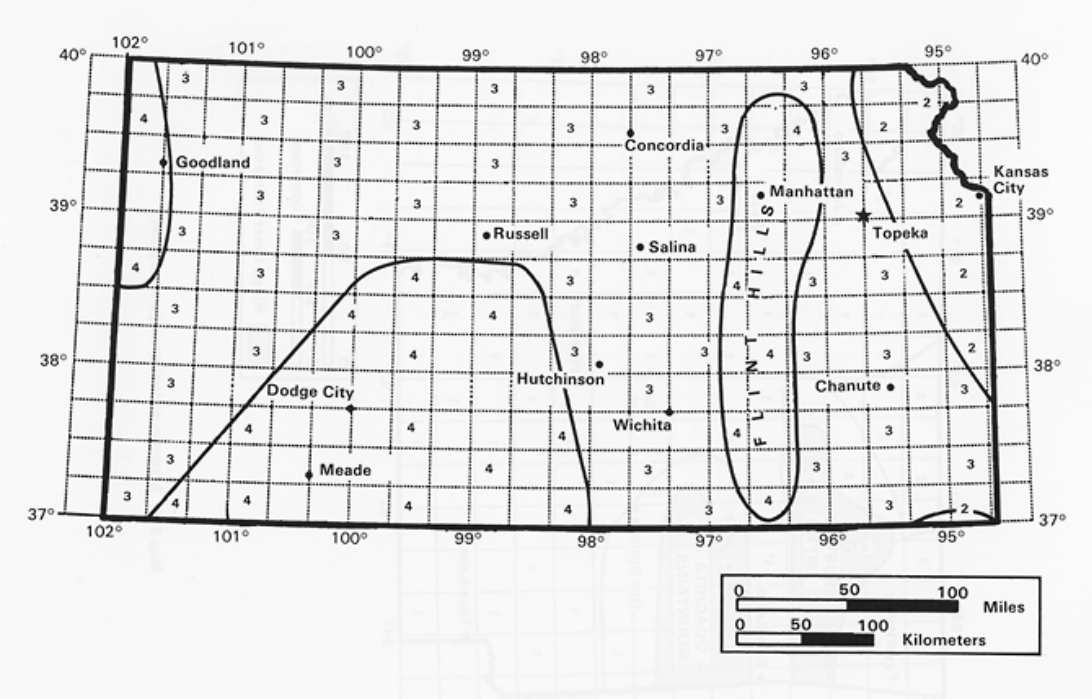

Figure 3.2 Kansas Wind Power (National Renewable Energy Laboratory 1982)

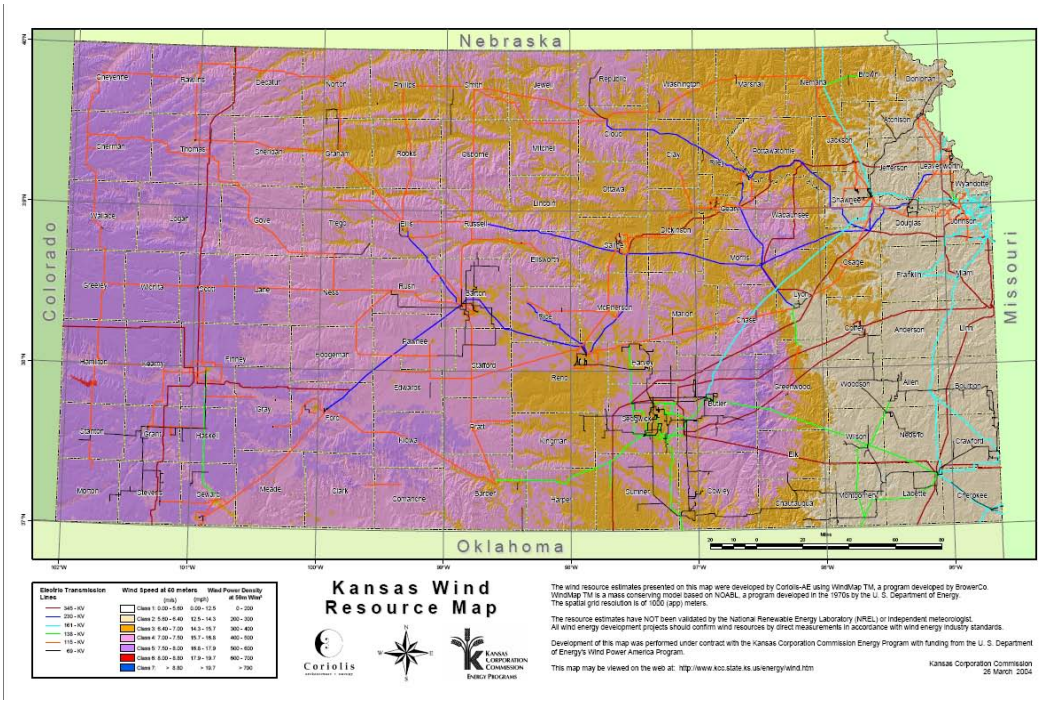

Figure 3.3 Kansas Wind Power (Kansas Corporation Commission 2004)

Figure 3.2 and Figure 3.3 are wind power maps of Kansas. Figure 3.2 was taken from the *Wind Energy Resource Atlas of the United States*. This publication was updated in 1983 and provides low-resolution maps for the entire United States. Figure 3.3 was taken from Kansas Corporation Commission Energy Program. This map was developed by a private company, Coriolis-AE, using WindMap^{TM} a (Kansas Corporation Commission 2004) program based on a mass conserving 1970s model developed by the U.S. Department of Energy. The model was verified by wind data collected at exposed ground level and projected to 50 meters (Kansas Corporation Commission 2004). Note that the 50-m reference height is an important feature and is the need for using Equation 2 to predict the velocity profile within the boundary layer.

3.5 Structure Inspection Database Discussion

The original inspection data included comments about each structure. Typically, the comments were limited to deficiency in the structure like “3 of 4 bolts are missing” (Kansas Department of Transportation 2005, LTB0628) or “4 inch longitudinal crack at splice” ((Kansas Department of Transportation 2005, LTB0703). However, non-structural comments like “Handrail pin is bent, preventing handrail from being lowered” were also included (Kansas Department of Transportation 2005, SPB5194) or “New pole, *Don’t know how to measure*” (WY-DOT 1998, SN2078). Each pole was given an importance factor of either a zero or one. Zero meant the pole had no reported cracking and one meant the structure was cracked in some location. Unless specified in the comment, cracking was assumed to be related to wind and was included in the statistical study. Some poles were cracked for non-wind-related reasons, like traffic collisions and projectile damage. These structures were not counted as cracked. In the descriptive comments, structures sometimes had multiple cracks. However, to not double count structures, each structure was categorized as either cracked or not cracked. The degree or amount of cracking was not quantified, nor typically available.

3.6 Statistical Analysis

Basic statistical analysis was completed once the inspection data for the structures were sorted. The first analysis was to get an approximate estimate of the percentage of cracked poles associated with each wind power classification. The number of cracked and uncracked poles in each WPC was determined and used to compute the percentage of cracked poles. This coarse statistic showed an increase in pole cracking as the wind power classification increases and a more in-depth analysis was warranted.

Of particular concern was if the wind power (or average wind velocity) was a significant predictor and if other parameters affect the pole fatigue cracking as well. Other parameters such as pole design, age, and orientation might provide other useful information and predictive metrics. These parameters were studied with a histogram of the cracked versus uncracked structures (e.g., Figure 3.4). The next step was to further sort each category by wind power classification (e.g., Figure 3.5). For each category that possessed 30 or more known elements, histograms were created. Figure 3.4 and Figure 3.5 are examples of typical histograms study and their interpretation of these particular figures is discussed later.

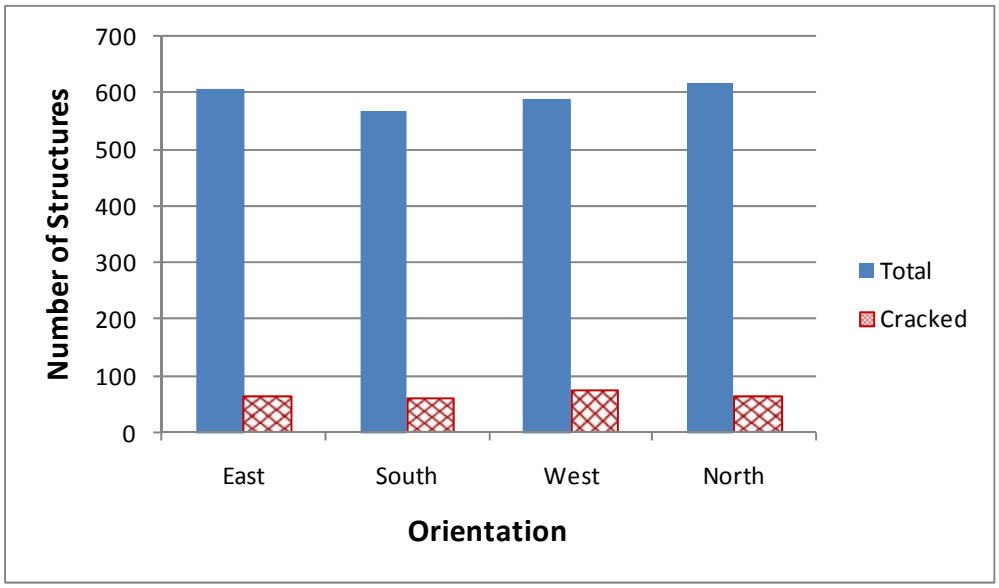

Figure 3.4 Sorted Structure Orientation

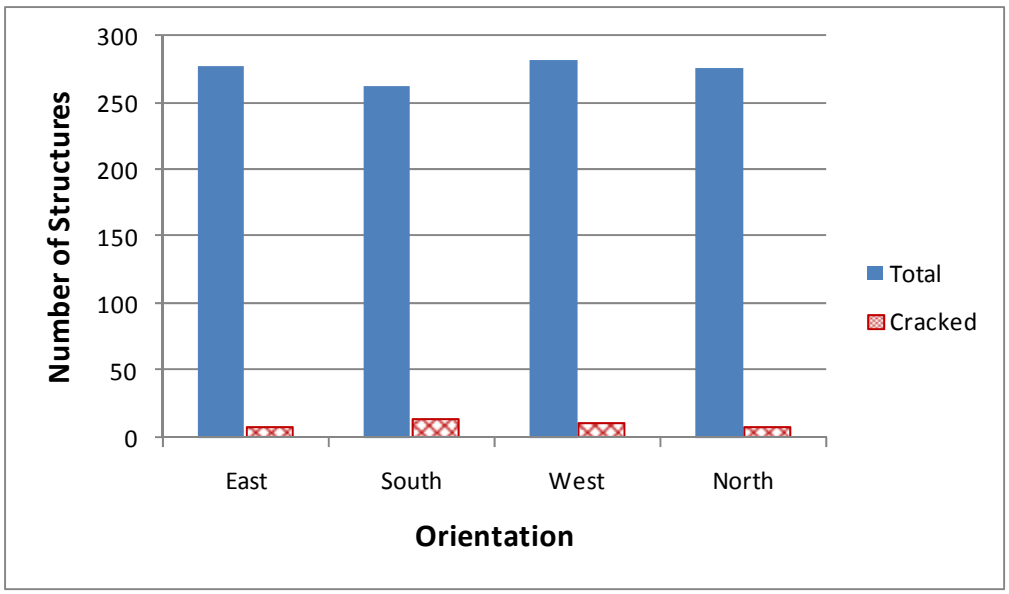

Figure 3.5 Sorted Structure Orientation for WPC-1

3.7 Modeling

The basic analyses were next supplemented with more advanced statistical analyses with several methods investigated. The first method was to use the percent of poles cracked in each WPC and fit an exponential regression. This method had several flaws: it only took into account the WPC-1, WPC-2, WPC-3, and WPC-4; it had no upper limit on the percentage of structures cracked and it did not fit the data well. The next method was to use the cumulative percentage of structures cracked. This method had the same flaws as the previous method, with an additional flaw of assuming a cracked structure in WPC-1 would also be cracked in WPC-2, WPC-3, and WPC-4. The final method to model the cracking behavior was using a *logistic* regression model. The binomial regression was chosen because it presumes a data set has only two responses (0 or 1, yes or no, tall or short, etc.) and the regression is limited to values between the values of the response (Taylor 2005).

The binomial regression lends itself to this study because a structure was either cracked or not cracked (one or zero). Another advantage of logistic regressions was, unlike linear regression which predicts the actual values of the response variable, logistic regression models the probability associated with each level of the response variable by finding a linear relationship between predictor variables and a link function of these probabilities. (Minitab 15, 2008)

Logistic binominial regression were done with the statistical package Minitab. The regression was run with the binominal regression option. Several different runs were completed to gain the best model for the crack prediction. For the regression, the average wind speed of each power class was used as a predictor (Table 3.1) and the response variable was the cracking status. The structures used were only in WPCs 1 through 4. Then several runs were completed using different combinations of average wind speed combined with the variables mast-arm length, structure age, structure orientation, and structure manufacturer as predictors.

Table 3.1 Wind Power Classification Wind Speed Categories

Wind Power Class (WPC)	Wind Speed At 50 m (mph)	Mean Speed
Class 1	0-12.5	6.25
Class 2	12.5-14.3	13.4
Class 3	14.3-15.7	15
Class 4	15.7-16.8	16.25
Class 5	16.8-17.9	17.35
Class 6	17.9-19.7	18.8
Class 7	>19.7	-

These models illustrated that WPC-1 needed to be subdivided to include several average wind speeds (data bins). Only WPC-1 was further subdivided because it has 12.5 miles per hour range of speeds, where the rest of the classes included in the model have a range of less than two miles per hour. For all of the poles in WPC-1, the average wind speed was reorganized using the mean annual wind speed at nearby airport sites, known county speeds, or known city speeds. Typically, these values came from the National Climatic Data Center (NCDC), a branch of NOAA (National Climatic Data Center (NCDC) n.d.). If a reasonable estimate for mean wind speed in WPC-1 could not be determined for the location of structure, it was assumed to be the mid-point of WPC-1, or 6.25 mph. The midpoint estimate was used for 49 out of the 1098 (4.5%). In addition to collecting the mean wind speed, the measured height reference was recorded and Equation 10 was used to place both sets on a common basis, i.e., the mean wind speed at 50 meters. A wind shear component (alpha) of 0.143 was used for all the locations. This number represents a wind profile in a well-mixed atmosphere over flat, open terrain. The model could be further refined by gathering site-specific terrain characteristics to determine alphas. An example of Equation 10 using the mean wind speed in Juneau, Alaska, of 8.2 mph measured at six meters above the ground results in a wind the speed at 50 meters above ground of 11.1 mph.

$$v_2 = v_1 \left[\frac{z_2}{z_1}\right]^{\alpha} \qquad \text{Equation 10}$$

where:

v_2 = the unknown mean wind speed at height z_2
v_1 = the known mean wind speed at height z_1
α = the wind shear exponent [0.143 (AWS Scientific Inc., 1997 pg 3-3)]

After the mean wind speed for WPC-1 was reassigned, the binary regression model was executed. Finally, approximate confidence bounds were placed on the regression, using the variance of the regression and the sample size.

4. ANALYSIS OF MAST-ARM AND HIGH-MAST FATIGUE FAILURES

4.1 Mast-Arm Crack Predictors

The structures were divided into two groups, mast-arms and high-mast luminaires. The following section pertains only to the mast-arm structures.The average wind speed, structure orientation, mast-arm length, structure age and manufacturer were available using inspection data for approximately 2,500 structures. The following tables and figures show the characteristics of these data.

Figure 4.1 Typical Mast-Arm Structure

4.1.1 Orientation

The traffic signal structures have mast arms that cantilever over a portion of a roadway. Typically signs, signals, or lights are attached to these and the direction the observer is facing is considered in their orientation (Figure 4.1). For example, a driver traveling north in Figure 4.2 would be able to read information from the sign on a structure in the northeast corner. This means that the structure located in the northeast corner would be oriented north, the southeast corner would be oriented east, and so forth.

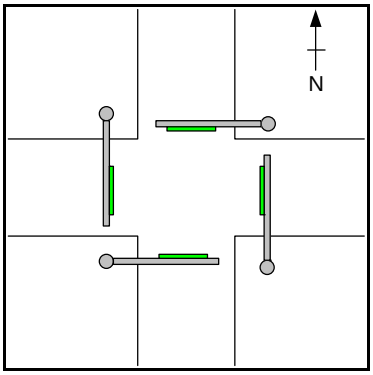

Figure 4.2 Structure Orientation

The orientation does not appear to play a significant role in the likelihood of a structure to crack. As illustrated in Figure 4.3, the total number of structures is approximately the same in each category, along with the number of cracked structures. The hatched bars on Figure 4.8 also show that the percent of structures cracked is approximately the same (a difference of 2.3% at most). Figure 4.4 through Figure 4.7 represent the orientation of the total and cracked structures divided into each WPC. For WPC-1 and WPC-2, no significant trend exists illustrating that cracking increases for one orientation versus another. However, in WPC-3 the structures with an eastern orientation have a high cracked percentage and when structures with an east or west orientation are compared with the south or north orientated structures, there is a difference of almost 15%. WPC-4 also shows a similar trend, with east and west structures having a combined cracking percentage 8.8% higher than the north and south. In summary, a trend with the orientation exists whereby structures in higher WPCs are more likely to be cracked with east-west orientation.

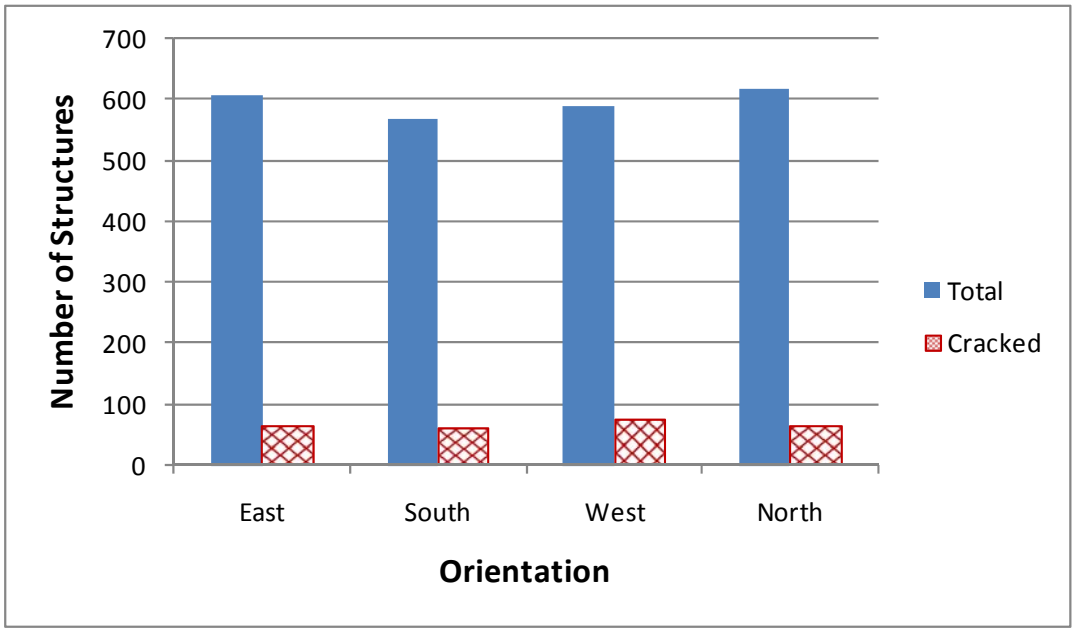

Figure 4.3 All WPCs Orientations and Cracking Status

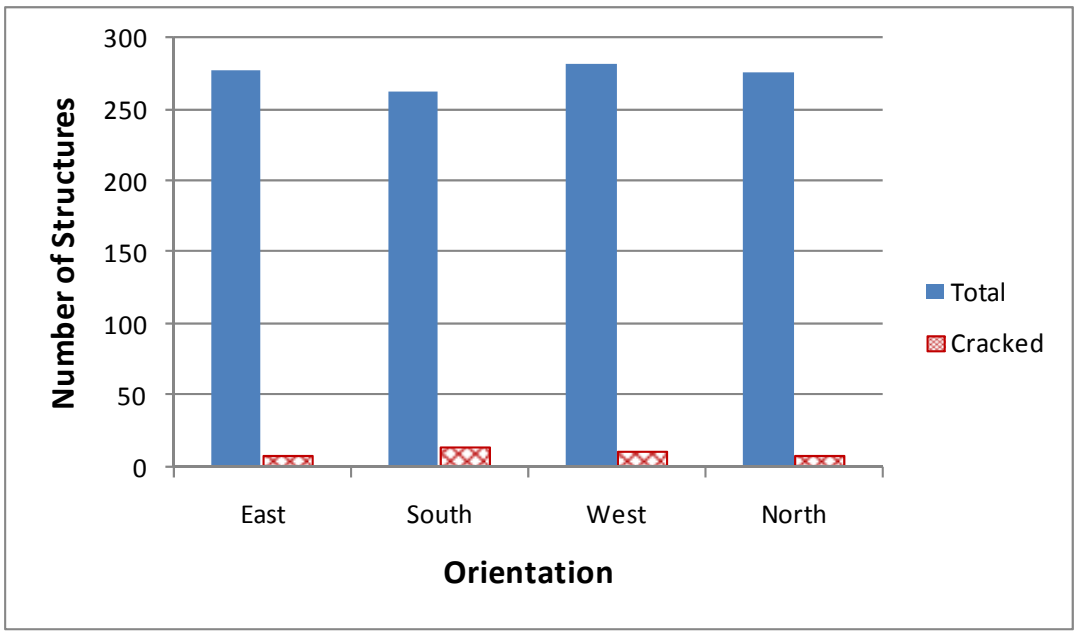

Figure 4.4 WPC-1 Orientations and Cracking Status

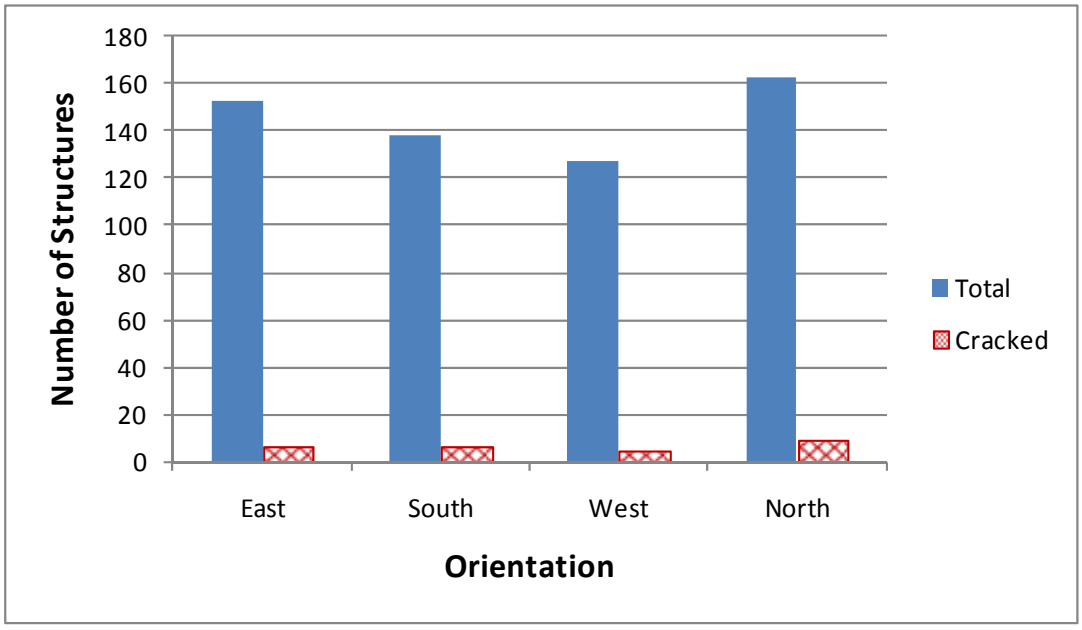

Figure 4.5 WPC-2 Orientations and Cracking Status

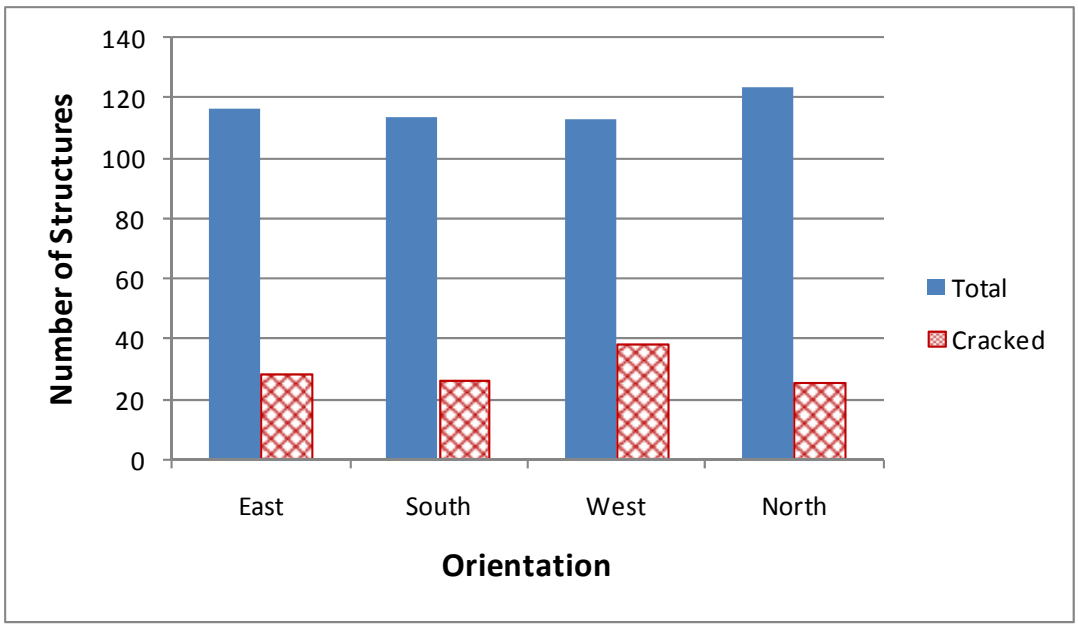

Figure 4.6 WPC-3 Orientations and Cracking Status

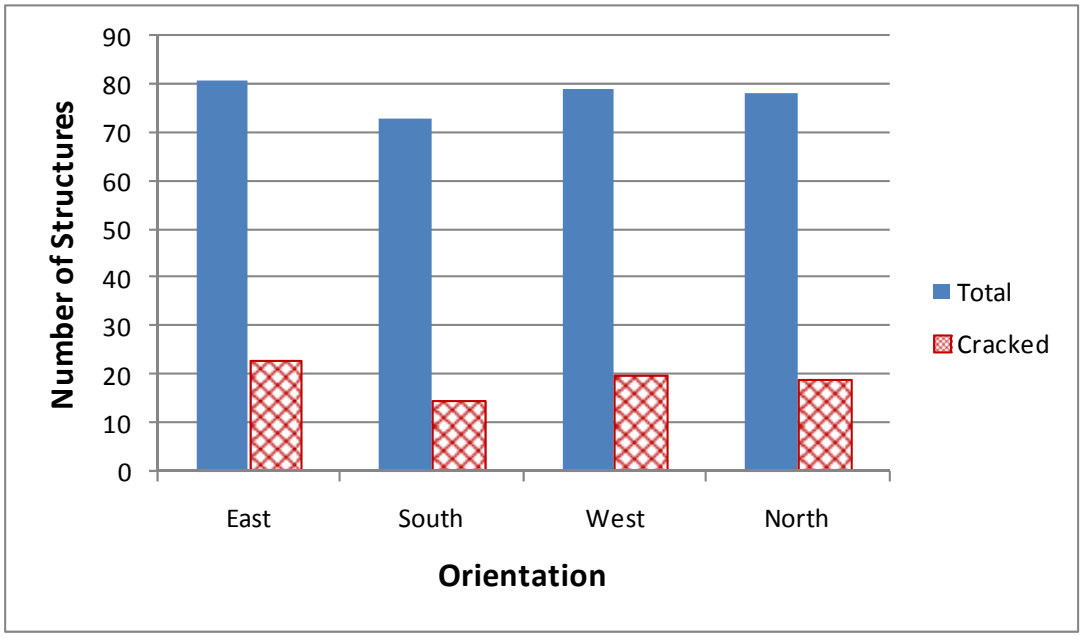

Figure 4.7 WPC-4 Orientations and Cracking Status

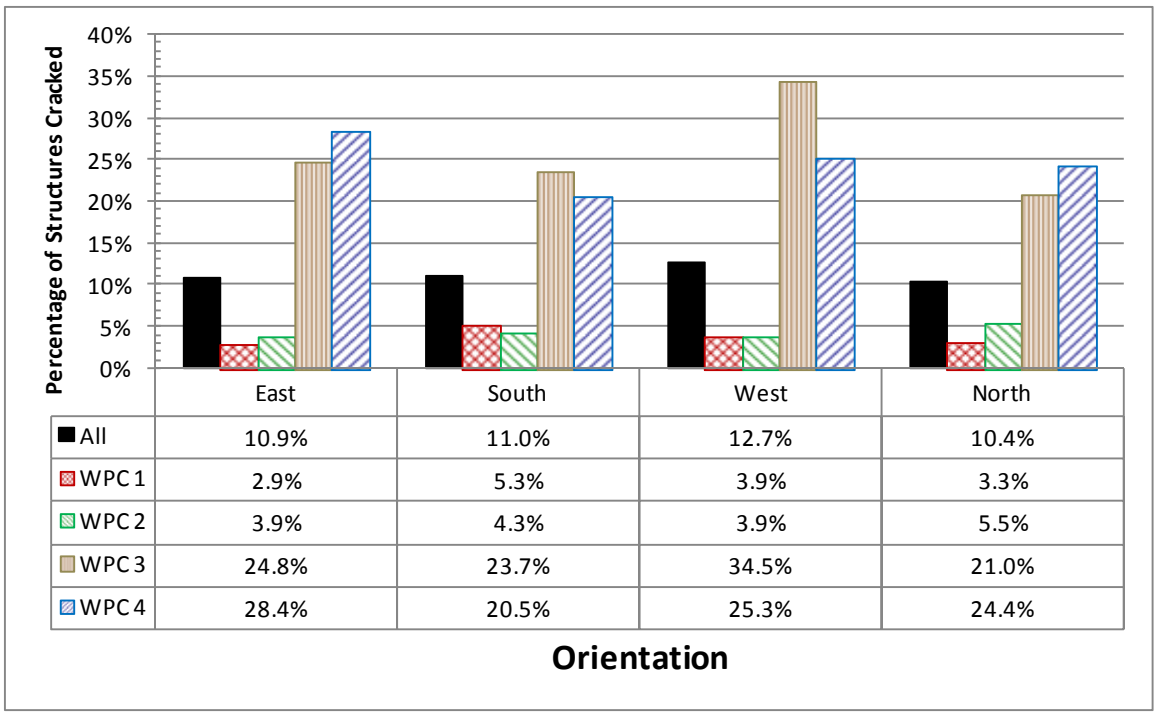

Figure 4.8 Orientations and Percentage of Cracked Structures

The aggregated inspection data shows no significant cracking trend related to orientation. However, this does not completely exclude orientation as a predictor. The aggregated inspection data does not take into account prevailing wind direction which may play a significant role. Figure 4.9 shows the annual prevailing wind direction for a few sites. These were made using records taken from the National Climatic Data Center (National Climatic Data Center (NCDC) n.d.) and cross-checked with a summary table from the Western Regional Climate Center (Western Regional Climate Center n.d.). Next, the inspection data were sorted for orientation and cracking status for each location in Figure 4.9. The results can be viewed in Table 4.1 and Table 4.2. In Table 4.2, the highlighted values show the maximum cracking percentage for each location. It can also be seen that the total number of poles in each orientation is roughly the same for the locations with a large number of poles. For the combination of north/south and east/west structures, the prevailing wind direction matches five out of nine times. Including the off angles, all the prevailing winds match for all locations. However, this is not particularly helpful on all locations because the prevailing wind direction is not constant or even available for all structure locations. With additional research in site specific trends, guidelines for inspection frequency could be influenced. The orientation of the structure does play a role in fatigue cracking and should be considered for future work. In summary, poles orientated perpendicular to the prevailing wind direction are more likely to crack.

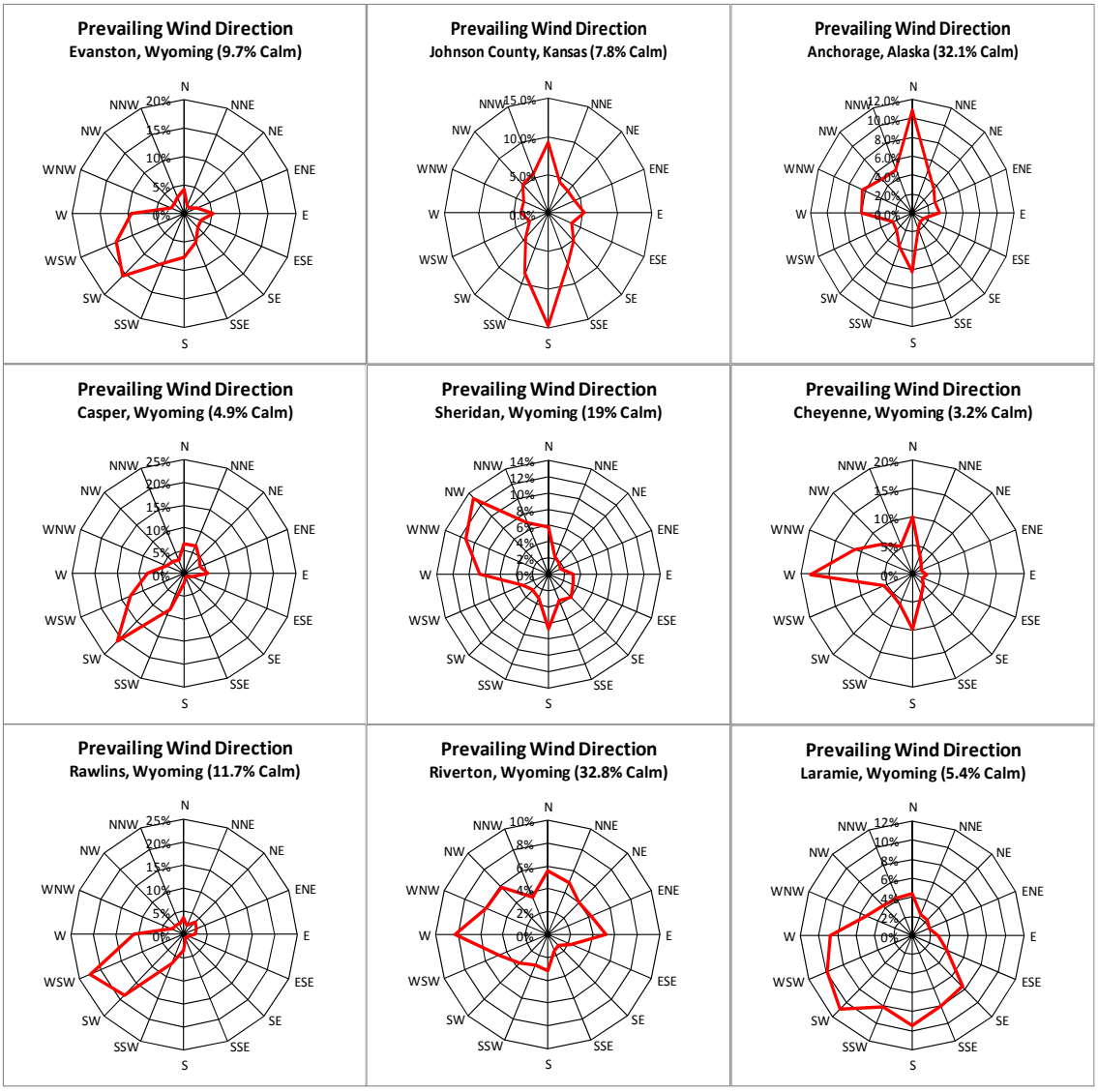

Figure 4.9 Wind Roses for Select Sites

Table 4.1 Mast-Arm Orientation and Cracking vs. Prevailing Wind Direction

	WPC	Prevailing Wind (Based on Wind Roses)	Maximum		Maximum	
			Direction	Cracking %	NS or EW	Cracking %
Evanston, Wyoming	WPC 2	Southwest	North and South	12.5%	NS	12.5%
Johnson County, Kansas	WPC 3	South	South	2.4%	NS	2.1%
Anchorage, AK	WPC 1	North	South	3.2%	NS	2.5%
Casper, WY	WPC 4	Southwest	East	50.0%	EW	48.1%
Sheridan, WY	WPC 1	Northwest	West	37.5%	EW	25.0%
Cheyenne, WY	WPC 3	West	West	28.3%	EW	21.6%
Rawlins, WY	WPC 4	West Southwest	South	50.0%	EW	40.0%
Riverton, WY	WPC 1	West	West	36.4%	EW	30.4%
Laramie, WY	WPC 3	Southwest	North	23.5%	EW	22.2%

Table 4.2 Mast-Arm Orientation and Cracking Percentage

	Orientation	North	East	South	West	North and South	East and West	All Directions
Evanston, Wyoming	Total	8	9	8	7	16	16	32
WPC 2	Cracked	1	0	1	0	2	0	2
	% Cracked	12.50%	0.00%	12.50%	0.00%	12.50%	0.00%	6.25%
Johnson County, Kansas	Total	55	27	41	20	96	47	143
WPC 3	Cracked	1	0	1	0	2	0	2
	% Cracked	1.82%	0.00%	2.44%	0.00%	2.08%	0.00%	1.40%
Anchorage, AK	Total	168	170	157	177	325	347	672
WPC 1	Cracked	3	3	5	3	8	6	14
	% Cracked	1.79%	1.76%	3.18%	1.69%	2.46%	1.73%	2.08%
Casper, WY	Total	38	42	40	39	78	81	159
WPC 4	Cracked	18	21	13	18	31	39	70
	% Cracked	47.37%	50.00%	32.50%	46.15%	39.74%	48.15%	44.03%
Sheridan, WY	Total	14	8	14	8	28	16	44
WPC 1	Cracked	1	1	3	3	4	4	8
	% Cracked	7.14%	12.50%	21.43%	37.50%	14.29%	25.00%	18.18%
Cheyenne, WY	Total	38	51	37	46	75	97	172
WPC 3	Cracked	7	8	8	13	15	21	36
	% Cracked	18.42%	15.69%	21.62%	28.26%	20.00%	21.65%	20.93%
Rawlins, WY	Total	6	5	4	5	10	10	20
WPC 4	Cracked	1	2	2	2	3	4	7
	% Cracked	16.67%	40.00%	50.00%	40.00%	30.00%	40.00%	35.00%
Riverton, WY	Total	9	12	7	11	16	23	39
WPC 1	Cracked	2	3	2	4	4	7	11
	% Cracked	22.22%	25.00%	28.57%	36.36%	25.00%	30.43%	28.21%
Laramie, WY	Total	17	18	16	18	33	36	69
WPC 3	Cracked	4	4	2	4	6	8	14
	% Cracked	23.53%	22.22%	12.50%	22.22%	18.18%	22.22%	20.29%
Rock Springs, WY	Total	16	14	14	13	30	27	57
WPC 3	Cracked	7	5	6	7	13	12	25
	% Cracked	43.75%	35.71%	42.86%	53.85%	43.33%	44.44%	43.86%

4.1.2 Mast-Arm Length

The length of a mast arm can amplify the movements resisted by welds and possibly increase the associated localized stress concentrations. The longer a mast arm, the longer the movement arm is which increases the movement at the connection to the vertical pole; this location is a likely place for cracking to occur. To examine if the mast-arm length was a significant predictor, the following figures and tables were developed. Table 4.3 shows that the mean length for all the mast arms are approximately 35 feet and that the mean length for all the cracked structures is 33 feet. There is no appreciable trend in the average arm length for structures depending on their wind power class for the total of the structures. There is a small increase in mean for the cracked structures with an increase in WPC, with the exception of WPC-2. Figure 4.10 through Figure 4.14 show histograms of mast-arm lengths for the total and cracked structures, and divides them into different WPCs. A left skewed distribution can be fitted to the mast arms in Figure 4.10 for both the total and cracked structures. However the trend does not hold for when the structures are divided among into their individual WPCs. Each WPC histogram has a different shape and different mean.

Table 4.3 Average and Extreme Mast-Arm Lengths

	Total Structures Mast-Arm Lengths (ft)				Cracked Structures Mast-Arm Lengths (ft)			
WPC	Mean	Minimum	Maximum	Standard Deviation	Mean	Minimum	Maximum	Standard Deviation
All	34.70	6.00	93.00	12.55	32.51	10.00	50.00	8.32
1	38.39	6.00	76.00	12.04	31.24	10.00	46.00	9.71
2	31.08	6.00	93.00	14.22	27.64	10.00	45.00	8.59
3	33.08	15.00	50.00	9.45	32.31	15.00	50.00	7.10
4	30.13	6.00	52.00	11.13	35.13	15.00	50.00	8.47

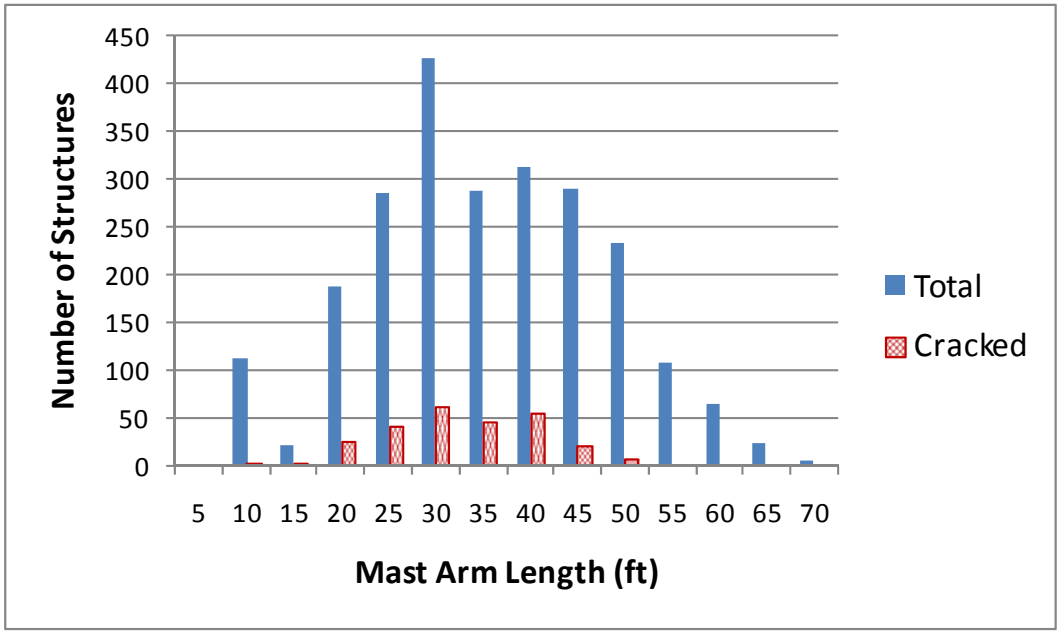

Figure 4.10 Lengths and Cracking Status for All WPC

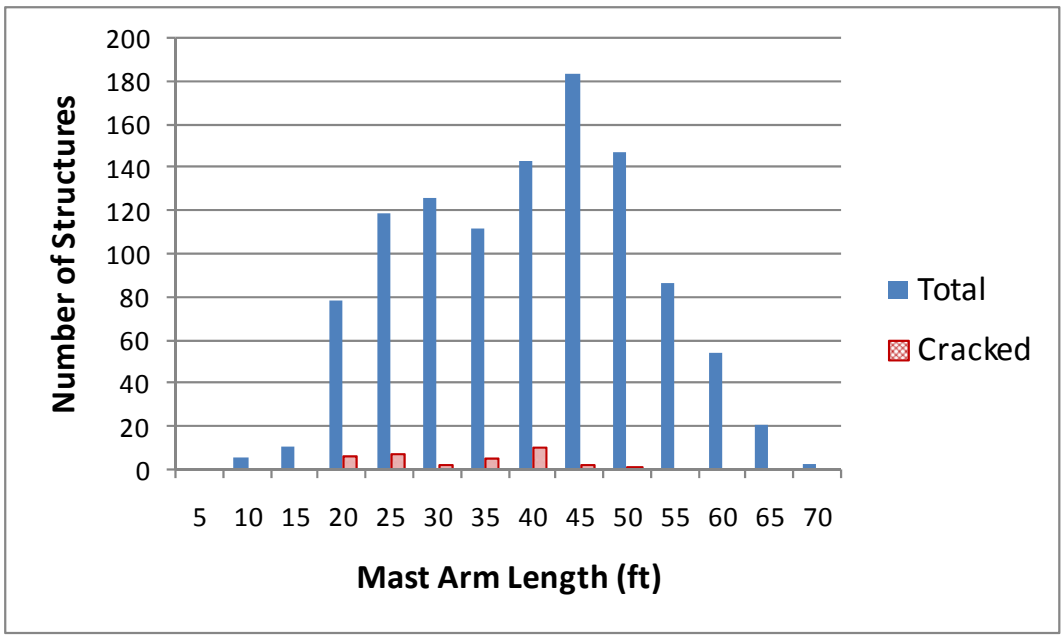

Figure 4.11 Lengths and Cracking Status for WPC-1

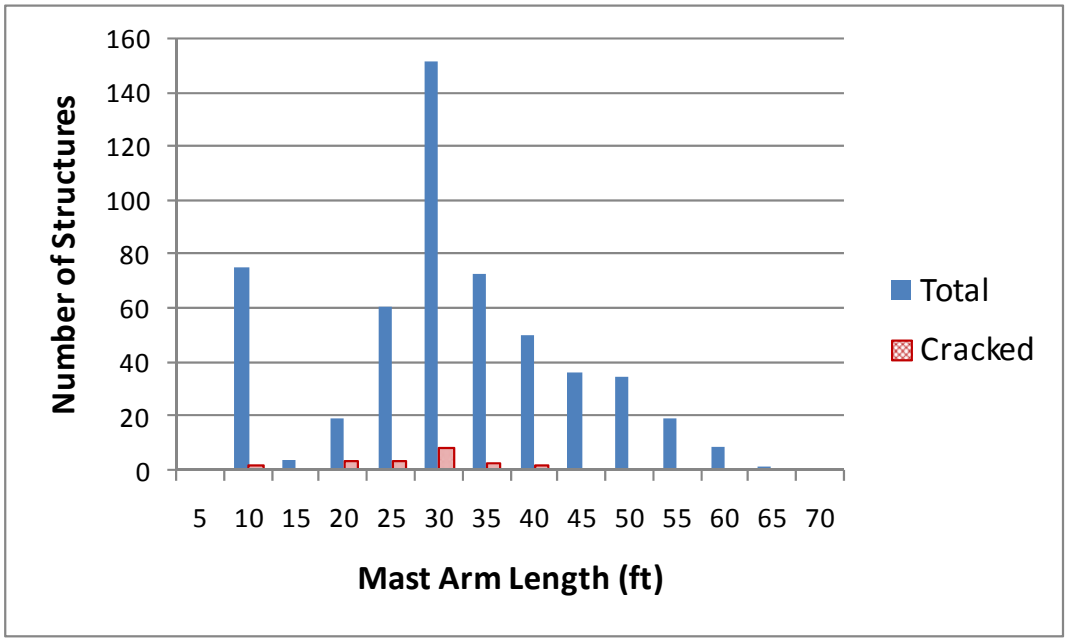

Figure 4.12 Lengths and Cracking Status for WPC-2

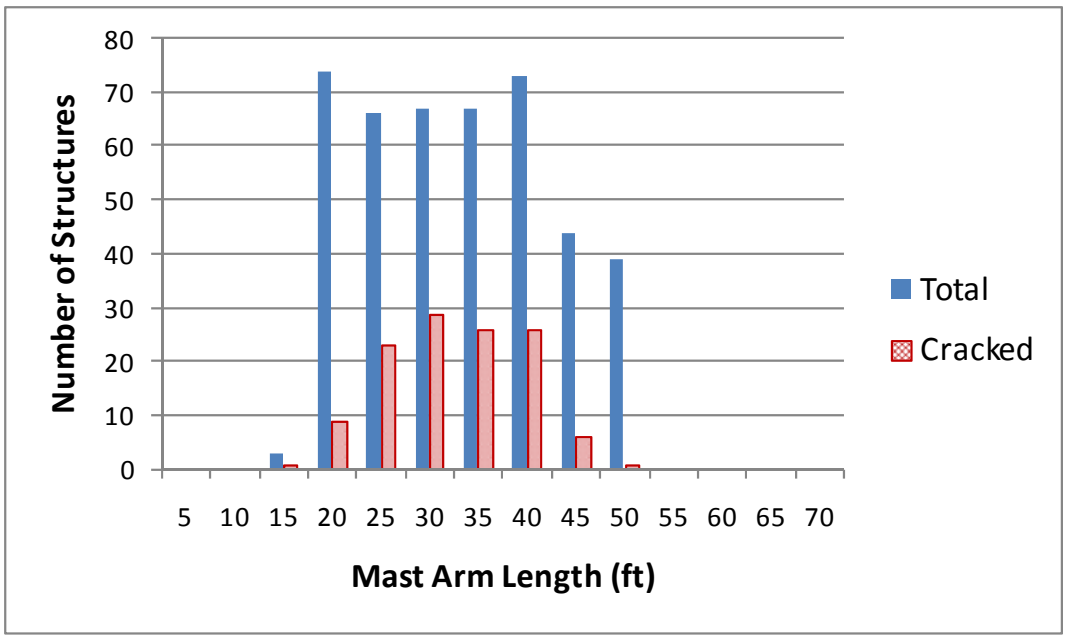

Figure 4.13 Lengths and Cracking Status for WPC-3

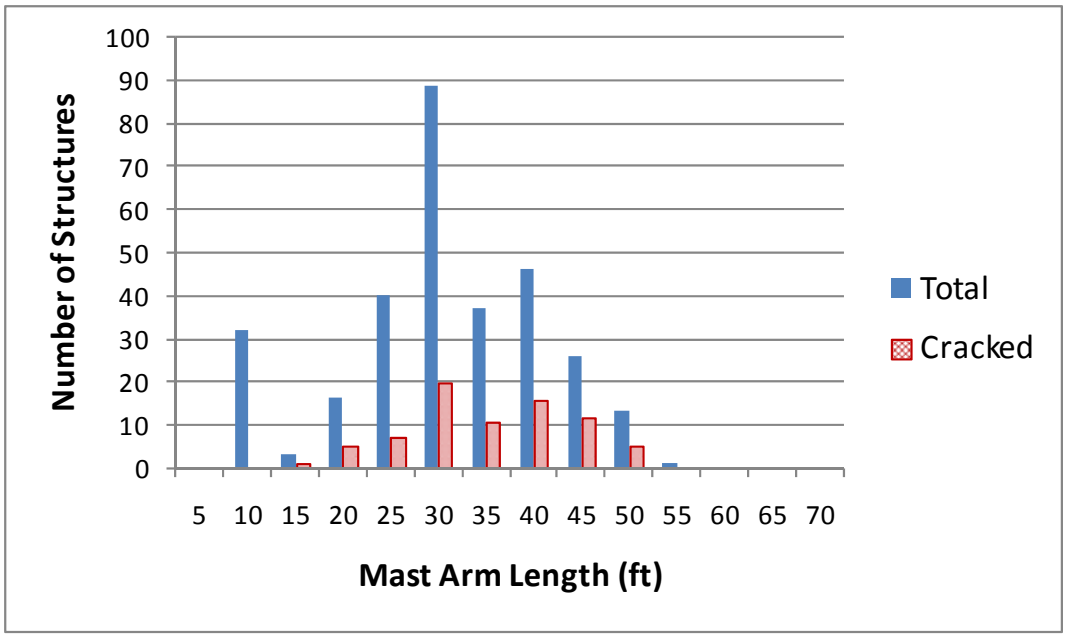

Figure 4.14 Lengths and Cracking Status for WPC-4

A more rigorous way to examine the effect of mast-arm length rather than just simple histograms is comparing the cracked percentage of structures with mast-arm lengths. Aggregating the data, no significant trend between length and cracking is demonstrated (Figure 4.15). However, when the structures are sorted and presented, some interesting trends appear. The percentage of poles cracked by length shown in Figure 4.16 and Figure 4.17 for WPC-1 and WPC-2, respectively, reflect a downward trend in cracking with an increase in arm length. WPC-1 has more poles cracked around 10 feet than any other power class, however this may not be meaningful because

the category has only six poles and one of those is cracked (1/6 = 16.7%). Figure 4.18 shows an initial high crack percentage at 15 feet, but it also has a lack of data (only three poles and one is cracked). Excluding the 15 feet bin, the cracking percentage increases until 30 feet and then decreases with longer arms. The WPC-4 (Figure 4.19) cracking percentage is in the low 30's for mast arms between 15 and 20 feet. For mast arms 25 feet and longer, there is a steady increase in cracking percentage with mast-arm length until the arm lengths exceed 45 feet. Figure 4.20 is a combination of the graphs presented in Figure 4.15 through Figure 4.19. Length as a sole predictor has varying value for this study. The cracking in WPC 1 through 3 peaks between 10 and 20 feet then steadily decreases with increasing length. For these wind power classes, length is valuable as a predictor, showing that shorter arm length increase fatigue cracking chances. This result is counter intuitive considering longer arms create larger stress ranges. For WPC 4, the results show a fairly constant cracking percentage for all lengths. This means that sustained winds do not affect the mast arms in the same manner areas with less sustained winds. While these are interesting results, they do not lend themselves to fatigue crack modeling as a function of mast-arm length alone.

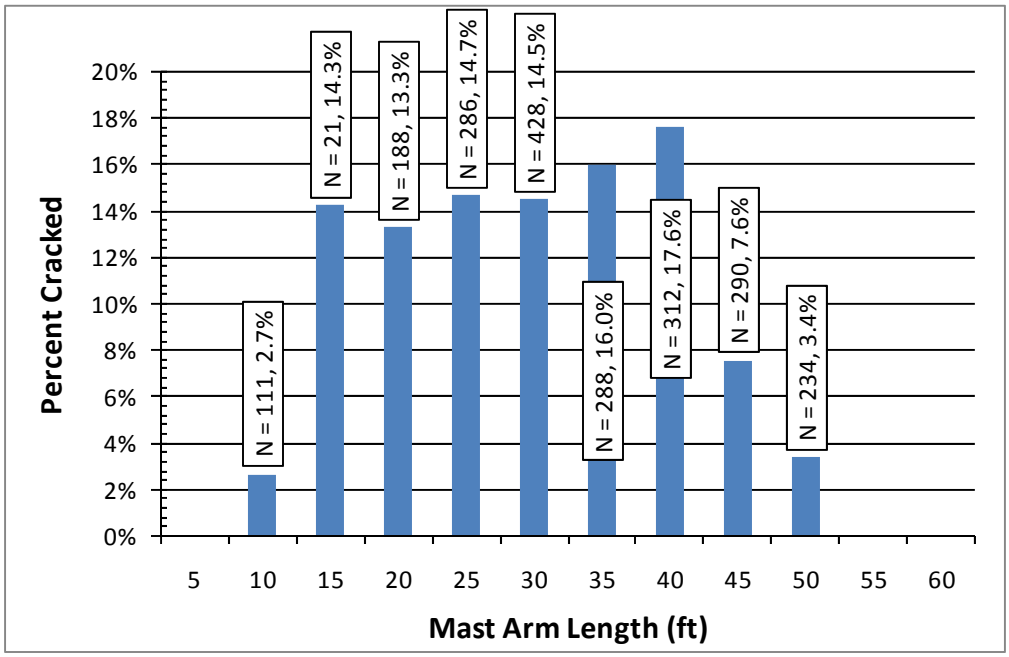

Figure 4.15 Percent of Structures Cracked in All WPCs by Mast-Arm Lengths

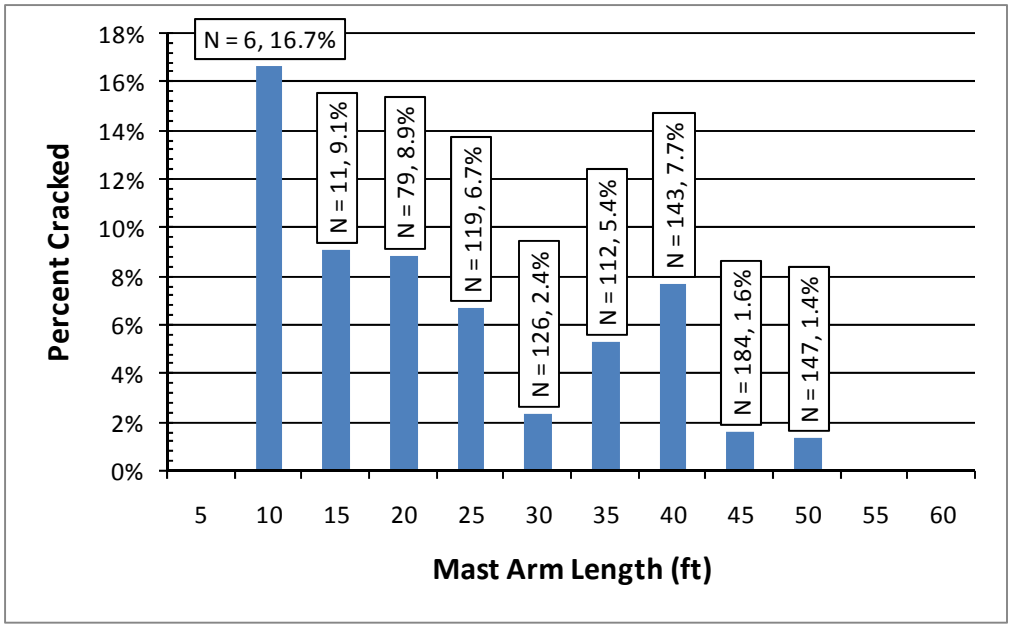

Figure 4.16 Percent of Structures cracked in WPC-1 by Mast-Arm Lengths

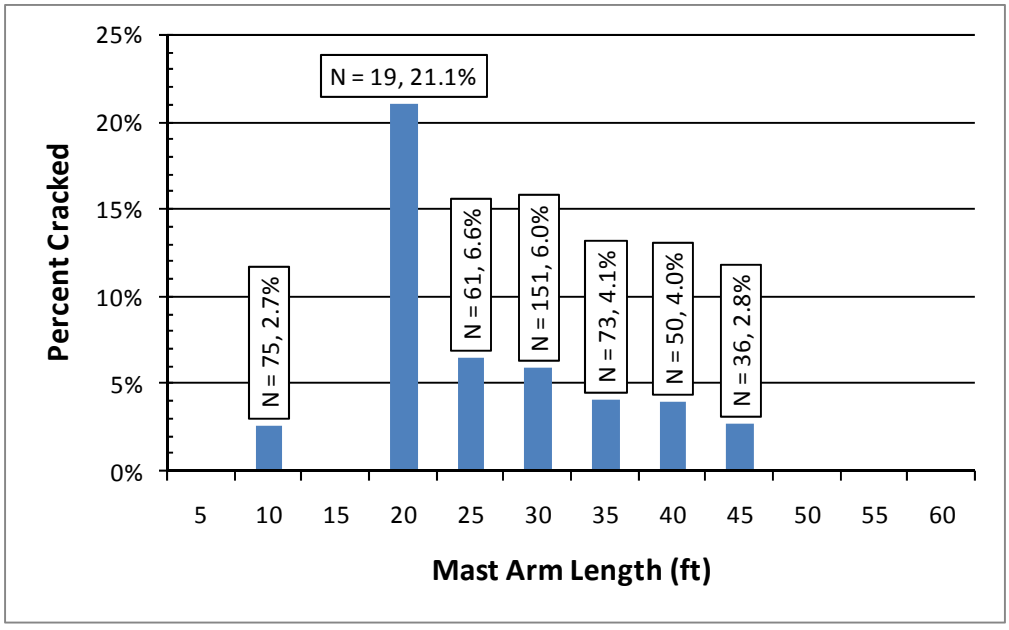

Figure 4.17 Percent of Structures Cracked in WPC-2 by Mast-Arm Lengths

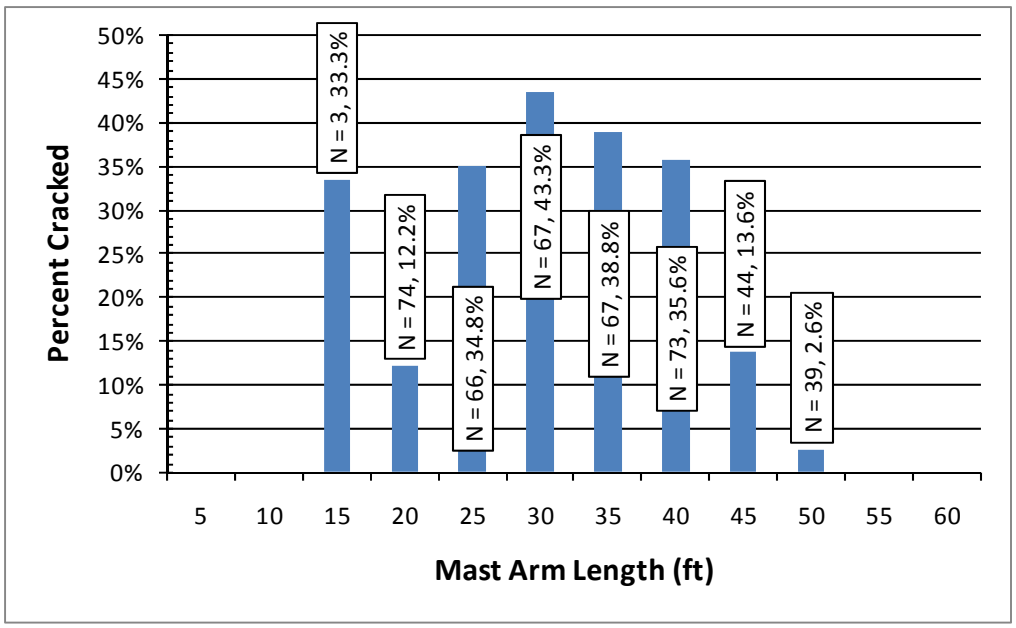

Figure 4.18 Percent of Structures Cracked in WPC- 3 by Mast-Arm Lengths

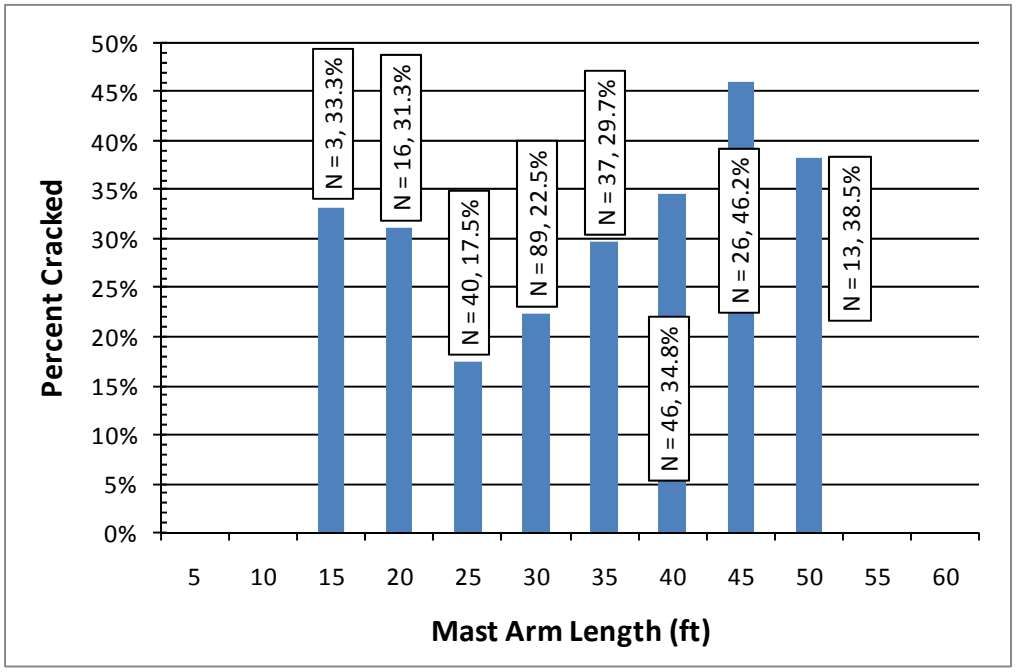

Figure 4.19 Percent of Structures Cracked in WPC-4 by Mast-Arm Lengths

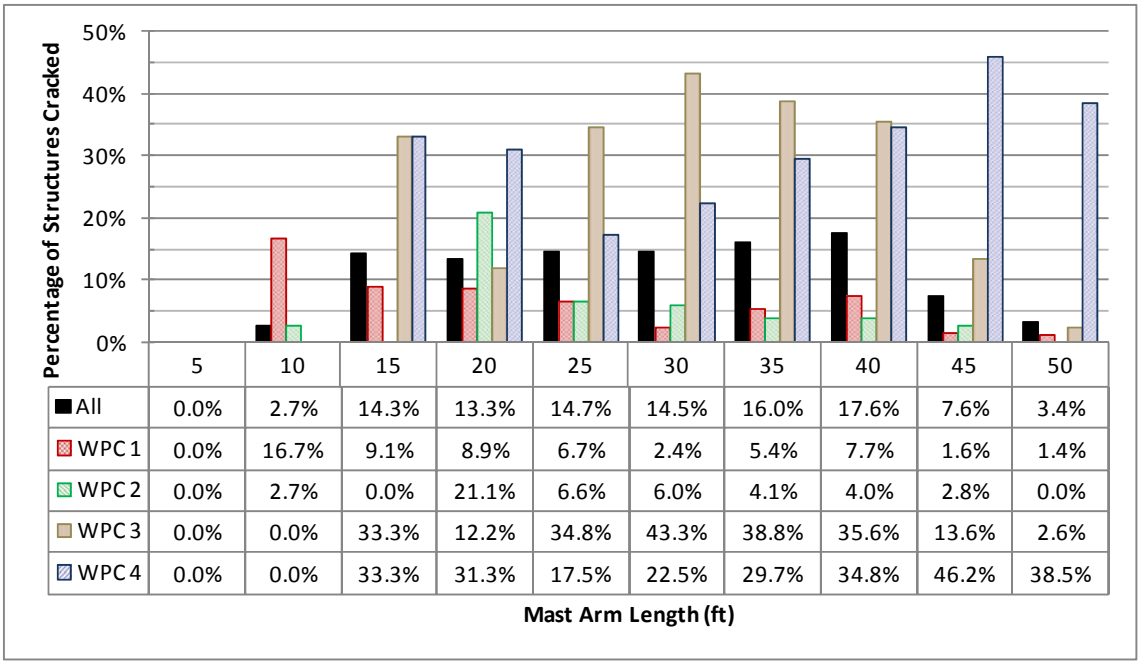

	5	10	15	20	25	30	35	40	45	50
All	0.0%	2.7%	14.3%	13.3%	14.7%	14.5%	16.0%	17.6%	7.6%	3.4%
WPC 1	0.0%	16.7%	9.1%	8.9%	6.7%	2.4%	5.4%	7.7%	1.6%	1.4%
WPC 2	0.0%	2.7%	0.0%	21.1%	6.6%	6.0%	4.1%	4.0%	2.8%	0.0%
WPC 3	0.0%	0.0%	33.3%	12.2%	34.8%	43.3%	38.8%	35.6%	13.6%	2.6%
WPC 4	0.0%	0.0%	33.3%	31.3%	17.5%	22.5%	29.7%	34.8%	46.2%	38.5%

Figure 4.20 Mast-Arm Length and Percentage of Cracked Structures

4.1.3 Age of Structure

A structure's age is associated with the potential number of load cycles experienced. Also, the older a structure is, the more likely it is to experience fatigue damage which could also potentially weaken the structure. To examine these effects, the following histograms and percentage graphs were created. Table 4.4 shows the average age of the structures along with the minimum and maximum age for both the total and cracked structures. The mean for each WPC is provided and for all classes combined (All). A minimum age of zero means the structure was erected during the same year the inspection was completed. By examining the minimum age for Cracked Structures Age, at least one structure was either cracked previous to erection or shortly after erection in WPC-3. Another noticeable observation from Table 4.4 is the average age of a cracked structure increased 2.5 years per WPC, which is the opposite of what was expected. No trend exists in the average age of the total structures in comparison to WPCs.

Table 4.4 Average and Extreme Ages

	Total Structures Age (years)				Cracked Structures Age (years)			
WPC	Mean	Minimum	Maximum	Standard Deviation	Mean	Minimum	Maximum	Standard Deviation
All	11.80	0.00	30.00	6.46	12.52	0.00	26.00	5.37
1	6.83	0.00	25.00	5.68	7.19	3.00	17.00	5.46
2	14.19	0.00	30.00	5.91	10.23	4.00	18.00	5.35
3	9.96	0.00	22.00	5.72	12.55	0.00	22.00	4.53
4	13.83	0.00	30.00	6.27	14.95	1.00	26.00	5.00

As illustrated in histograms shown in Figure 4.21 through Figure 4.25, the majority of the structures are between 10 and 22 years old. Also, approximately 110 structures are one year old or less. Unfortunately, few structures are older than 23years. The histograms also show that the distribution of poles is not even between the WPCs. WPC-1 has a large number of new poles (0-5 years old), few middle age poles (6-15 years old) and some old structures (older than 15 years).

WPC 2 has a large number of middle and old age structures, WPC-3 is mostly middle age and WPC-4 is mostly old age structures. It is interesting that the older poles are located in the highest WPC (Table 4.4 and Figure 4.21). One reason for this is urban centers are typically located in the lower wind power areas, and as towns and road expanded, structures are replaced more frequently. It also can be just a characteristic of the sample available.

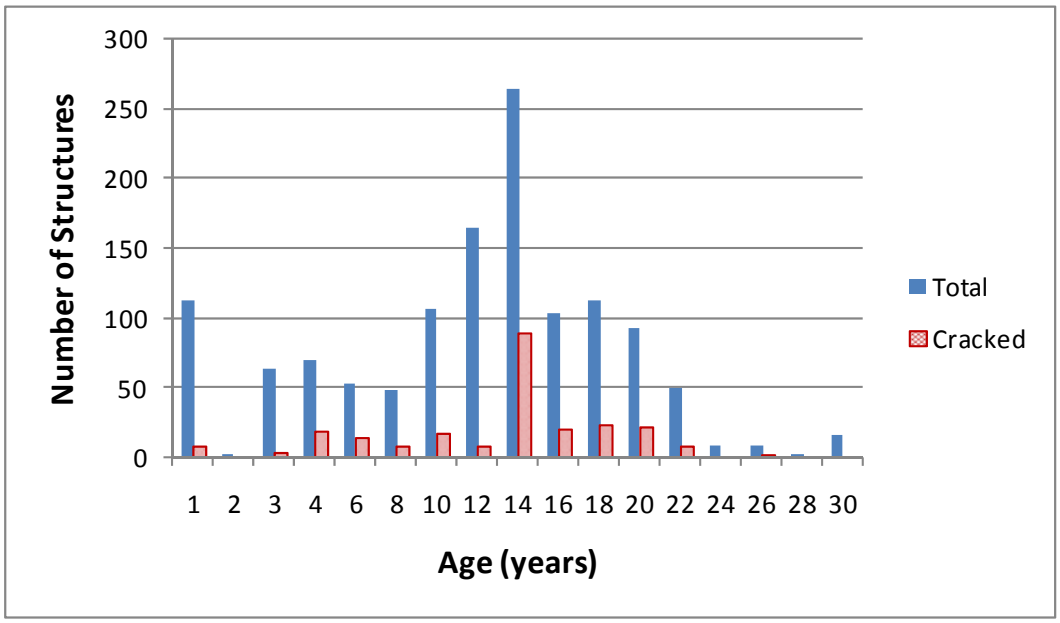

Figure 4.21 Age and Cracking Status for All WPC

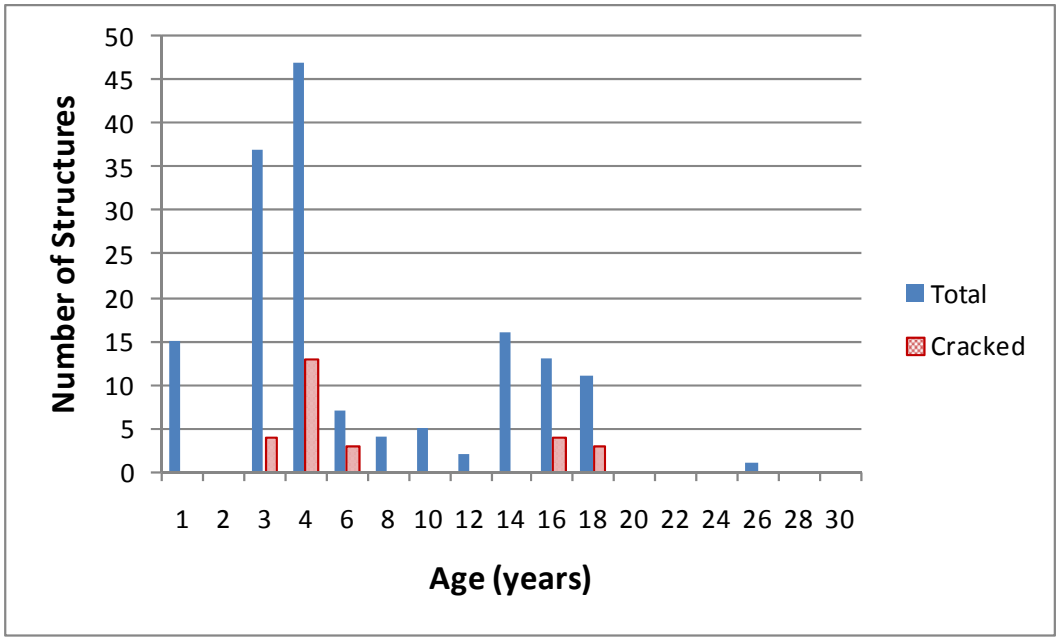

Figure 4.22 Age and Cracking Status for WPC-1

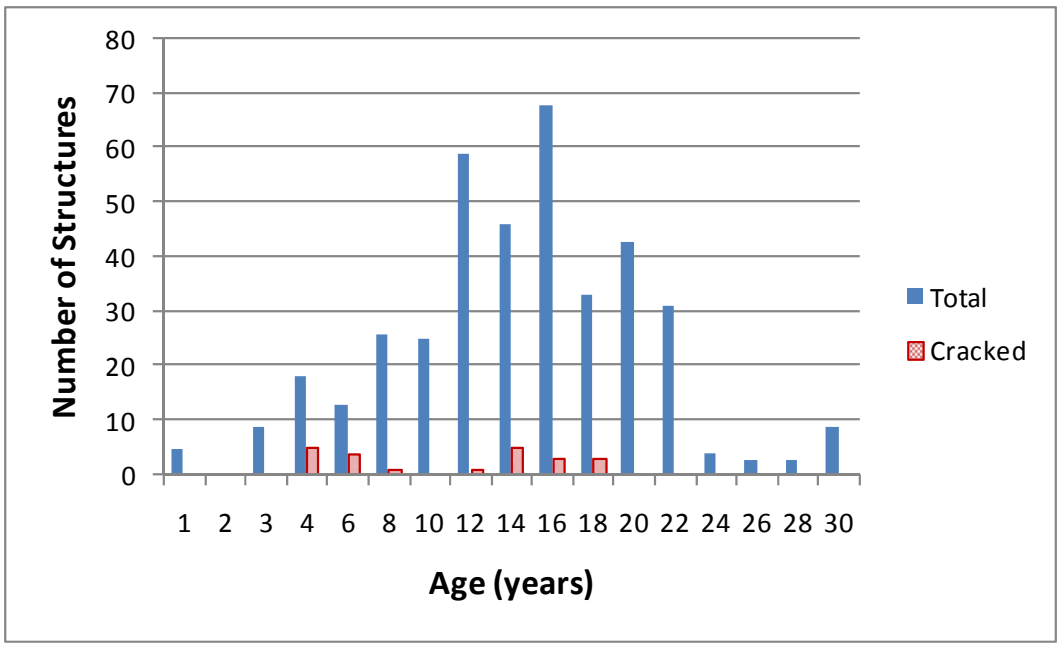

Figure 4.23 Age and Cracking Status for WPC-2

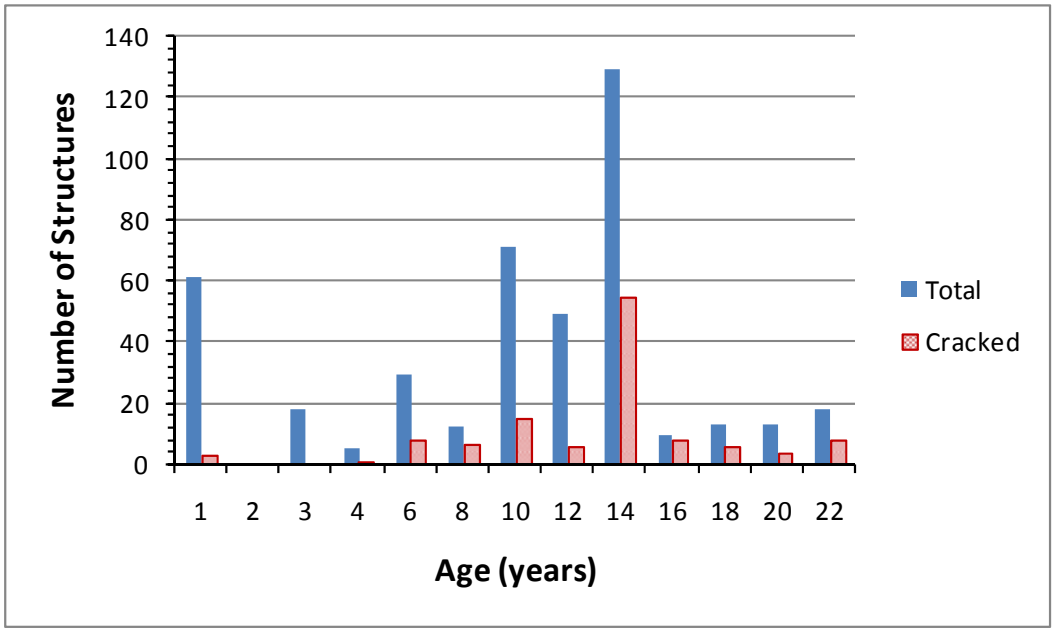

Figure 4.24 Age and Cracking Status for WPC-3

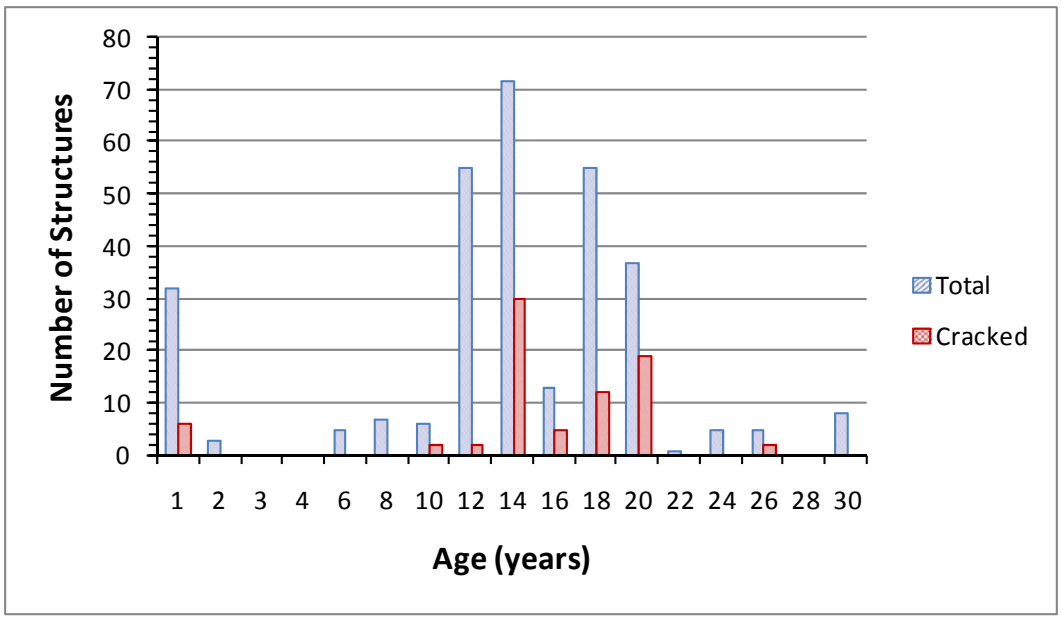

Figure 4.25 Age and Cracking Status for WPC-4

Examine the percentage of structures cracked with age. Figure 4.26 shows the crack percentage for all the WPCs combined with two peak cracking periods, one for structures between four and six years old and the second one for structures between 13 and 14 years old. A high percentage of poles cracked every year after year six (with the exception of year 12), so there no real trend of increased cracking with age.

Once the structures were split into WPCs some interesting trends were observed. Figure 4.27 is the cracking percentage for WPC-1. This graph shows that if a structure survives through year six, it is not likely to crack until year 16. Potentially, this means a structure located in WPC-1 could be inspected regularly early in its life and then inspected less frequently thereafter. The same trend is illustrated in Figure 4.28 for WPC-2 with some small amount of cracking occurring between the two peak times. For both of these WPCs, the mean annual wind speed is relatively low, which creates fewer load cycles. This means structures would have to be older before they would see enough significant load cycles to crack from fatigue. The earlier cracking could be from any material or weld flaws, which lower the fatigue life of the structure.

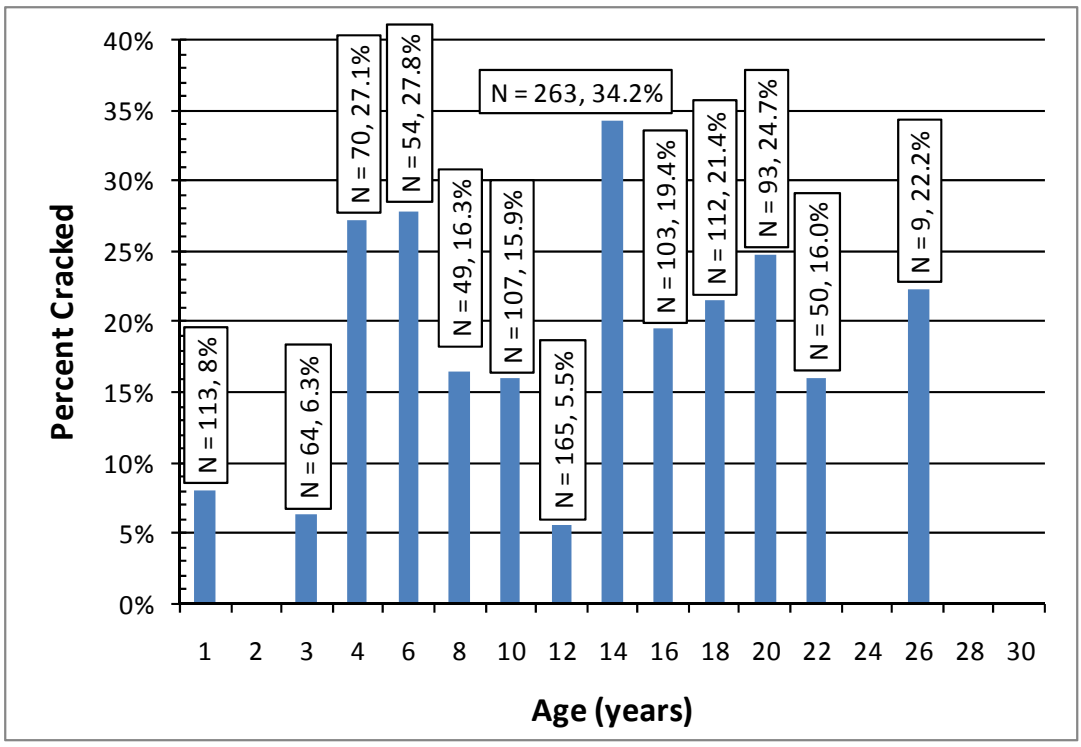

Figure 4.26 Percent of Structures Cracked in All WPCs by Age

The cracked percentage for WPC-3 shows (Figure 4.29) peak cracking to occur at eight and 16 years of age. This is a similar cracking trend as in WPC-1 and WPC-2, but with more cracking between the two high points. Figure 4.30 shows the cracked percentage per age for WPC-4. Structures one year old or less have a cracking percent of 19%, years 10 through 20 have varying cracking percentages and year 26 has a high cracking percentage. In Figure 4.31, the cracking percentages for each WPC is shown along with all classes combined. Here, the result of each is compared to the others. The age data shows that for all wind powers, fatigue cracking occurs early and then later in life. This Darwinian behavior is an important observation for fatigue cracking in low wind powers and might guide inspection strategies.

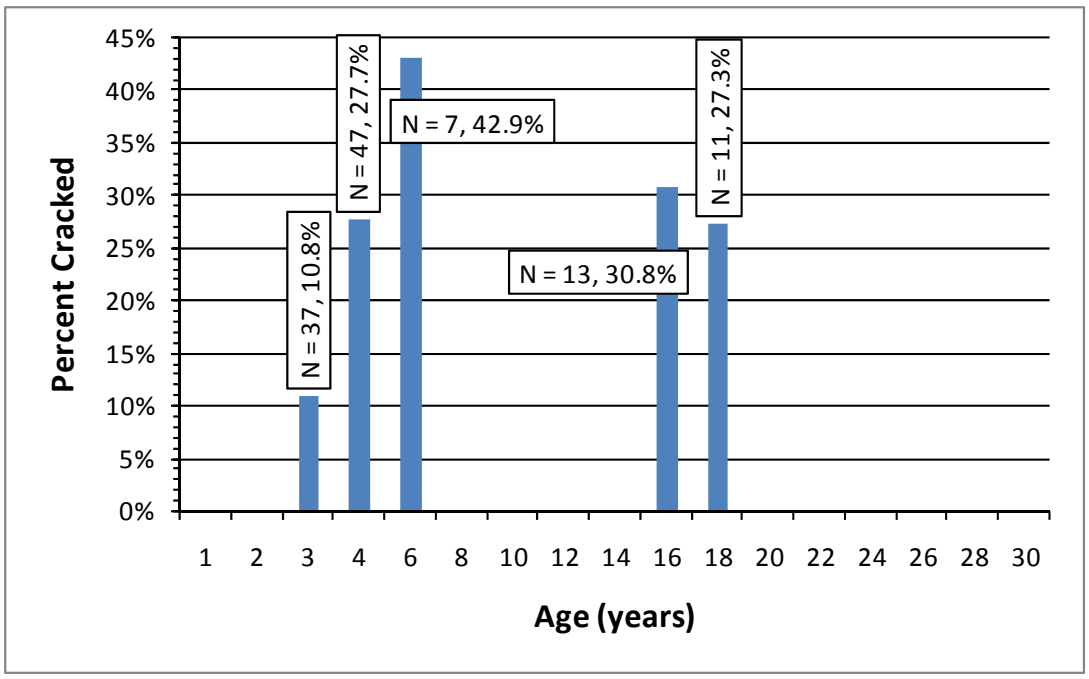

Figure 4.27 Percent of Structures Cracked in WPC-1 by Age

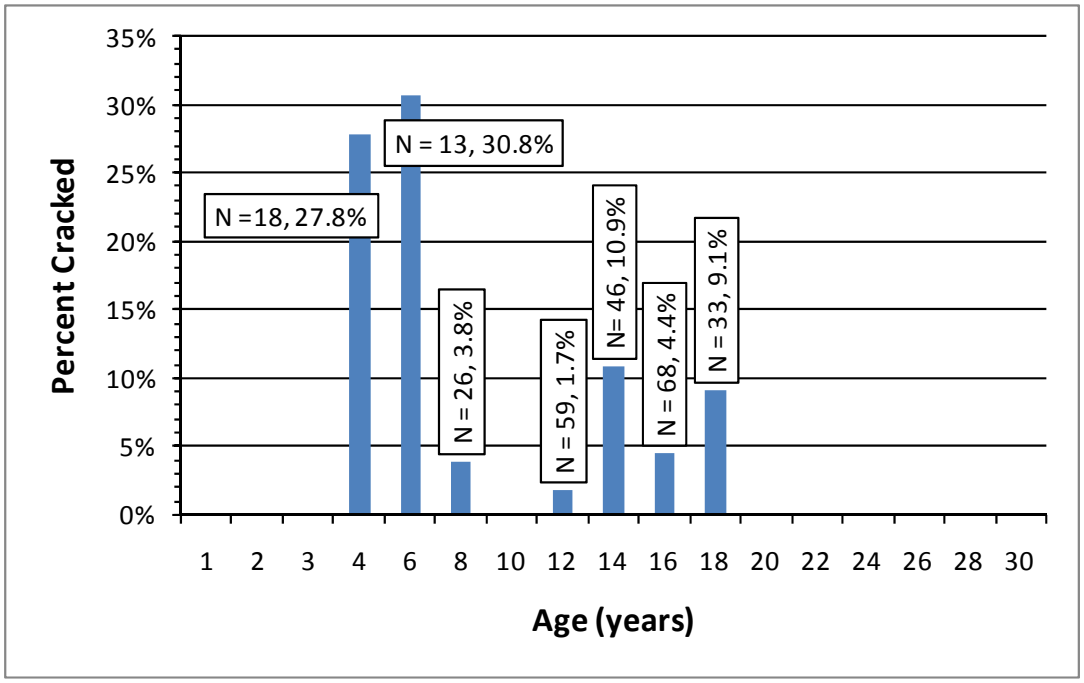

Figure 4.28 Percent of Structures Cracked in WPC-2 by Age

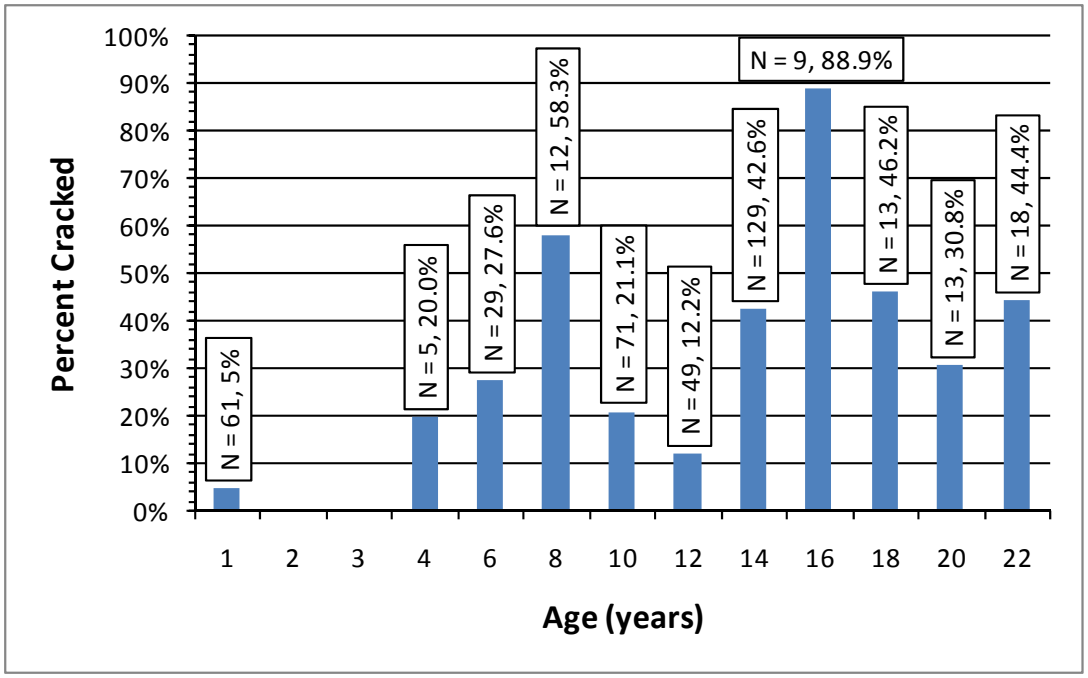

Figure 4.29 Percent of Structures Cracked in WPC-3 by Age

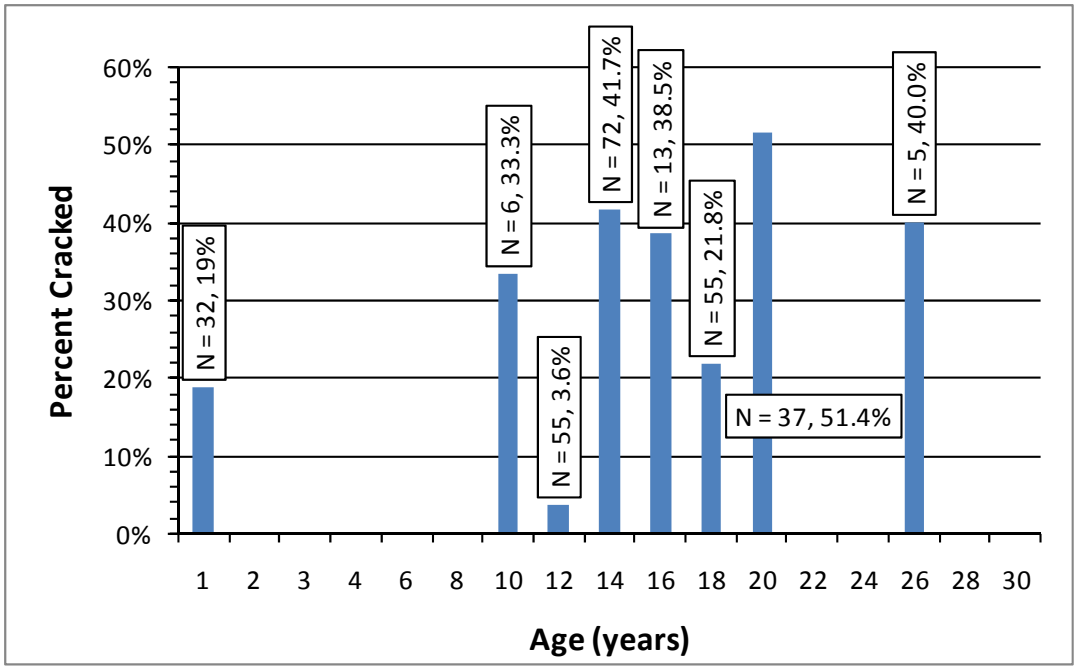

Figure 4.30 Percent of Structures Cracked in WPC-4 by Age

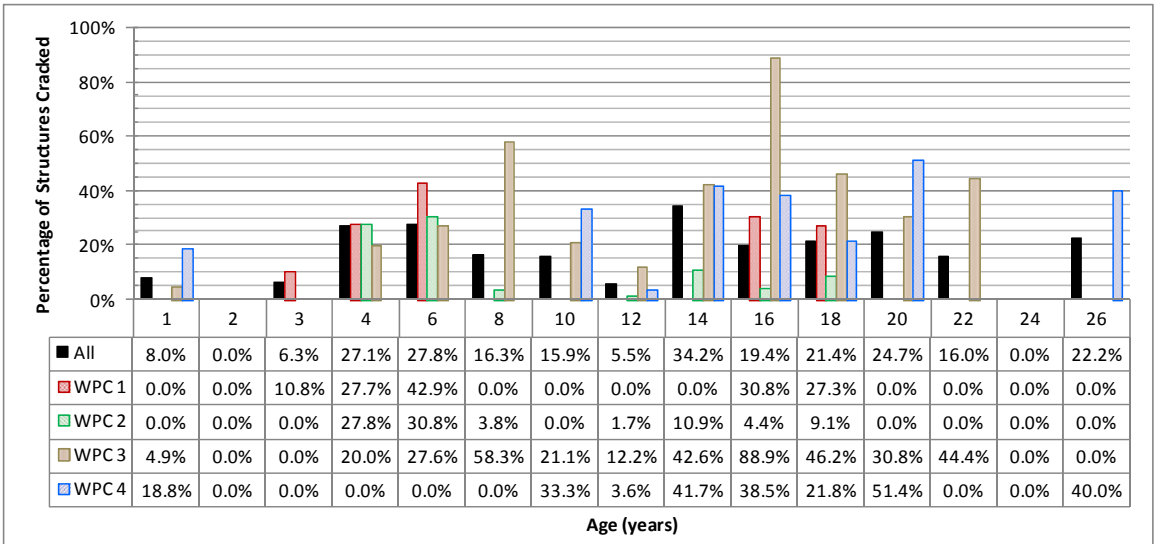

	1	2	3	4	6	8	10	12	14	16	18	20	22	24	26
All	8.0%	0.0%	6.3%	27.1%	27.8%	16.3%	15.9%	5.5%	34.2%	19.4%	21.4%	24.7%	16.0%	0.0%	22.2%
WPC 1	0.0%	0.0%	10.8%	27.7%	42.9%	0.0%	0.0%	0.0%	0.0%	30.8%	27.3%	0.0%	0.0%	0.0%	0.0%
WPC 2	0.0%	0.0%	0.0%	27.8%	30.8%	3.8%	0.0%	1.7%	10.9%	4.4%	9.1%	0.0%	0.0%	0.0%	0.0%
WPC 3	4.9%	0.0%	0.0%	20.0%	27.6%	58.3%	21.1%	12.2%	42.6%	88.9%	46.2%	30.8%	44.4%	0.0%	0.0%
WPC 4	18.8%	0.0%	0.0%	0.0%	0.0%	0.0%	33.3%	3.6%	41.7%	38.5%	21.8%	51.4%	0.0%	0.0%	40.0%

Figure 4.31 Age and Percentage of Cracked Structures

4.1.4 Manufacturer

In Wyoming only, inspection data included the manufacturer for a significant number of structures. There are only 261 structures for which the manufacturer is known (~10 %). There were four different manufacturers. For privacy reasons, no manufacturers are listed, instead each manufacturer was assigned and referred to by a number. This study is in no way a comparison of individual manufacturers, because there are many variables other than just the manufacturers that play a role in fatigue cracking.

Table 4.5 shows the results of sorting the structures by manufacturer. Manufacturer 2 has the highest cracking percentage; however it represents only three structures in the sample. Manufacturer 1 has the most number of poles and a mid-range for cracking percentage and Manufacturer 3 represents roughly half as many structures as Manufacturer 1 but 1.4 % more cracking. When looking at the structures sorted by both Manufacturer and WPC, there is an increasing trend of cracking for increasing class. The results of the sort for WPC-2 should be ignored because there are not enough structures to show meaningful results. Figure 4.32 shows the cracking percentage for each grouping in a side-by-side comparison. From this figure, it is apparent that the sample size is too small to be included in the binomial regression model. The manufacturer as a predictor is not of value at this point due to the lack of data. Also because each manufacturer makes only certain types of connections and they do not all make the same type (see Figure 4.33) comparing them side-by-side has no significant value.

Table 4.5 Mast-Arm Inspection Data Sorted by Manufacturer

Grouping	Manufacturer	Total	Cracked	Percent Cracked
All	1	163	22	13.5%
	2	3	2	66.7%
	3	74	11	14.9%
	4	21	0	0.0%
WPC-1	1	36	1	2.8%
	2	1	0	0.0%
	3	15	0	0.0%
	4	2	0	0.0%
WPC-2	1	6	0	0.0%
	2	0	0	-
	3	3	0	0.0%
	4	1	0	0.0%
WPC-3	1	95	8	8.4%
	2	0	0	-
	3	18	3	16.7%
	4	18	0	0.0%
WPC-4	1	26	13	50.0%
	2	2	2	100.0%
	3	38	8	21.1%
	4	0	0	-

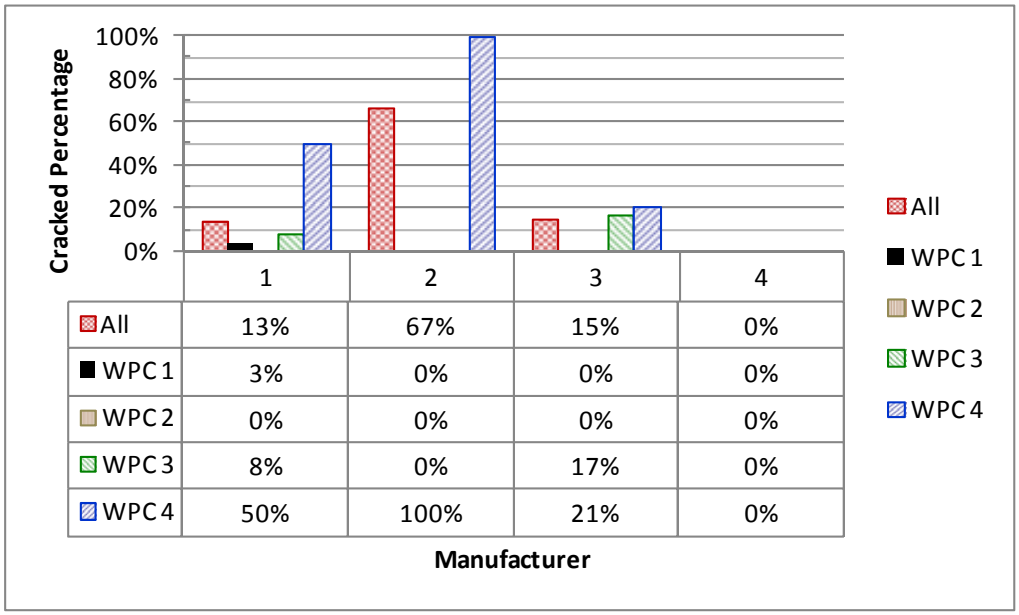

Figure 4.32 Mast-Arm Cracking Percentage By Manufacturer

4.1.5 Connection Type

The final parameter considered for inclusion in the mast-arm cracking binomial regression model was the connection type. Typical connections are illustrated in Figure 4.33. For this sorting, 246 structures had known connection types from the inspection data (see Table 4.6). The connection category has the same lack of data problems as the manufacturer category and is therefore not included in the regression analysis. There is a correlation between connection types and manufacturers, which is expected as manufacturers prefer a particular connection type for their assembled structures (Figure 4.34). Manufacturer 1 used closed connections for 71% of its structures and ring stiffened connections for the remainder. Manufacturer 3 used solely ring stiffened connections and manufacturer 4 used 72% open and 28% ring stiffened connections.

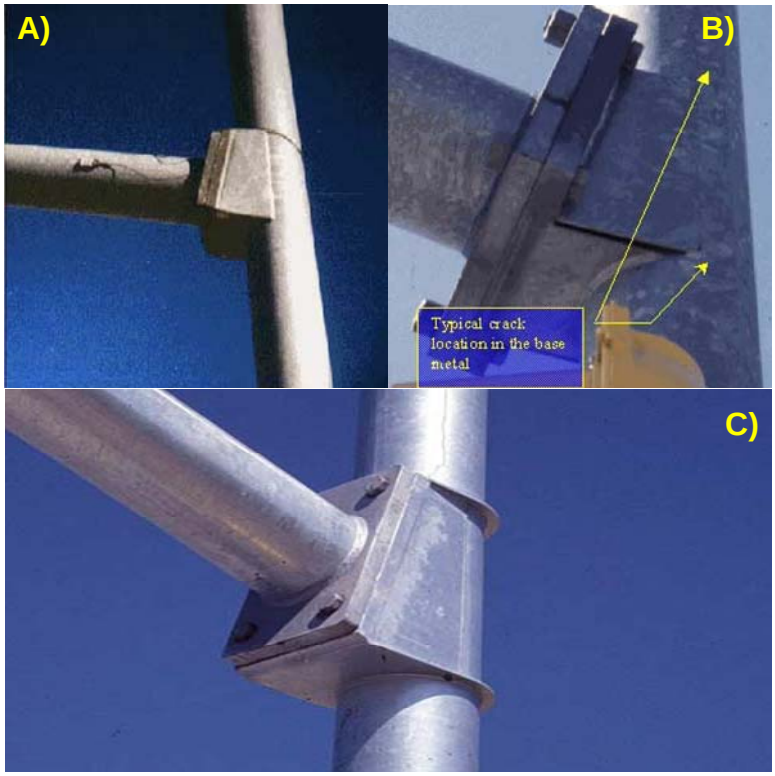

Figure 4.33 Connection Types: A) Closed, B) Open, and C) Ring Stiffened

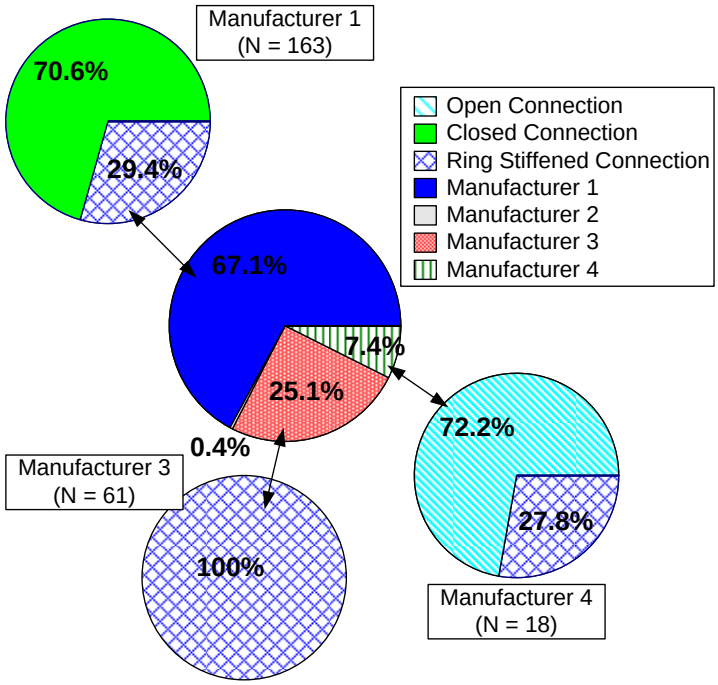

Figure 4.34 Manufacturer-Connection Relationship

WPC-2 should be ignored again because the sample size is too small to draw reasonable conclusions. However, even with a lack of data, an upward trend is observed in cracking as the WPC increases. Also, the ring stiffened connection has less cracking at each WPC when compared to the closed connection. Another interesting trend is the different increase rate between cracking percentages when comparing the ring-stiffened to the closed design. For the closed design, the cracking percentage increases quickly, going from 3.2% in WPC-1 to 50% in WPC-4. On the other hand, the ring-stiffened design increases from 0 to 17.1% over the four WPCs. Interestingly, the connection type does seem to make a difference but more data are needed to use this as a predictor. With further data, this category could be used as an additional predictor, but at present there is not enough data spread over a wide enough area to use as a predictor.

Table 4.6 Mast-Arm Inspection Data Sorted by Connection

Grouping	Connection	Total	Cracked	Percent Cracked
All	Closed	115	22	19.1%
	Open	14	0	0.0%
	Ring Stiffened	117	9	7.7%
WPC 1	Closed	31	1	3.2%
	Open	3	0	0.0%
	Ring Stiffened	16	0	0.0%
WPC 2	Closed	3	0	0.0%
	Open	1	0	0.0%
	Ring Stiffened	5	0	0.0%
WPC 3	Closed	55	8	14.5%
	Open	10	0	0.0%
	Ring Stiffened	61	3	4.9%
WPC 4	Closed	26	13	50.0%
	Open	0	0	-
	Ring Stiffened	35	6	17.1%

4.2 Mast-Arm Binomial Regression

A binomial regression analysis was completed for the sorted inspection data. Several analyses were completed to determine the combination of predictors that yields the best model to predict cracking percentage for traffic signal structures. Each analysis included the mean wind speed at 50m as a predictor, and then various other predictors were included. To obtain an initial trial for which combination of predictors to use, the Best Subset Regression function inside of Minitab was used. Table 4.7 shows the results. Based on this table, the following analyses were completed: Cracking vs. Wind (*W*), Cracking vs. Wind and Length (*W, L*), Cracking vs. Wind, Length, and Age (*W, L, A*), Cracking vs. Wind, Length, and Orientation (*W, L, O*), and Cracking versus Wind, Length, Age, and Orientation (*W, L, A, O*).

Table 4.7 Best Subsets Regression Results

Vars	R-Sq	R-Sq(adj)	Mallows C_p	S	Ave Wind Speed	Length	Age	Orientation
1	1.9	1.8	8.8	0.39	x	-	-	-
1	0.6	0.5	26.2	0.39	-	x	-	-
2	2.5	2.3	3.1	0.39	x	x	-	-
2	1.9	1.8	10.3	0.39	x	-	x	-
3	2.6	2.4	3.2	0.39	x	x	x	-
3	2.5	2.3	4.8	0.39	x	x	-	x
4	2.6	2.3	5	0.39	x	x	x	x

A complete record of binominal regression results from Minitab for each analysis is provided in Appendix A. A sample summary of results from the binary regression is Figure 4.35. The important aspects are highlighted. The *P* value is use to determine if the null hypothesis is an appropriate assumption. A low *P* value means that null hypothesis is not true. For Figure 4.35, the *P* values are high, which led to rejecting this combination of predictors. Any combination predictors including more than average wind speed alone showed similar trends for *P* values, so these models were also rejected. However, when the combinations are run using combinations of WxL, WxLxO, etc. the interaction *P* value is zero. (x implies multiplication here).

This means that a relationship exists between wind and length, or any of the terms related to each other. As *individual* overall predictors, length, orientation, and age are not significant, however when these values are multiplied by wind and/or each other, they become significant. This leads to complex models and the need for much more data. Because the data are limited at this time, this study uses wind as the sole predictor.

3 Var

Binary Logistic Regression: Cracked versus Ave Wind Speed, Length, Orientation

Logistic Regression Table

Predictor	Coef	SE Coef	Z	P	Odds Ratio	95% CI Lower	95% CI Upper
Constant	-7.24166	0.552725	-13.1	0			
Ave Wind Speed	0.378699	0.031853	11.89	0	1.46	1.37	1.55
Length	0.0028834	0.0057984	0.5	0.619	1	0.99	1.01
Orientation	0.232294	0.0600478	0.39	0.699	1.02	0.91	1.15

Log-Likelihood = -729.303

Test That all slopes are zero: G = 207.107 DF = 3 P-Value = 0

Goodness-of-Fit Tests

Method	Chi-Square	DF	P
Pearson	807.394	690	0.001
Deviance	504.717	690	1
Hosmer-Lemeshow	67.554	8	0

Figure 4.35 Binary Regression Results for Cracking vs. Wind, Length, and Orientation

A graphical representation of the regression results is shown in Figure 4.36. The grouped data points are also included (refer to Appendix B for grouping process and rationale). When the regressions are compared to the actual data, the *W, L, A, O* regression can be rejected immediately because it is obviously not a good fit. Likewise the regression of *W, L, A* can be excluded, and when looking at the age data individually (Figure 4.26), there is no apparent trend. The regression combinations of *W*; *W, L*; and *W, L, O* are similar. For the *P*-value reasons *W, L* and *W, L, O* are rejected, but ignoring that still provides a reasonable fit to the data. Here, the regression with only average wind speed (W) is used. Figure 4.37 shows the binary regression results using mean wind speed at 50m as the predictor. The red dotted lines are 95% confidence intervals based on the regression and sample size. The dashed blue line extrapolates the regression line for regions where no known data exists. The shaded areas reflect the zones for the WPCs. The limits to the probability of cracking for each class as provided in Table 4.8.

This model does not show the whole story, because length, age, and orientation do play a role in cracking. However, without more data modeling, the interaction of all the variables is premature and may lead to inaccurate models. The model presented in Figure 4.37 is an accurate model using solely the mean wind speed as the predictor. This model shows a trend of increasing cracking probability with increasing wind velocity. Also shown is for low wind velocities (WPC-1) there is smaller chance of cracking (8.3%) and for structures in WPC 4 the cracking percentage is 30.8%. This is an important finding and coincides with reported fatigue cracking in various states with low and high wind velocities. Note that the presence of a crack does not necessarily imply structural collapse.

Table 4.8 Wind Power Cracking Probability

	Lower Bound (mph)	Upper Bound (mph)	Δ Speed (mph)	Lower Bound	Upper Bound	Δ (%)	Δ% / Δ mph
WPC 1	0	12.5	12.5	0.1%	8.3%	8.3%	0.7%
WPC 2	12.5	14.5	2	8.3%	16.0%	7.7%	3.8%
WPC 3	14.5	15.7	1.2	16.0%	22.9%	6.9%	5.7%
WPC 4	15.7	16.8	1.1	22.9%	30.8%	7.9%	7.2%
WPC 5	16.8	17.9	1.1	30.8%	40.0%	9.2%	8.4%
WPC 6	17.9	19.7	1.8	40.0%	56.5%	16.4%	9.1%
WPC 7	19.7	LARGE	LARGE	56.5%	-	-	-

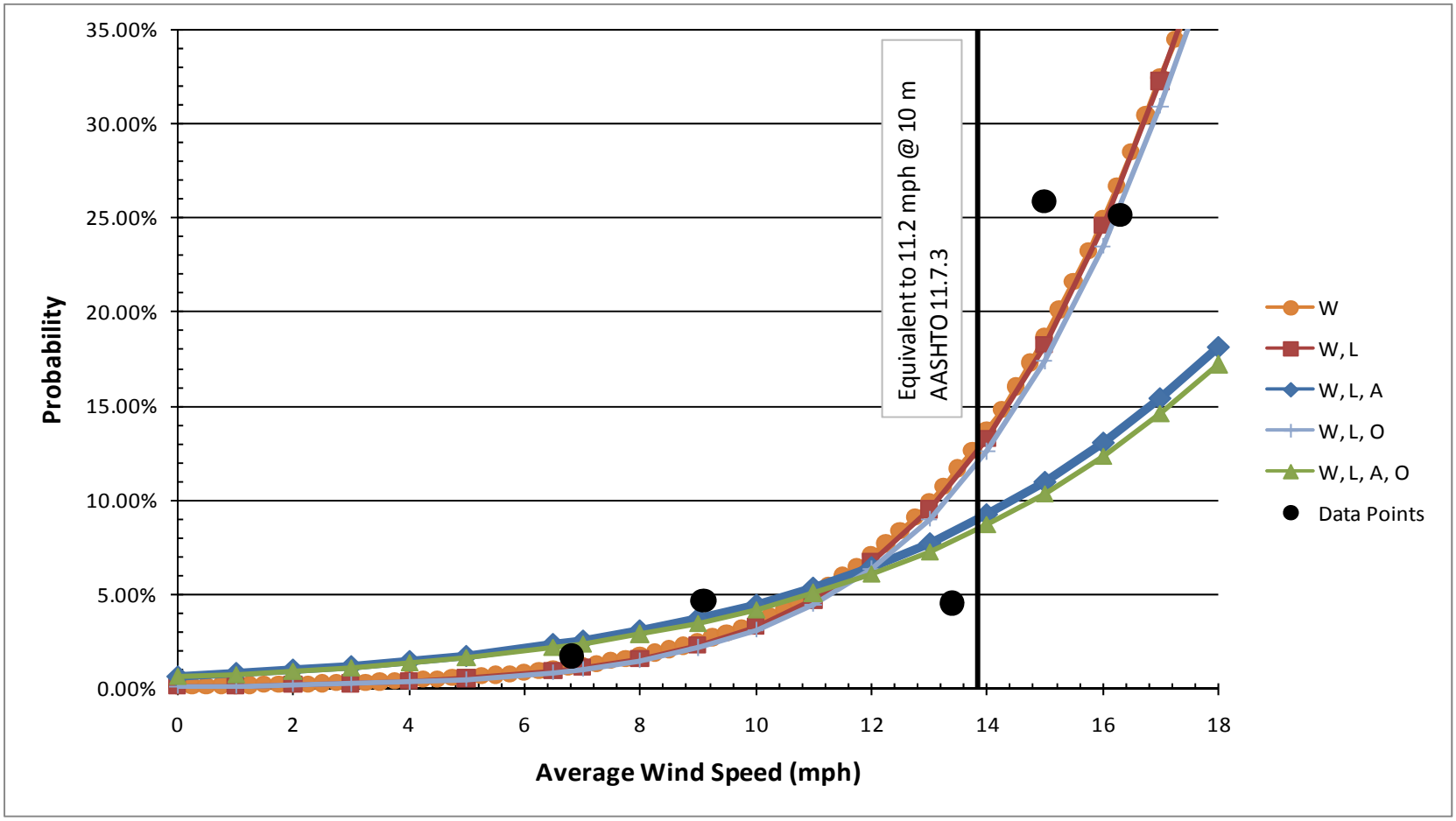

Figure 4.36 Mast-Arm Cracking vs. Mean Wind Speed at 50m

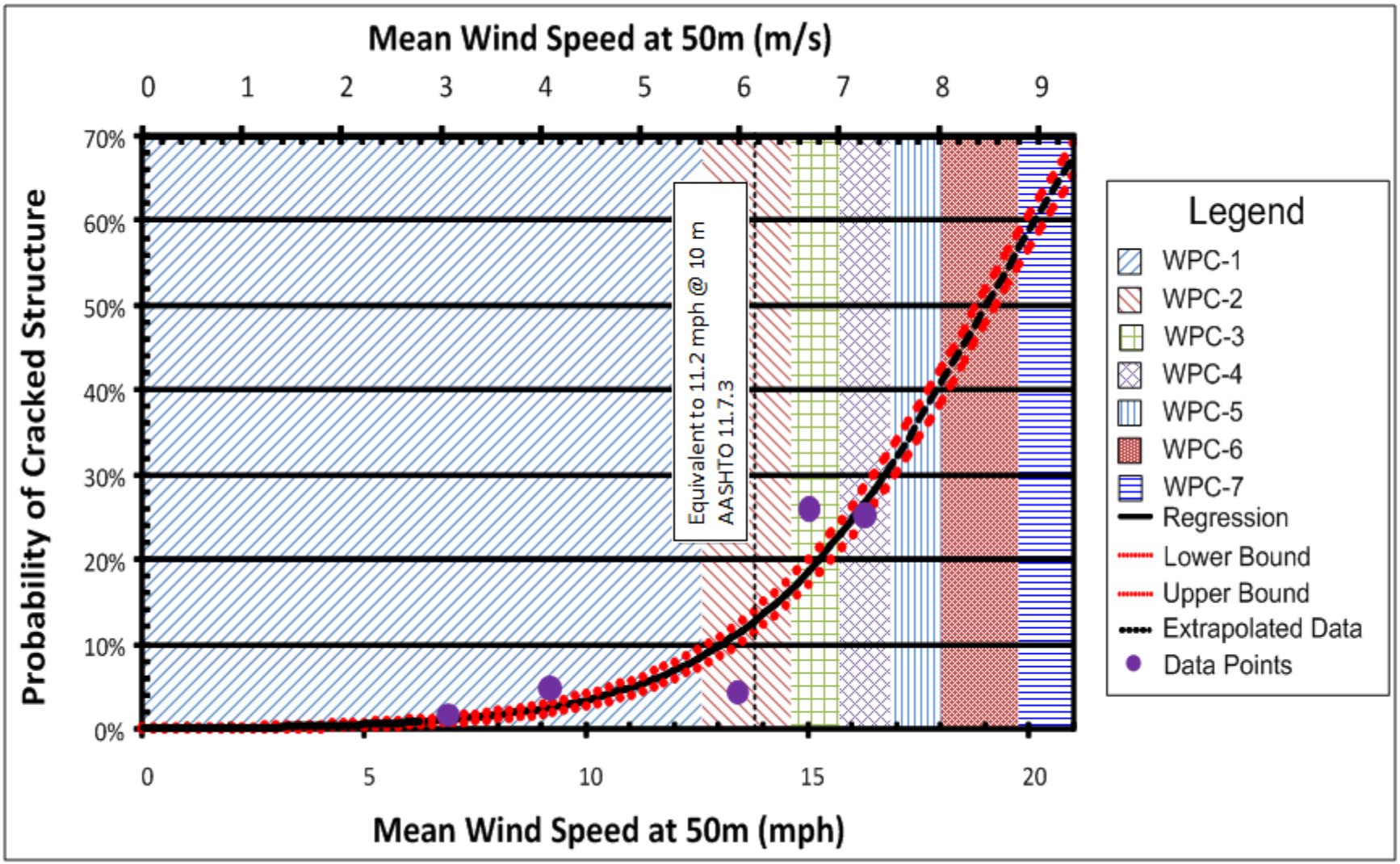

Figure 4.37 Mast-Arm Cracking Probability

4.3 High-Mast Luminaire Predictors

The structures were divided into two groups, mast arms and high-mast luminaires. This section pertains only to the high-mast luminaires structures. The average wind speed, structure shape, base diameter, and base plate thickness were available using inspection data for approximately 700 structures. The following tables and figures show the characteristics of these data.

4.3.1 Structure Shape

High-mast luminaire structures typically consist of a single tube with light fixtures on top (Figure 4.38). The tube is typically formed by welding lengths of bent steel plates together. These lengths are then spliced together to form a 50-foot to 200-foot structure. The tubing is bent in several different shapes, and these shapes could potentially have different wind shedding properties. For the inspection data considered, the tubing shapes were square, hexagonal and octagonal. Table 4.9 shows the data for each shape. Approximately 60% of the tubes are hexagonal; 39% are square, and less than 1% are octagonal.

Table 4.9 High-Mast Luminaire Tube Shape Cracking Status

Shape	Total	Cracked	Cracked Percentage
Hexagonal	415	52	12.5%
Octagonal	2	0	0.0%
Square	268	29	10.8%
Not Known	14	2	14.3%
Total	**699**	**83**	**11.9%**

Figure 4.38 Typical High-Mast Luminaire Structure
(Road Traffic Technology Lighting Solutions Image Gallery n.d.)

4.3.2 Base Plate Thickness

Base plates attach the tubing to the structure's foundation (Figure 4.39). The thickness of the base plate helps to resist the movement generated by the wind acting on lighting system on the top of the high-mast pole. Base plate thickness and cracking percentage are presented in Table 4.10. There is an increase in cracking events with an increase in base plate thickness. This trend is unexpected because the thicker the material is, the less plate distortion is expected. However, a potential cause could be lack of weld penetration because it is more difficult to weld thick plates to thin tubes (Chen, et al. 2003).

Table 4.10 High-Mast Luminaire Base Plate Thickness Cracking Status

Base Plate Thickness	Total	Cracked	Cracked Percentage
1.175	1	0	0.0%
1.25	62	0	0.0%
1.5	336	39	11.6%
1.75	76	10	13.2%
2	178	30	16.9%
2.25	3	0	0.0%
2.5	2	0	0.0%
Not Known	41	4	9.8%
Total	**699**	**83**	**11.9%**

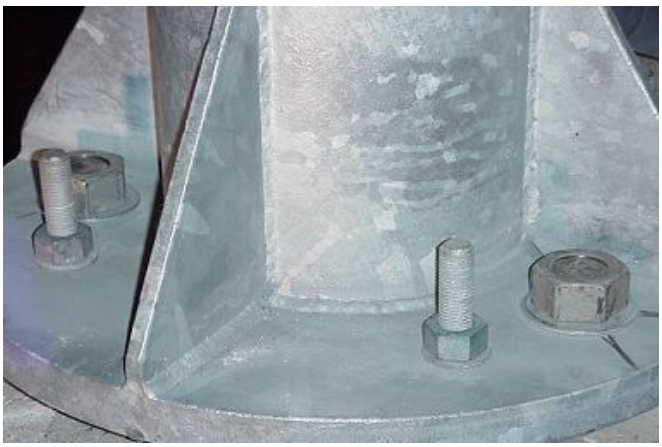

Figure 4.39 Typical Base Plate
(U.S. Department of Transportation Federal Highway Administration n.d.)

4.3.3 Base Diameter

The pole base diameter is the diameter referenced just above the connection see Figure 4.39. For this study, the presence of gussets or stiffeners was not known. Overall, there is no trend of cracking with pole base diameter Figure 4.40. Sample size is a problem for seeing any relevant trends for the overall data. However, if the samples were sorted into bins, there is a trend of increased cracking with increased diameter. Figure 4.40 through Figure 4.44 show the different cracking percentages divided by wind power class. Again sample size is a problem, but for WPC 4 there is a trend of increased cracking with increase in pole diameter.

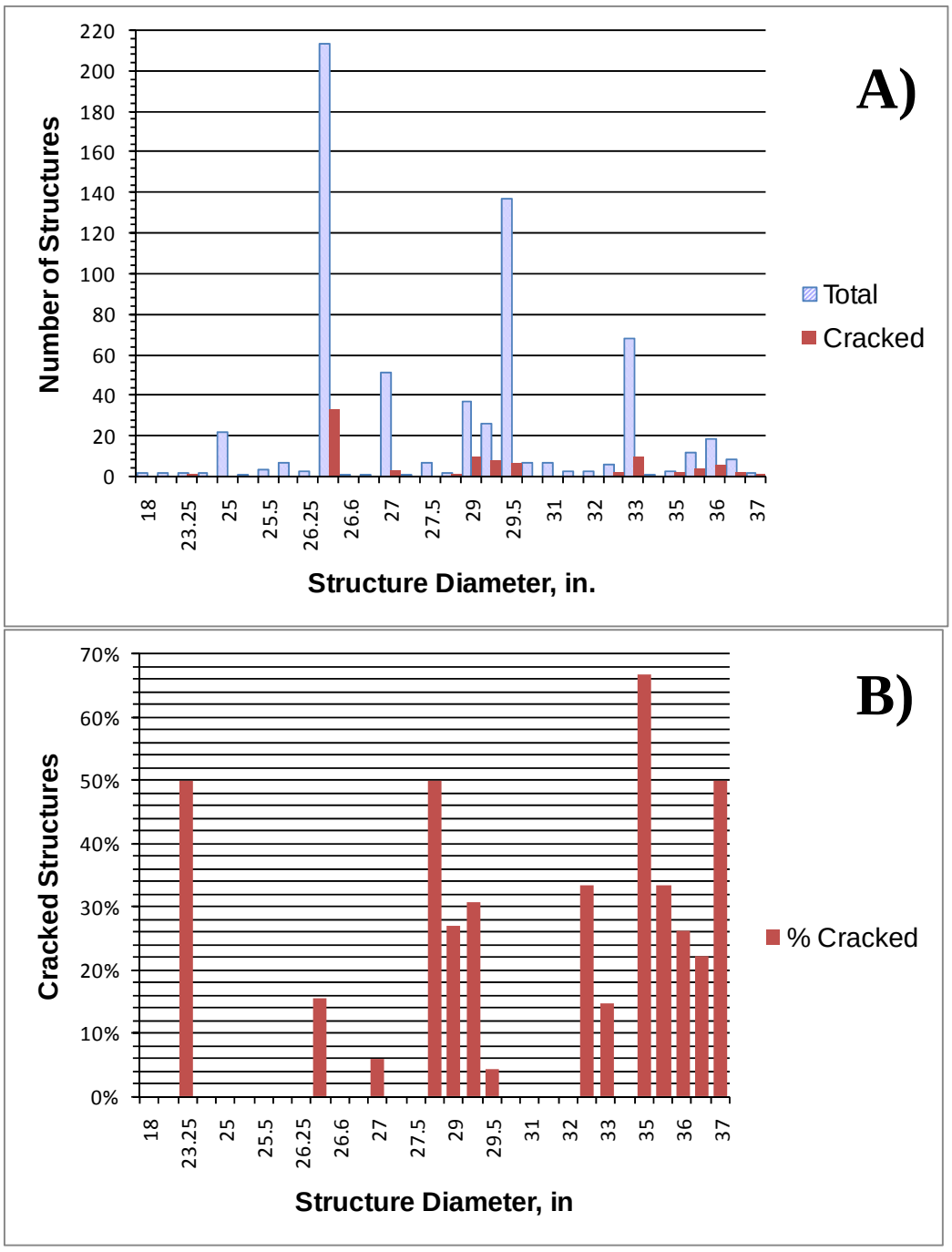

Figure 4.40 All WPCs Base Diameter A) Cracking Status and B) Percent Cracked

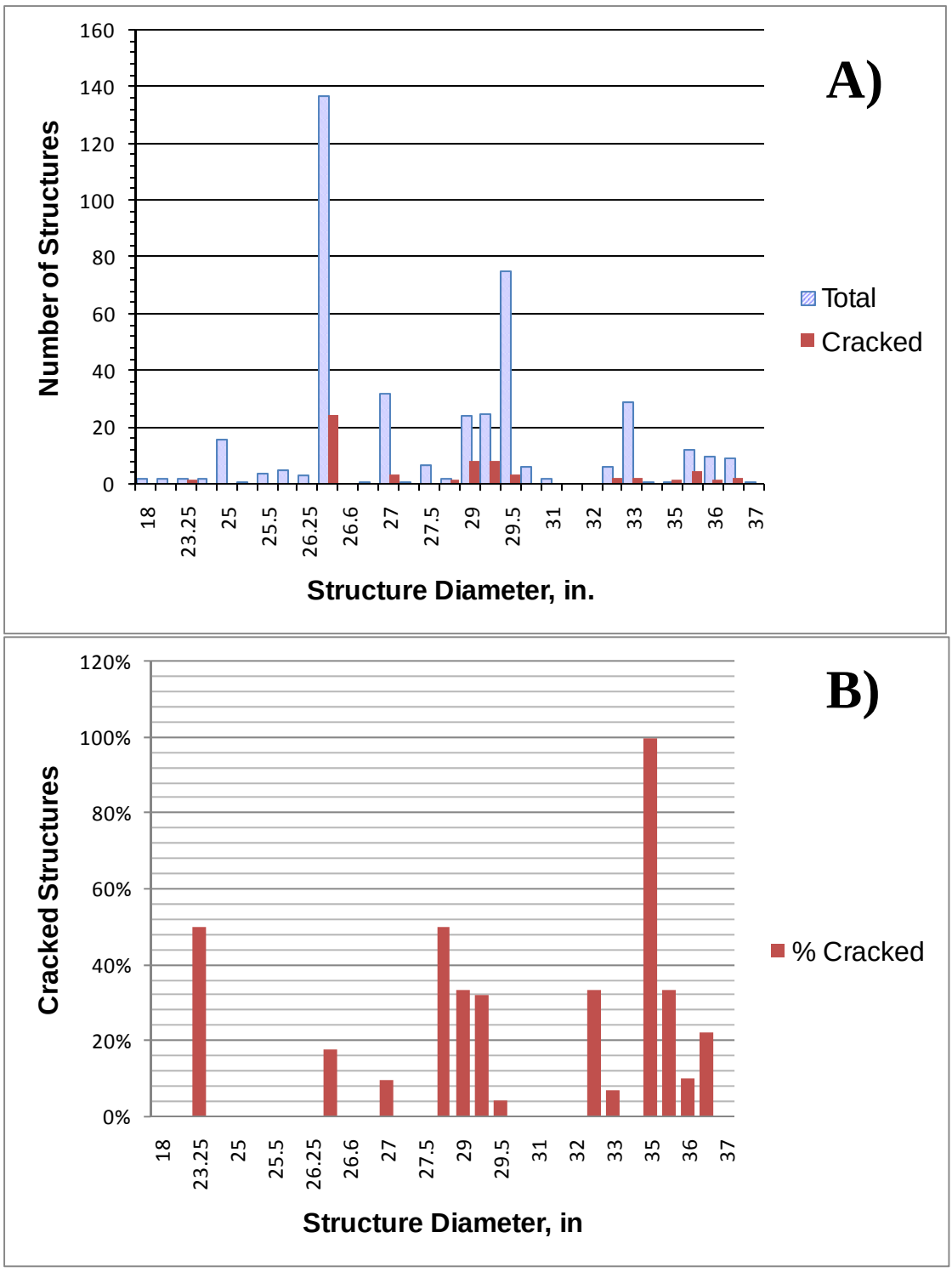

Figure 4.41 WPC-2 Base Diameter A) Cracking Status and B) Percent Cracked

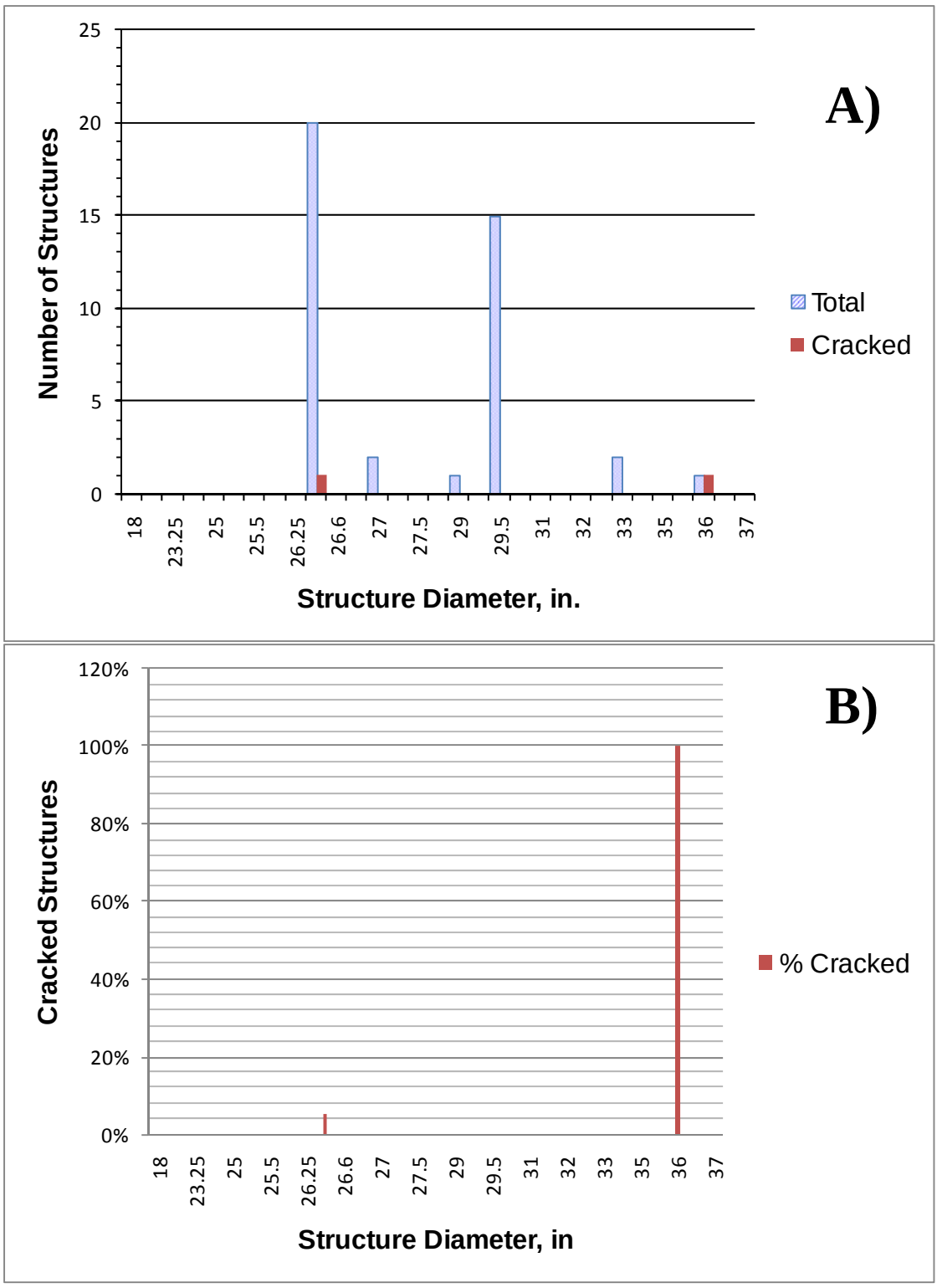

Figure 4.42 WPC-3 Base Diameter A) Cracking Status and B) Percent Cracked

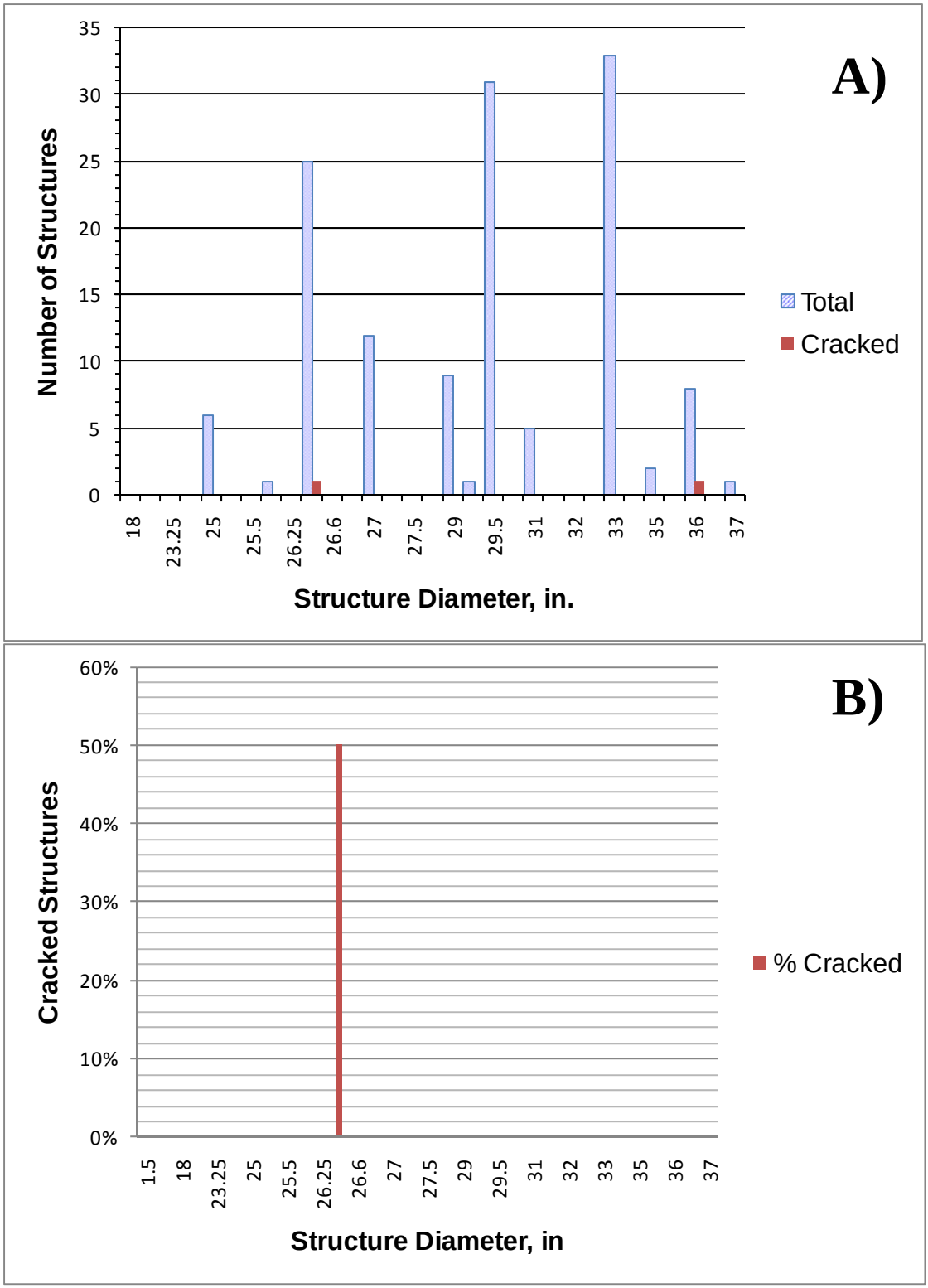

Figure 4.43 WPC-4 Base Diameter A) Cracking Status and B) Percent Cracked

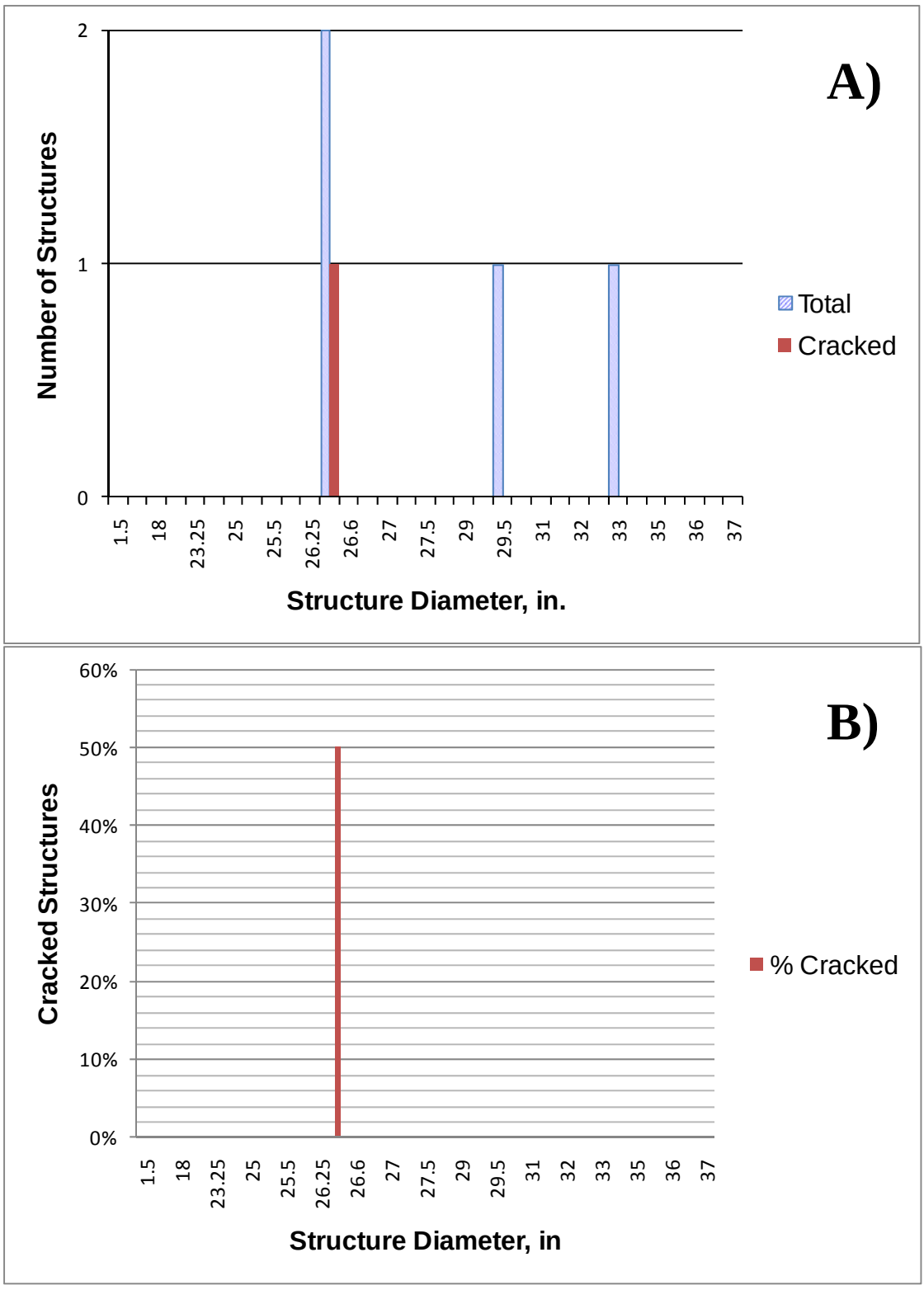

Figure 4.44 WPC-5 Base Diameter A) Cracking Status and B) Percent Cracked

4.3.4 Base Plate Thickness versus Base Diameter

Next, a relationship between base pole diameter and base plate thickness was investigated. Figure 4.45 shows the relationship between these two attributes. The purpose of this comparison was to find if an increase or decrease in diameter divided by thickness (D/t) would yield an increase or decrease in cracking. The data were divided into D/t values of 0-12, 12-14, 14-16, 16-18, 18-20, and 20+. The area with largest cracking percentage was 12-14. However, directly following that was an area of zero cracking. The reported ratios on the figure are cracked structures to total structures. This figure also shows that as the diameter of the pole increases, the cracking increases. However, this may not be a great correlation given the number of bin sizes. The overall data shown in Figure 4.45 shows no conclusive relationship between cracking percentages and D/t ratios. Like the other predictors, more data are needed before this can be used or ruled out as a predictor. Also, a study should be conducted to relate plate thickness and pole diameter to other structure properties because stress magnitudes vary with arm lengths, structure heights and other properties.

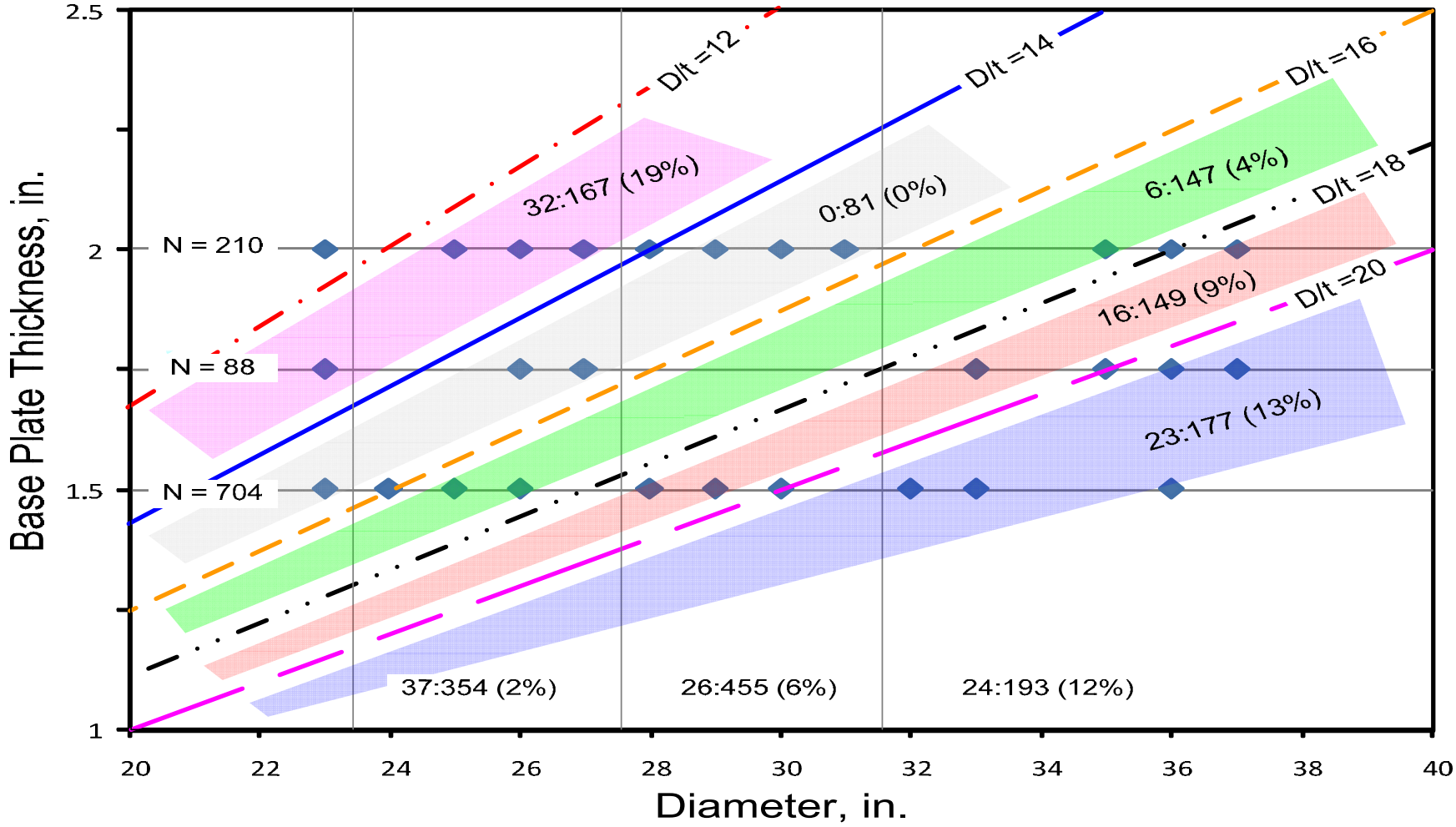

Figure 4.45 Cracking for Base Plate Thickness versus Base Diameter

4.3.5 Average Wind Speed

The average wind speed for each high-mast luminaire structure was found using the method described earlier. Table 4.11 shows the results of the primary sorting by wind power class. Table 4.8 shows the average wind speeds for each WPC. While there are almost 700 structures, they are only located in WPC 2, 3 and 4. This limitation does not lead to conclusive trends.

Table 4.11 High-Mast Luminaire WPC VS. Cracking Status

WPC	Total	Cracked	Cracked Percentage
WPC 1	0	0	-
WPC 2	440	58	13.2%
WPC 3	51	2	3.9%
WPC 4	139	23	16.5%
WPC 5	3	0	0.0%
Not Known	66	0	0.0%
Total	**699**	**83**	**11.9%**

4.3.6 High-Mast Luminaire Binomial Regression

A binomial regression analysis was completed for the sorted inspection data. Several analyses were completed to see what combination of predictors would yield the best model to predict cracking. Each analysis included the mean wind speed at 50m as a predictor, and then various other predictors were included. The results of each model are provided in Figure 4.46 through Figure 4.49. Following analysis were completed: Cracking vs. Wind (*W*); Cracking vs. Wind and Base Plate Thickness (*W, T*); Cracking vs. Wind, Base Plate Thickness, and Tube Shape (*W, T, S*); and Cracking vs. Wind and Tube Shape (*W, S*).

For these models, the recorded *P* value is used to determine if the null hypothesis is an appropriate assumption. The lower this value is, the smaller the probability that rejecting the null hypothesis is a mistake. Any combination of the predictors showed *P* values greater than zero, so all these models were rejected. Figure 4.50 displays the graphical results of each combination; however, because the models are not valid, neither is this figure. The current data has no wind power class one samples, which excludes a 12 mph range. With more data in various wind power classes it may be possible to make a predictive model. However, a model based on wind power class may not be appropriate for high-mast luminaires. In Appendix D, a predictive model based on vortex shedding is briefly presented.

1 Var

Binary Logistic Regression: Cracked versus Ave Wind Speed

Logistic Regression Table						95% CI	
Predictor	Coef	SE Coef	Z	P	Odds Ratio	Lower	Upper
Constant	-2.50032	1.3417	-1.86	0.062			
Ave Wind Speed	0.0428779	0.0939028	0.46	0.648	1.04	0.87	1.25

Log-Likelihood = -245.826

Test That all slopes are zero: G = 0.206 DF = 1 P-Value = 0.65

Goodness-of-Fit Tests

Method	Chi-Square	DF	P
Pearson	5.25866	2	0.072
Deviance	7.00963	2	0.03
Hosmer-Lemeshow	0.71209	1	0.399

Figure 4.46 High-Mast Luminaire Binary Regression Results for Average Wind Speed Only

2 Var

Binary Logistic Regression: Cracked versus Ave Wind Speed, Base Plate Thickness

Logistic Regression Table						95% CI	
Predictor	Coef	SE Coef	Z	P	Odds Ratio	Lower	Upper
Constant	-2.73665	1.41981	-1.93	0.054			
Ave Wind Speed	0.0416573	0.095926	0.43	0.664	1.04	0.86	1.26
Base Plate Thickness	0.156561	0.185539	1.84	0.399	1.17	0.81	1.68

Log-Likelihood = -232.911

Test That all slopes are zero: G = 0.78 DF = 2 P-Value = 0.677

Goodness-of-Fit Tests

Method	Chi-Square	DF	P
Pearson	20.369	14	0.119
Deviance	30.4433	14	0.007
Hosmer-Lemeshow	8.0237	4	0.091

Figure 4.47 High-Mast Luminaire Binary Regression Results for Average Wind Speed Only and Base Plate Thickness

3 Var

Binary Logistic Regression: Cracked versus Ave Wind Speed, Base Plate Thickness, Tube Shape

Logistic Regression Table						95% CI	
Predictor	Coef	SE Coef	Z	P	Odds Ratio	Lower	Upper
Constant	-2.610138	1.4129	-1.77	0.077			
Ave Wind Speed	0.0363553	0.0971319	0.37	0.708	1.04	0.86	1.25
Base Plate Thickness	0.166168	0.186289	0.89	0.372	1.18	0.82	1.7
Tube Shape	-0.0434708	0.128697	-0.34	0.736	0.96	0.74	1.23

Log-Likelihood = -232.853

Test That all slopes are zero: G = 0.895 DF = 3 P-Value = 0.827

Goodness-of-Fit Tests

Method	Chi-Square	DF	P
Pearson	47.6455	24	0.003
Deviance	64.138	24	0
Hosmer-Lemeshow	20.0029	5	0.001

Figure 4.48 High-Mast Luminaire Binary Regression Results Average Wind Speed Only, Base Plate Thickness and Tube Shape

2 Var

Binary Logistic Regression: Cracked versus Ave Wind Speed, Tube Shape

Logistic Regression Table						95% CI	
Predictor	Coef	SE Coef	Z	P	Odds Ratio	Lower	Upper
Constant	-2.41932	1.41679	-1.71	0.088			
Ave Wind Speed	0.0410507	0.0955532	0.43	0.667	1.04	0.86	1.26
Tube Shape	-0.033029	0.126057	-0.26	0.793	0.97	0.76	1.24

Log-Likelihood = -240.031

Test That all slopes are zero: G = 0.295 DF = 2 P-Value = 0.863

Goodness-of-Fit Tests

Method	Chi-Square	DF	P
Pearson	6.8181	6	0.338
Deviance	10.8002	6	0.095
Hosmer-Lemeshow	1.3914	2	0.499

Figure 4.49 High-Mast Luminaire Binary Regression Results Average Wind Speed Only and Tube Shape

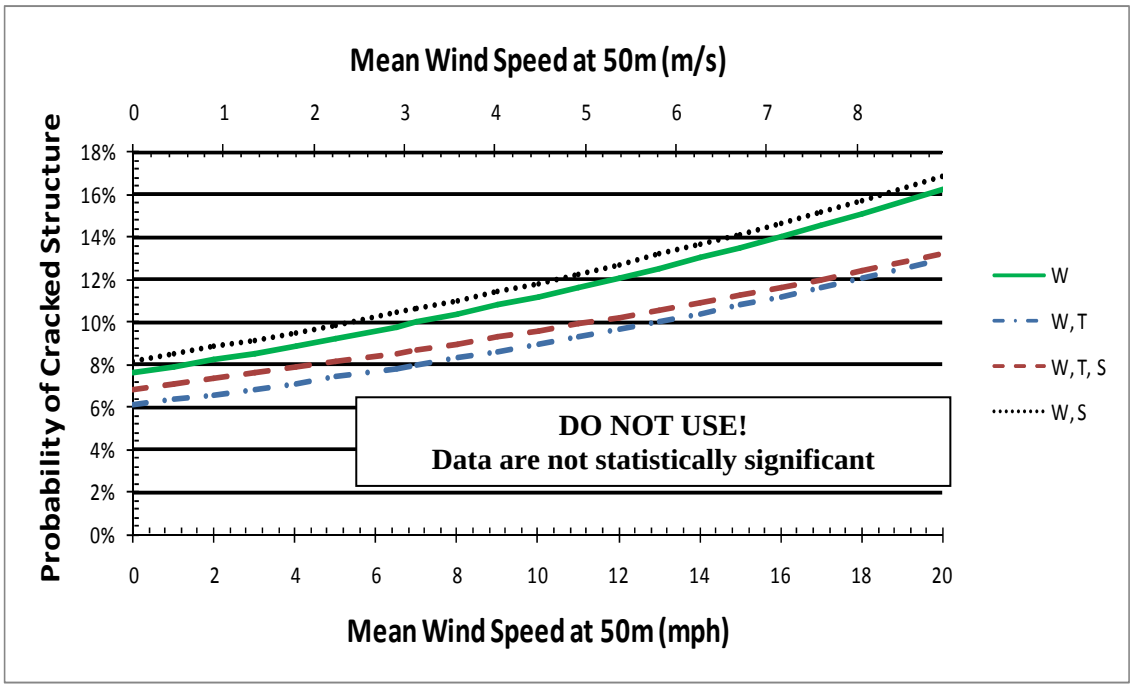

Figure 4.50 High-Mast Luminaire Cracking Probability

5. DISCUSSION

This section discusses the relevant results of this project. It is divided similarly to the Section 4, Analysis of Mast-Arm and High Mast Fatigue Failures section to make referencing figures and tables easier.

5.1 Data Collection

The current state of inspections for cantilever traffic structures is minimalistic in most areas with few states having very complete inspections. Only recently has there been a trend to comprehensively inspect these types of structures. Only four states reported having complete inspections of their inventory and another four reported partial inspections (Figure 3.1). However, some states like Colorado, New Mexico, and Washington are currently completing inspection cycles and will hopefully have data available in the future. Alaska, Wyoming, Kansas, and Michigan were used in this study for a variety of reasons: each state provided complete inspection data, each state had cracked structures, and each state had a variety of WPCs.

5.2 Wind Power Maps

The wind power resource maps used for each state can be viewed in Appendix C. The use of wind power maps helps to establish the average annual wind velocity at 50 meters, which can be related to each structure's height by Equation10. The wind power classifications provided a convenient data grouping method with the exception of WPC-1, which had to be further divided because it held such a wide range of velocities.

5.3 Mast-Arm Structures

Mast-arm structures had the most complete inspection data. This study included approximately 2,500 mast arms. Cracking in mast arms were investigated using average wind velocity, along with structure age, length, orientation, manufacturer, and connection type. The inspection data showed an equal distribution of structures in each orientation, along with an equal distribution of cracked structures in each orientation (Figure 4.3 through Figure 4.8). However, investigation into the prevailing wind direction versus cracking orientation shows that if a structure is orientated perpendicular to the prevailing wind, it has a higher probability of cracking (Figure 4.9, Table 4.1 and Table 4.2). Also, it does not seem to matter if the prevailing wind is blowing on the front or back face. This fact can be used on a site-specific basis, but not when comparing multiple sites because the prevailing wind direction varies from location to location.

Mast-arm length was investigated as a contributor to cracking. This factor showed no firm evidence that mast-arm length plays a role in the structure cracking (Table 4.3 and Figure 4.20). The average length of a mast arm is approximately 35 feet and the cracking shows a range of 10 to 45 feet with cracking in the range of 14% to 17%.

Age has the potential to play a large role in the crack prediction. The older a structure is, the greater number of load cycles will have occurred. The age data shows this when viewed per WPC (Figure 4.27 through Figure 4.31). For each WPC, except WPC-3, the structures show a "Darwinian relationship." There are a higher percentage of structures cracked initially followed by a period of relatively no cracking and then another period of high cracking. This trend could be related to the quality of the welds. Mast-arm structures with poor quality manufacturing/ welding will be much more likely to crack before similar structures of higher quality. This is

reflected in two periods of high cracking separated by a number of years. The structure of poor quality would crack under fewer load cycles and the structure of higher quality would have to be older before a critical number of cycles would be observed. This trend can be distinctly seen with WPC-4 (Figure 4.30), which in year one, 19% of the structures are cracked and then cracking starts again in year 10.

A key aspect to the age analysis is the fact this study is just a random pick in time, i.e., a snapshot. The statement that a structure is cracked at 10 years means that sometime in the last 10 years the structure cracked. This means that without a complete life history of the structure, there is no way to get the actually age at which a structure cracks. This study does not take into account replacement protocols for the DOTs. For example, a DOT may inspect and replace any pole that cracks in the first five years, or it may repair the cracking and the pole could be in service for another 20 years. Overall, a centralized database for all these types of structures similar to the bridge database would be extremely helpful. Age plays an interesting role in fatigue cracking for mast arms and shows that poles fatigue crack earlier or after aging long enough to experience a significant number of load cycles.

For the mast arms located in Wyoming, the manufacturer and mast-arm connection was known for some of the structures. The connection type and manufacturer were also investigated. A structure's manufacturer plays a definite role in structure cracking. For this study, there were four different manufacturers, and each one had a different cracking percentage (Figure 4.32). Each manufacturer did show an increase in cracked structures with an increase in WPC. There were three different connection types for which cracking status was known: closed, open, and ring stiffened (Figure 4.33). The open connection type did not have enough samples to be statistically significant. The ring stiffened connection has the lowest fatigue cracking percentage of all the different connections. A correlation exists between connection type and manufacturer. This study does not conclude, in any way, a relationship between manufacturers and poor product quality of what they were asked to provide.

Wind power class is the most valuable predictor of mast-arm cracking. There is a trend of increased cracking for each increase in WPC. Using the WPC (average velocity) as a predictor, multiple regressions were completed in an effort to predict the chance of a pole cracking. Table 5.1 summarizes the results of the different regression methods used to predict pole cracking. Overall, the best prediction model is the logistic binary regression model. This model has the capacity of including multiple predictors (wind velocity, length, age, orientation, etc.) but for these data, only wind velocity was a valid predictor (see Section 4.2). Figure 4.37 shows the graphical results. This figure can be used to predict the chance of a mast-arm structure being cracked at any given time. For instance, a structure in a location with average wind speed at 15 mph at 164 ft (50m) (19 mph @ 33ft (10m)) has an 18.6% chance of being cracked.

Table 5.1 WPC vs. Mast-Arm Cracking

	Data	Binary Regression Model		Exponential Regression		Cumulative Exponential Regression Model	
WPC	% Cracked	% Cracked	% Difference	% Cracked	% Difference	% Cracked	% Difference
1	3.8%	4.2%	10%	2.8%	-26%	3.2%	-16%
2	4.5%	12.2%	172%	10.6%	177%	6.3%	64%
3	25.9%	19.4%	-25%	14.2%	272%	7.3%	90%
4	25.1%	26.8%	7%	18.1%	372%	8.2%	114%

5.4 High-Mast Structures

From the inspection data received, approximately 700 high-mast structures were investigated. These structures were in WPC-2 through WPC-4 and had cracked structures in WPC-2, 3, and 4. There is no apparent overall cracking trend with these structures (Table 4.11). WPC-2 and 4 have high cracked percentages, but WPC 3 has a low percentage. There are more than 30 structures in WPC-3, so this not a sample size problem. Because there is no apparent trend, no overall graph to predict the cracking status of high-mast structures was developed.

The high-mast structure inspection data included information of the base plate thickness, base plate diameter, and tubing shape for each structure. From these data, it can be concluded that the thicker the base plate, the higher the probability that a structure will be cracked (Table 4.10). This could be from lack of weld penetration when working with materials of different thickness or that typically thicker base plates are attached to higher structures which increases the movement that the base plate welds have to resist. Also, the greater the pole diameter, the higher the probability of fatigue cracking (Figure 4.45). Again this is probably related to the increasing diameter with increasing height issue. The diameter-to-thickness ratio was also compared but this did not yield any trends Figure 4.45. From the tubing shape, it can be shown that the shape of the tubing does not play a significant role in cracking (Table 4.9).

5.5 Specification Implications

This average annual wind velocity can be related to the cyclic loading of the structure by the principle that if a location has a higher mean wind velocity, it will have higher gust values and/or more frequent wind activity. The higher a mean wind velocity, the greater the number of wind loads occur. For mast-arm cantilever structures, the probability of cracking increases rapidly with increases in wind speeds (Figure 4.36). This effect is magnified when heights less than 50 meters are considered see Figure 5.1. However, this is important information and can potentially be related to fatigue importance factors in Section 11.7.6 of AASHTO's *Standard Specifications for Structural Supports for Highway Signs, Luminaires, and Traffic Signals* (AASHTO 2001, 11-6). For structures on rural highways that are not subjected to significant average wind speeds (i.e., less than 5 mph), some level of cracking may be considered acceptable and a low priority Fatigue Category could be used. This decision could potentially move structures from Fatigue Category I into Fatigue Category III, which yields a reduction in the Specification-based importance factor (I_F). Galloping loads could be reduced by up to 70% ($I_F = 1$ to $I_F = 0.30$) and natural wind gusts loads by 50% ($I_F = 1$ to $I_F = 0.50$).

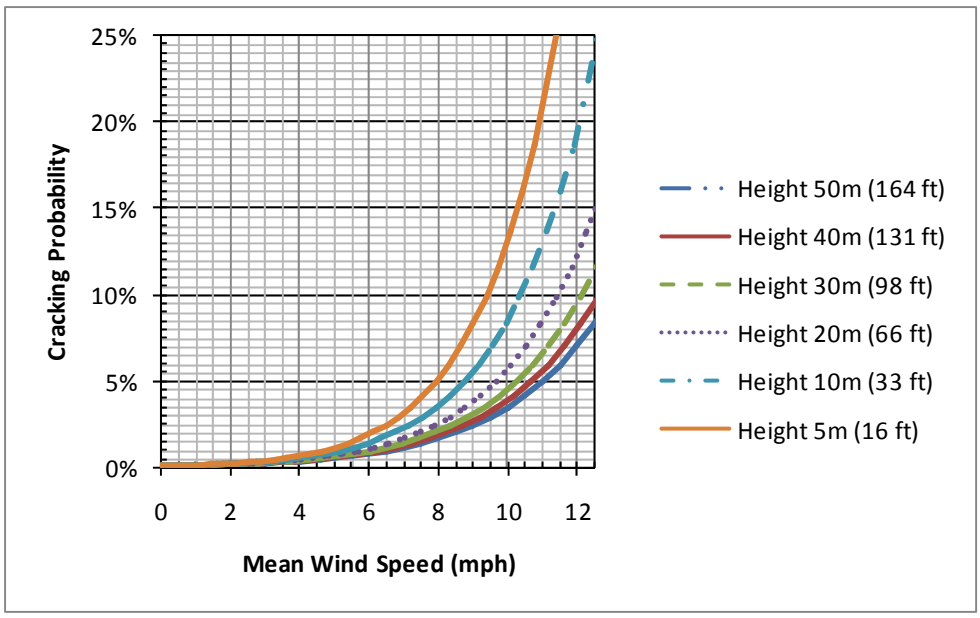

Figure 5.1 Cracking Probability for WPC-1 Per Structure Height

Also, the average annual wind velocity can be related directly to section 11.7.3 of AASHTO's Standard Specifications for Structural Supports for Highway Signs, Luminaires, and Traffic Signals. In this section, the equivalent static natural wind gust pressure range is determined using yearly mean wind velocity of 5 m/s (11.2 mph) (AASHTO 2001, 11-12). By following the commentary, the equivalent static pressure can be computed using Equation 11. This equation could rationally reduce loads using the wind power maps to determine the yearly mean wind velocity (V_{mean}) coupled with the potential change in importance factor (I_F) described previously.

$$P_{NW} = 5.2 C_d \left(\frac{V_{mean}}{11.2\ mph}\right)^2 I_F\ (psf)$$ Equation 11 (AASHTO 2001)

This study also serves as a check to the following comment presented in the Commentary: "The largest natural wind gust loading for an arm or pole with a single arm is from a wind gust perpendicular to the arm" (AASHTO 2001, 11-13). The investigation into the prevailing wind versus the structure orientation cracking status corroborates the quoted statement.

5.5.1 Specification Implications Examples

5.5.1.1 Natural Wind Gusts

For this example, a cantilever signal structure similar to Figure 1.2 is located in Wind Power Class 1 and has an average velocity at 50 meters of 8.5 mph. Using Equation 10, the 10-m average velocity is computed as:

$$v_2 = v_1 \left(\frac{z_2}{z_1}\right)^N$$
$$= 8.5\ mph \left(\frac{10m}{50m}\right)^{0.148}$$
$$= 6.75\ mph$$

Using the Specifications directly, the equivalent static natural wind gust pressure range is found using:

$$P_{NW} = 5.2 C_d I_F \ (psf)$$

where:

C_d = Drag Coefficient (1.1 for this example)
I_F = Importance Factor (Category I for this example)

Fatigue Category	I_F
I	1
II	0.80
III	0.55

$$P_{NW} = 5.2(1.1)(1) = 5.72\ psf$$

However, in the commentary Equation 11 is provided, and using wind power maps as a guide, the new equivalent natural wind gust pressure is:

$$P_{NW} = 5.2 C_d \left(\frac{V_{mean}}{11.2\ mph}\right)^2 I_F \ (psf)$$

Category I:

$$P_{NW} = 5.2(1.1)\left(\frac{6.75\ mph}{11.2\ mph}\right)^2 1 = 2.08\ psf$$

Now, if we consider the fact that this structure is built in a low wind power class area, and lower the importance factor to Category II or III:

Category II:

$$P_{NW} = 5.2(1.1)\left(\frac{6.75\ mph}{11.2\ mph}\right)^2 0.80 = 1.66\ psf$$

Category III:

$$P_{NW} = 5.2(1.1)\left(\frac{6.75\ mph}{11.2\ mph}\right)^2 0.55 = 1.14\ psf$$

Summary:

Change	Pressure (psf)	Ratio
None	5.27	1.0
Commentary Equation	2.08	0.39
Commentary Equation, Category II	1.66	0.31
Commentary Equation, Category III	1.14	0.22

From the direct application of the Specifications, the natural wind gust pressure is 5.27 psf. When the wind maps are used to get the wind speed, this gives a 71% reduction in the expected loads. If the loads are further reduced by changing their Importance Category to II or III (for instance a pole is located in region with no history of cracking), then a reduction of 69% or 78% respectively can be expected. Overall, this is a significant reduction in fatigue loads. Therefore, the strength limit state would govern.

5.5.1.2 Galloping

For this example, a cantilever signal structure similar to Figure 1.2 is located in Wind Power Class 1 and has an average velocity at 50 meters of 8.5 mph (6.75 mph at 10m). Using the Specifications directly, the equivalent static galloping range is found using:

$$P_{NW} = 21 I_F \ (psf)$$

where:

I_F = Importance Factor (Category I for this example)

Fatigue Category	I_F
I	1
II	0.65
III	0.30

Category I:

$$P_{NW} = 21(1) = 21 \ psf$$

Category II:

$$P_{NW} = 21(0.65) = 13.65 \ psf$$

Category III:

$$P_{NW} = 21(0.30) = 6.3 \ psf$$

Summary:

Category	Pressure (psf)	Ratio
I	21	1.0
II	13.65	0.65
III	6.3	0.30

From the direct application of the Specifications the galloping pressure is 21 psf. If the loads are reduced by changing their Importance Category to II or III (for instance a pole is located in region with no history of cracking) then a load reduction of 35 or 70 respectively can be expected. These load reductions are potentially a great savings in structure costs. Note that average wind velocity was not used in this example. Future work may determine that it is applicable. Certainly, the present work indicates that lower categories are appropriate for lower WPC.

5.5.1.3 Truck Gust

For this example, a cantilever signal structure similar to Figure 1.2 is located in Wind Power Class 1 and has an average velocity at 50 meters of 8.5 mph (6.75 mph at 10m). Using the Specifications directly, the equivalent static galloping range is found using:

$$P_{NW} = 18.8 C_d I_F \ (psf)$$

where:

I_F = Importance Factor (Category I for this example)

Fatigue Category	I_F
I	1
II	0.85
III	0.70

Category I:

$$P_{NW} = 18.8(1) = 18.8 \ psf$$

Category II:

$$P_{NW} = 18.8(0.85) = 16.0 \ psf$$

Category III:

$$P_{NW} = 18.8(0.70) = 13.2 \ psf$$

Summary:

Category	Pressure (psf)	Ratio
I	18.8	1.0
II	16.0	0.85
III	13.2	0.70

From the direct application of the Specifications, the Truck-Induced Gust pressure is 18.8 psf. If the loads are reduced by changing their Importance Category to II or III (for instance a pole is located in region with no history of cracking), then a load reduction of 15 or 30 respectively can be expected. These load reductions are the lowest reductions for the different wind phenomena, but still provide for potential savings in structure costs. This example was included because of completeness as truck gust behavior is not expected to be related to WPC.

6. CONCLUSIONS AND RECOMMENDATIONS

Design improvements for traffic signal and sign structures incorporated in the AASHTO Luminaire and Traffic Signal Specification 4th Edition for fatigue load criteria related to wind are producing significant increases in joint size and cost. The specification is based upon limited wind loading and fatigue resistance data and analysis provided by NCHRP Report 411 and NCHRP 469. Based on these reports, a generalized fatigue load criteria was developed and implemented. This represents a significant change to past practice and typically results in larger and more costly structures. Thus, states have been hesitant to adopt the changes. The revised specification applies conservative principles (envelope wind demands and infinite fatigue life) for design in all regions; hence, the larger and more costly structures. Thus, the states that do not have sustained wind and have not experienced significant fatigue failures have concerns with the larger and more costly structures. States are searching for justification before accepting the new fatigue design requirements. Presented below are the conclusions and recommendations of the current study which should provide additional data for states to consider when approaching the new fatigue design requirements.

6.1 Conclusions

The conclusions and recommendations presented herein are based on the limited data samples collected and should be verified through additional research with additional data. This initial study is an important investigation into mast-arm and high-mast structure design that may benefit states with rational structure design procedures. It is a preliminary study and a significant effort would be required before implementation. The purpose of this study is to investigate fatigue cracking in cantilever traffic structures with respect to wind power maps and make design code suggestions based on the findings. Inspection data were collected for high-mast and mast-arm cantilever structures and analyzed separately. The mast-arm cantilever structures showed an increase in cracking with an increase in WPC (Figure 4.37). The high-mast structures display no trend when compared to WPC (Table 4.11) however there are limited data so more investigation should be conducted to completely rule out WPC as a predictor. When different structure aspects were investigated, some interesting trends did appear with respect to high-mast and mast arm independently. For mast-arm structure failures, the prevailing wind direction is generally perpendicular to the orientation of the structure, the structure age illustrates a Darwinian effect, and the structure length plays no significant role in cracking. For high-mast structures, the tubing shape does not seem to matter in terms of crack occurrences; and, the thicker or larger diameter a base plate is, the more likely the structure will be cracked which is converse to the expected results.

This suggests that the fatigue importance factors in Section 11.7.6 of AASHTO's *Standard Specifications for Structural Supports for Highway Signs, Luminaires, and Traffic Signals* could use further refinement with respect to historical fatigue cracking. The low number of poles cracked in areas with low average wind speeds (little sustained winds) suggests that mast arms without mitigation devices in these areas could be placed in Fatigue Category II or III to lower the potential size and costs of the structure and connection details. Changing the importance factor will decrease all the fatigue loads and should allow areas with historically no problems to potentially return to structures similar to past practice size and cost.

6.2 Recommendations

It is recommended that an addition qualification to the fatigue categories be added for mast-arm structures in areas of wind velocities less than 8.5 mph at 50m (10.7 mph at 10m) so they can be given lower importance factors. Historically, structures in these areas have a less than 2% probability of cracking at any given time due to wind. Note that cracking does not necessarily imply collapse will occur. Further research is needed in the high-mast structures area before similar qualifications could be made.

Additionally, the use of wind power maps to predict annual mean wind speed could be incorporated into the specifications. Site-specific data are readily available from the National Climatic Data Center (NCDC), but the wind power resource maps provide a greater area of coverage across the United States.

From the age comparisons incorporated in this study, it is suggested that inspection strategies pay close attention to mast-arm structures cracking during the first six years of the structure's service. After 15 years in service, all mast arms have a much higher chance of cracking, so additional inspections may be warranted. The age study also suggests the results as a single point in time may not be accurate. For this reason, it's suggested that a national database be initiated for all cantilever structures (similar to the bridge data base).

A national database could provide invalible stastical information from service life expecations to what type of connections are the most fatigue resistance. Finally, from the surveys completed, additional inspection data should be available within the next year that should include both high-mast and mast-arm structures. These data should be gathered and added to the current inspection data to see if the correlations remain. Additionally a large number of high-mast structures should be inventoried for height, cracking status, splice locations, and tube thickness. These data could yield results comparable to the current mast-arm results – or it may be the average velocity ranges associated with vortex shedding that may be appropriate.

7. REFERENCES

AASHTO, American Association of State Highway and Transportation. *Standard Specifications for Structural Supports for Highway Signs, Luminaires, and Traffic Signals.* 4th. Washington, District of Columbia: American Association of State Highway and Transportation, 2001.

AWS Scientific Inc. *Wind Resource Assessment Handbook.* National Renewable Energy Laboratory, 1997.

Chen, Genda, M. Barker, L. R. Dharani, and C. Ramsay. *Signal Mast Arm Fatigue Failure Investigation.* Final Report, Jefferson City, MO: MoDOT, 2003.

Dexter, R. J., and M. J. Ricker. *Fatigue-Resistant Design of Cantilevered Signal, Sign, and Light Supports.* NCHRP Report 469, Transportation Research Board, Washington, D.C.: National Academy Press, 2002.

Dexter, R. J., M. R. Kaczinski, and J. P. Van Dien. *Fatigue-Resistant Design of Catilevered Signal, Sign and Light Supports.* NCHRP Report 412, Transportation Research Board, Washington, D.C.: National Academy Press, 1998.

Fouad, Fouad H., Elizabeth A. Calvert, and Edgar Nunez. *Structural Supports for Highway Signs, Luminaires, and Traffic Signals.* NCHRP Report 411, Transportation Research Board, Washington, D.C.: National Academy Press, 1998.

Fouad, Fouad H., et al. *Structural Supports for Highway Signs, Luminaires, and Traffic Signals.* NCHRP 494, Washington, D.C.: Transportation Research Board, 2003.

Hadjicostas, Petros. "Maximizing Proportions of Correct Classifications in Binary Logistic Regression." *Journal of Applied Statistics* 33, No. 6 (July 2006): 629-640.

Hamilton, H. R., J. A. Puckett, Brian Grey, Wang Peili, Brent Deschamp, and Patrick McManus. *Traffic Signal Pole Research.* Final Report, Cheyenne, WY: Wyoming Department of Transportation, 2004.

Iowa Energy Center. *Wind Energy Manual.* 2006. http://www.energy.iastate.edu/renewable/wind/wem/wem-08_power.html (accessed May 18, 2007).

Kansas Corporation Commission. *KSwindmap.* March 25, 2004. http://kcc.ks.gov/energy/kswindmap.pdf (accessed September 28, 2007).

Kansas Department of Transportation. "tblStructure." *KDot Sign and Light Tower Database.* 2005.

Lin, Hui-Yi, and Leann Myers. "Power and Type I Error Rates of Good-of-Fit Statistics for Binomial Generalized Estimating Equations (GEE) Models." *Computational Statistics & Data Analysis* 50 (2006): 3432-3448.

Minitab 15. "Binary Logistic Regression." *Minitab Help.* Minitab Inc., February 15, 2008.

National Climatic Data Center (NCDC). *Climate Data Online - Surface Data, Hourly Global.* http://gis.ncdc.noaa.gov/website/ims-cdo/ish/viewer.htm (accessed April 7, 2008).

National Renewable Energy Laboratory. *Wind Energy Resource Atlas of the United States.* 1982. http://rredc.nrel.gov/wind/pubs/atlas/atlas_index.html (accessed September 25, 2007).

Oral, E. "Binary Regression with Stochastic Covariates." *Communications in Statistics - Theory and Methods* 35 (2006): 1429-1447.

Perkins, Anthony J., Colleen A. McHorney, Patrick O. Monahan, and Timothy E. Stump. "Odds Ratio, Delta, ETS Classifications, and Standardization Measures of DIF Magnitude for Binary Logistic Regression." *Journal of Educational and Behavioral Statistics* 32, No. 1 (March 2007): 92-109.

Phares, Brent M., Partha P. Sarkar, Terry J. Wipf, and Byungik Chang. *Development of Fatigue Procedures for Slender, Tapered Support Structures for Highway Signs, Luminaries, and Traffic Signals Subjected to Wind-Induced Excitation form Vortex-Shedding and Buffeting.* Final Report, Ames, IA: MIdwest Transportation Consortium, 2007.

Puckett, J. A. *Traffic Signal Pole Fatigue in Wyoming − A Research Overview.* http://wwweng.uwyo.edu/civil/Kester-Lab/fatigue.html (accessed April 7, 2008).

Road Traffic Technology Lighting Solutions Image Gallery. http://images.google.com/imgres?imgurl=http://www.roadtraffic-technology.com/contractor_images/millerbernd/2s-highmast.jpg&imgrefurl=http://www.roadtraffic-technology.com/contractors/lighting_solutions/gallery.html&h=198&w=150&sz=5&hl=en&start=8&tbnid=xGV (accessed March 25, 2008).

Phares, Brent M., Partha P. Sarkar, Terry J. Wipf, and Byungik Chang. *Development of Fatigue Design Procedures for Slender, Tapered Support Structures for Highway Signs, Luminaries, and Traffic Signals Subjected to Wind-Induced Excitation from Vortex Shedding and Buffeting.* Midwest Transportation Consortium, 2007.

Taylor, Jonathan. *stat.stanford.edu.* May 17, 2005. http://www-stat.stanford.edu/~jtaylo/courses/stats191/notes/logistic.pdf (accessed February 25, 2008).

U.S. Department of Energy. *Wind Powering America: State and United States Wind Resource Maps.* http://www.eere.energy.gov/windandhydro/windpoweringamerica/wind_maps.asp (accessed September 15, 2007).

U.S. Department of Transportation Federal Highway Administration. *Guidelines for the Installation, Inspection, Maintenance and Repair of Structural Supports for Highway Signs, Luminaries, and Traffic Signals.* http://www.fhwa.dot.gov/bridge/signinspection04.cfm (accessed April 7, 2008).

Western Regional Climate Center. *Western Regional Climate Center Wind Directory.* http://www.wrcc.dri.edu/htmlfiles/westwinddir.html (accessed April 7, 2008).

APPENDIX A

This appendix provides the output from Minitab for each binominal regression analysis completed.

Best Subsets Regression

Best Subsets Regression: Cracked (1) versus Average Wind, Length, Age, Orientation

```
Response is Cracked (1)
1280 cases used, 1178 cases contain missing values
```

Vars	R-Sq	R-Sq(adj)	Mallows Cp	S	Average Wind Speed	Length	Age	Orientation
1	1.9	1.8	8.8	0.39181	X			
1	0.6	0.5	26.2	0.39445		X		
2	2.5	2.3	3.1	0.39077	X	X		
2	1.9	1.8	10.3	0.39187	X		X	
3	2.6	2.4	3.2	0.39064	X	X	X	
3	2.5	2.3	4.8	0.39089	X	X		X
4	2.6	2.3	5.0	0.39076	X	X	X	X

Cracking versus Wind

Binary Logistic Regression: Cracked (1) versus Average Wind Speed

```
Link Function: Logit


Response Information

Variable     Value  Count
Cracked (1)  1        267  (Event)
             0       2191
             Total   2458
```

Logistic Regression Table

Predictor	Coef	SE Coef	Z	P	Odds Ratio	95% CI Lower	95% CI Upper
Constant	-7.00747	0.452633	-15.48	0.000			
Average Wind Speed	0.368931	0.0314638	11.73	0.000	1.45	1.36	1.54

Log-Likelihood = -746.244
Test that all slopes are zero: G = 196.801, DF = 1, P-Value = 0.000

Goodness-of-Fit Tests

Method	Chi-Square	DF	P
Pearson	119.611	10	0.000
Deviance	94.273	10	0.000
Hosmer-Lemeshow	30.594	3	0.000

Table of Observed and Expected Frequencies:
(See Hosmer-Lemeshow Test for the Pearson Chi-Square Statistic)

	Group					
Value	1	2	3	4	5	Total
1						
Obs	3	24	41	121	78	267
Exp	3.3	22.0	70.4	87.2	84.0	
0						
Obs	278	707	626	347	233	2191
Exp	277.7	709.0	596.6	380.8	227.0	
Total	281	731	667	468	311	2458

Measures of Association:
(Between the Response Variable and Predicted Probabilities)

Pairs	Number	Percent	Summary Measures	
Concordant	394452	67.4	Somers' D	0.51
Discordant	96788	16.5	Goodman-Kruskal Gamma	0.61
Ties	93757	16.0	Kendall's Tau-a	0.10
Total	584997	100.0		

Cracking versus Wind and Length

Binary Logistic Regression: Cracked (1) versus Average Wind Speed, Length

Link Function: Logit

Response Information

Variable	Value	Count	
Cracked (1)	1	266	(Event)
	0	2109	
	Total	2375	

* NOTE * 2375 cases were used
* NOTE * 83 cases contained missing values

Logistic Regression Table

Predictor	Coef	SE Coef	Z	P	Odds Ratio	95% CI Lower	95% CI Upper
Constant	-7.17760	0.526695	-13.63	0.000			
Average Wind Speed	0.378508	0.0318454	11.89	0.000	1.46	1.37	1.55
Length	0.0027845	0.0057920	0.48	0.631	1.00	0.99	1.01

Log-Likelihood = -729.378
Test that all slopes are zero: G = 206.957, DF = 2, P-Value = 0.000

Goodness-of-Fit Tests

Method	Chi-Square	DF	P
Pearson	464.812	265	0.000
Deviance	369.107	265	0.000
Hosmer-Lemeshow	67.963	8	0.000

Table of Observed and Expected Frequencies:
(See Hosmer-Lemeshow Test for the Pearson Chi-Square Statistic)

	Group									
Value	1	2	3	4	5	6	7	8	9	10
1										
Obs	3	12	10	4	23	12	36	87	46	33
Exp	2.7	7.0	7.4	7.9	24.1	27.7	45.4	49.7	69.0	25.1
0										
Obs	235	249	227	241	251	225	254	164	210	53
Exp	235.3	254.0	229.6	237.1	249.9	209.3	244.6	201.3	187.0	60.9
Total	238	261	237	245	274	237	290	251	256	86

Value	Total
1	
Obs	266
Exp	
0	
Obs	2109
Exp	
Total	2375

Measures of Association:
(Between the Response Variable and Predicted Probabilities)

Pairs	Number	Percent	Summary Measures	
Concordant	416231	74.2	Somers' D	0.52
Discordant	125149	22.3	Goodman-Kruskal Gamma	0.54
Ties	19614	3.5	Kendall's Tau-a	0.10
Total	560994	100.0		

Cracking versus Wind, Length and Age

Binary Logistic Regression: Cracked (1) versus Average Wind, Length, Age

Link Function: Logit

Response Information

Variable	Value	Count	
Cracked (1)	1	248	(Event)
	0	1032	
	Total	1280	

* NOTE * 1280 cases were used
* NOTE * 1178 cases contained missing values

Logistic Regression Table

Predictor	Coef	SE Coef	Z	P	Odds Ratio	95% CI Lower	95% CI Upper
Constant	-5.01194	0.664416	-7.54	0.000			
Average Wind Speed	0.194604	0.0427606	4.55	0.000	1.21	1.12	1.32
Length	0.0184841	0.0062986	2.93	0.003	1.02	1.01	1.03
Age	0.0169198	0.0115291	1.47	0.142	1.02	0.99	1.04

Log-Likelihood = -610.491
Test that all slopes are zero: G = 37.553, DF = 3, P-Value = 0.000

Goodness-of-Fit Tests

Method	Chi-Square	DF	P
Pearson	722.668	451	0.000
Deviance	666.058	451	0.000
Hosmer-Lemeshow	51.771	8	0.000

Table of Observed and Expected Frequencies:
(See Hosmer-Lemeshow Test for the Pearson Chi-Square Statistic)

	Group										
Value	1	2	3	4	5	6	7	8	9	10	Total
1											
Obs	21	12	10	10	17	23	47	30	39	39	248
Exp	9.2	16.1	20.1	22.7	23.6	25.5	28.2	30.9	34.0	37.6	
0											
Obs	107	116	119	121	111	106	81	98	89	84	1032
Exp	118.8	111.9	108.9	108.3	104.4	103.5	99.8	97.1	94.0	85.4	
Total	128	128	129	131	128	129	128	128	128	123	1280

Measures of Association:
(Between the Response Variable and Predicted Probabilities)

Pairs	Number	Percent	Summary Measures	
Concordant	164633	64.3	Somers' D	0.30
Discordant	88262	34.5	Goodman-Kruskal Gamma	0.30
Ties	3041	1.2	Kendall's Tau-a	0.09
Total	255936	100.0		

Cracking Versus Wind, Length, and Orientation

Binary Logistic Regression: Cracked (1) versus Average Wind, Length, Orientation

```
Link Function: Logit


Response Information

Variable     Value  Count
Cracked (1)  1        266  (Event)
             0       2109
             Total   2375

* NOTE * 2375 cases were used
* NOTE * 83 cases contained missing values


Logistic Regression Table

                                                           Odds     95% CI
Predictor                Coef    SE Coef       Z      P  Ratio  Lower  Upper
Constant              -7.24166   0.552725  -13.10  0.000
Average Wind Speed   0.378699  0.0318530   11.89  0.000   1.46   1.37   1.55
Length              0.0028834  0.0057984    0.50  0.619   1.00   0.99   1.01
Orientation         0.0232294  0.0600478    0.39  0.699   1.02   0.91   1.15


Log-Likelihood = -729.303
Test that all slopes are zero: G = 207.107, DF = 3, P-Value = 0.000


Goodness-of-Fit Tests

Method           Chi-Square   DF      P
Pearson             807.394  690  0.001
Deviance            504.717  690  1.000
Hosmer-Lemeshow      67.554    8  0.000


Table of Observed and Expected Frequencies:
(See Hosmer-Lemeshow Test for the Pearson Chi-Square Statistic)

                                    Group
Value      1      2      3      4      5      6      7      8      9     10
1
  Obs      3     11     11      5     19     14     15     84     43     61
  Exp    2.7    6.3    7.5    7.9   18.8   28.6   34.3   47.8   57.7   54.4
0
  Obs    234    231    231    239    222    232    233    161    199    127
  Exp  234.3  235.7  234.5  236.1  222.2  217.4  213.7  197.2  184.3  133.6
Total    237    242    242    244    241    246    248    245    242    188


Value  Total
1
  Obs    266
  Exp
0
  Obs   2109
  Exp
Total   2375
```

Measures of Association:
(Between the Response Variable and Predicted Probabilities)

Pairs	Number	Percent	Summary Measures	
Concordant	418817	74.7	Somers' D	0.52
Discordant	126491	22.5	Goodman-Kruskal Gamma	0.54
Ties	15686	2.8	Kendall's Tau-a	0.10
Total	560994	100.0		

Cracking Versus Wind, Length, Age, and Orientation

Binary Logistic Regression: Cracked (1) versus Average Wind, Length, Age, Orientation

Link Function: Logit

Response Information

Variable	Value	Count	
Cracked (1)	1	248	(Event)
	0	1032	
	Total	1280	

* NOTE * 1280 cases were used
* NOTE * 1178 cases contained missing values

Logistic Regression Table

Predictor	Coef	SE Coef	Z	P	Odds Ratio	95% CI Lower	95% CI Upper
Constant	-5.08211	0.686615	-7.40	0.000			
Average Wind Speed	0.194909	0.0427595	4.56	0.000	1.22	1.12	1.32
Length	0.0185852	0.0063036	2.95	0.003	1.02	1.01	1.03
Age	0.0167463	0.0115299	1.45	0.146	1.02	0.99	1.04
Orientation	0.0258289	0.0632881	0.41	0.683	1.03	0.91	1.16

Log-Likelihood = -610.408
Test that all slopes are zero: G = 37.719, DF = 4, P-Value = 0.000

Goodness-of-Fit Tests

Method	Chi-Square	DF	P
Pearson	971.418	804	0.000
Deviance	905.334	804	0.007
Hosmer-Lemeshow	47.025	8	0.000

Table of Observed and Expected Frequencies:
(See Hosmer-Lemeshow Test for the Pearson Chi-Square Statistic)

	Group										
Value	1	2	3	4	5	6	7	8	9	10	Total
1											
Obs	21	12	10	10	17	24	44	29	40	41	248
Exp	9.2	16.0	19.9	22.1	23.5	25.5	28.1	31.1	33.9	38.5	
0											
Obs	107	116	118	118	111	105	84	100	88	85	1032
Exp	118.8	112.0	108.1	105.9	104.5	103.5	99.9	97.9	94.1	87.5	
Total	128	128	128	128	128	129	128	129	128	126	1280

Measures of Association:
(Between the Response Variable and Predicted Probabilities)

Pairs	Number	Percent	Summary Measures	
Concordant	164845	64.4	Somers' D	0.30
Discordant	88706	34.7	Goodman-Kruskal Gamma	0.30
Ties	2385	0.9	Kendall's Tau-a	0.09
Total	255936	100.0		

APPENDIX B

The results of the binominal regression predicting structure cracking is contained in Appendix B. The graphs below show the probability of cracking using a binary regression with the average annual wind speed of a structure location in WPC-1 and the average wind speed of each subsequent power (WPC 1 Refined). For each graph, different groupings of the known cracking data are displayed as purple dots. The first graph shows all the data (Figure B.1), the subsequent graphs show different groupings of the data in WPC-1. Grouping in WPC-1 was done using a weighted average wind speed and the total cracking percentage. For example, in Figure B.3 for the known data at 5.2 mph the average wind speed and cracking percentage was computed by: (4.4*29+6.8*203+7.2*15)/(29+203+15) = 6.5 mph (0+0+2)/(29+203+15)*100 = 0.81 %. The purpose of this section is to show how well the data fits the regression analysis.

The Table B.1 shows counts of structures in each average wind speed (mph), the number of cracked structures and the percentage of cracked structures. Because the binominal regression works on weighted data the greater quantity of data points in a group, the more it affects the regression, meaning the 203 structures at 5.4 mph with 0% cracking is more significant and will influence the regression more than the 15 structures at 5.7 mph with 13.3% cracking. Figure B.1 shows all the data points over the top of the regression. At first glance, this figure makes the reader assume the regression is not a well fit nor an adequate predictor. However, understanding of how the binominal regression analysis works, it is acceptable. Figure B.1 through Figure B.5 show data groupings to account for weighting the known quantity and location of data points. For the results shown in the report body, variations of Figure B.4 will be used because it groups the WPC-1 data together the best. For this grouping, average wind speeds 4.4 to 8.2 mph are placed together and 8.9 to 12.0 are placed together.

Table B.1 Cracking Data Used in Binomial Regression

Ave Wind	Total	Cracked	Percentage
4.4	29	-	0.0%
6.8	203	-	0.0%
7.2	15	2	13.3%
8.2	49	3	6.1%
8.9	716	22	3.1%
9.1	29	4	13.8%
10.1	2	-	0.0%
10.8	39	11	28.2%
12.0	16	-	0.0%
13.4	581	26	4.5
15.0	468	121	25.9%
16.3	311	78	25.1%

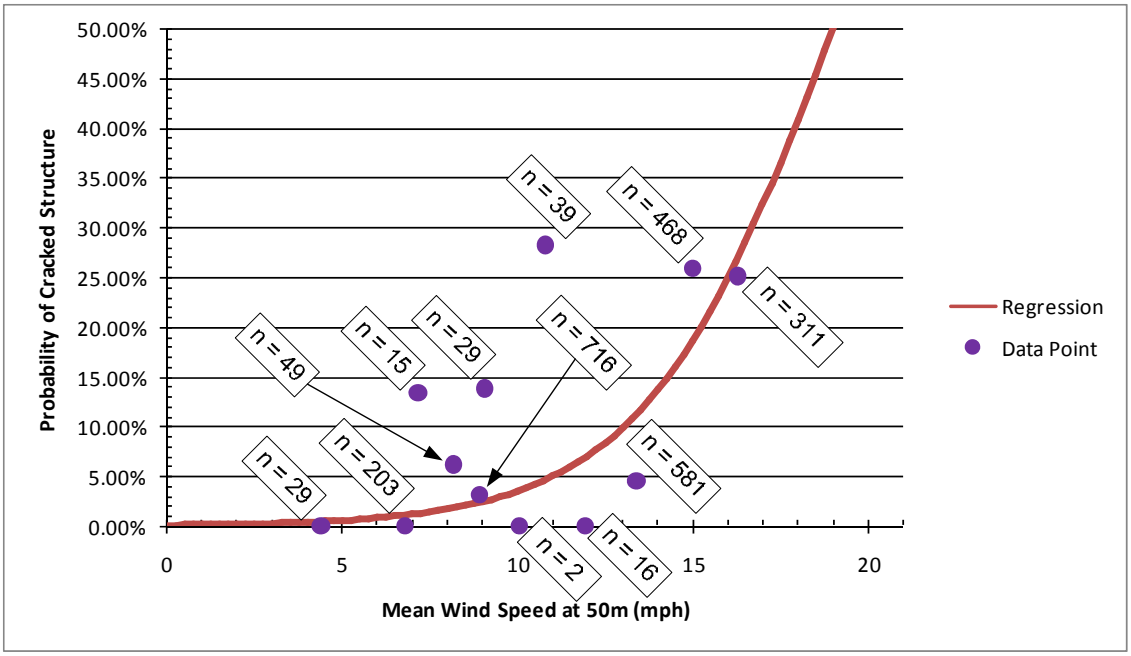

Figure B.1 Mast-Arm Cracking with All Known Data

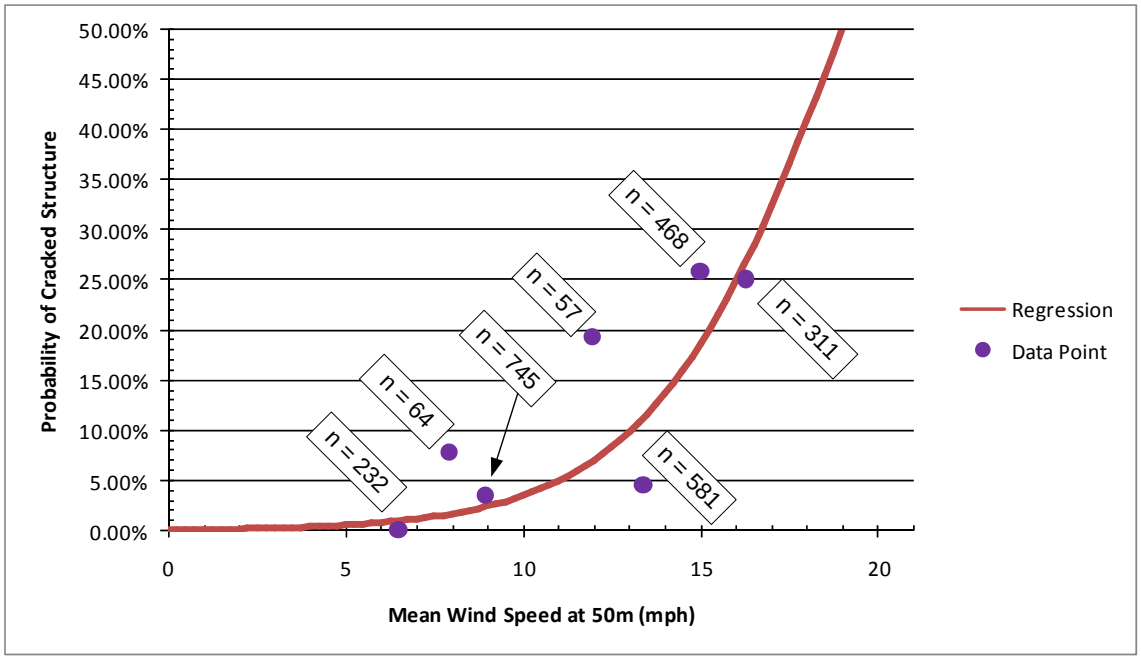

Figure B.2 Mast-Arm Cracking with WPC-1 in Four Groupings

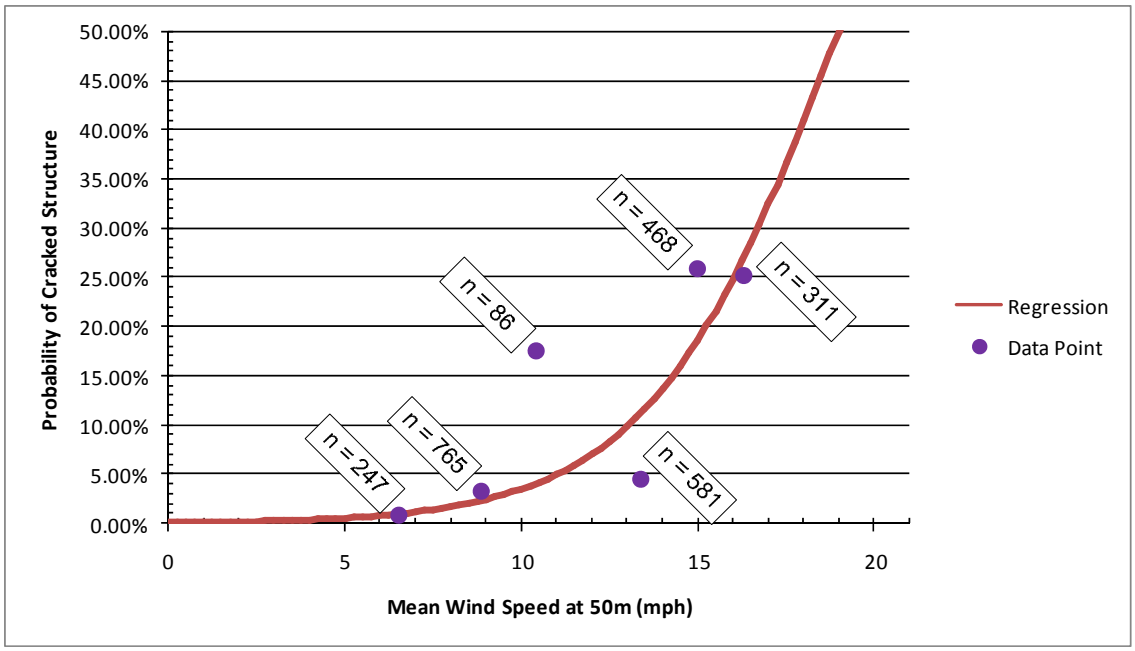

Figure B.3 Mast-Arm Cracking with WPC-1 in Three Groupings

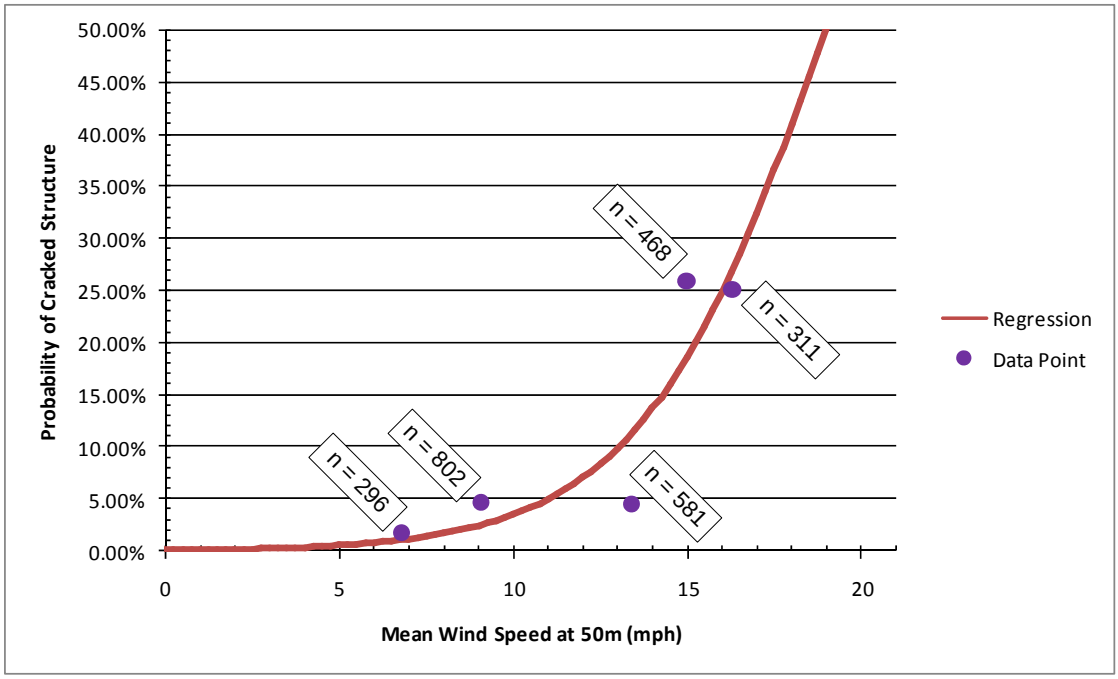

Figure B.4 Mast-Arm Cracking with WPC-1 in Two Groupings

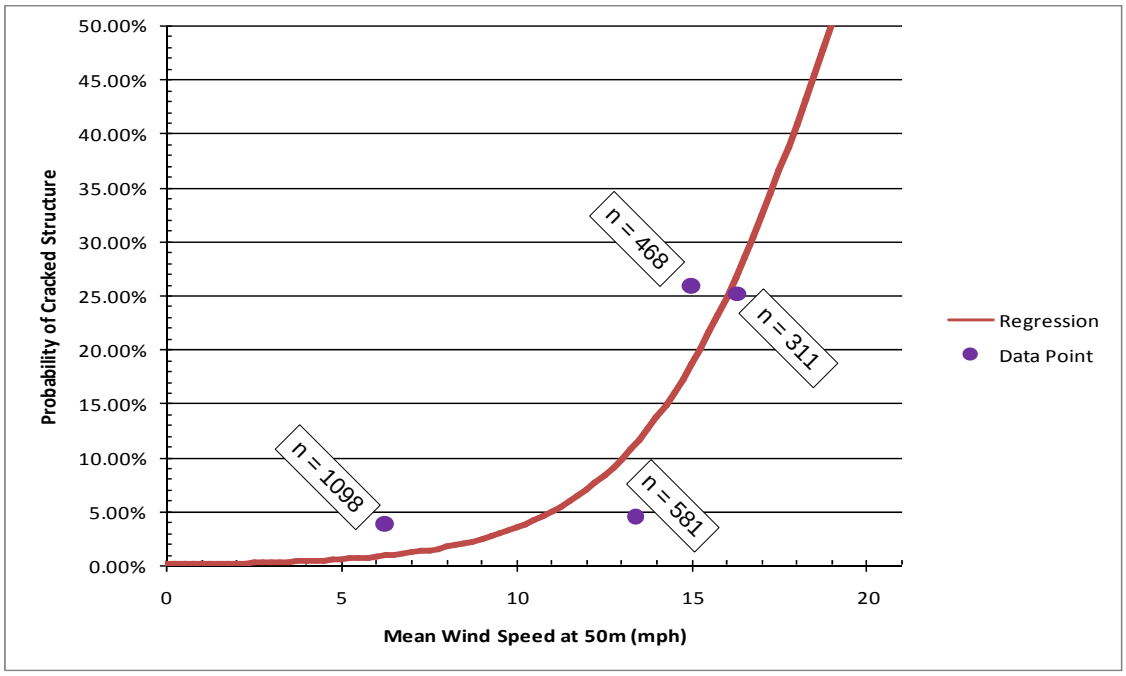

Figure B.5 Mast-Arm Cracking with WPC-1 in One Grouping

APPENDIX C

This appendix provides the wind power resource maps used in this study to classify each structure.

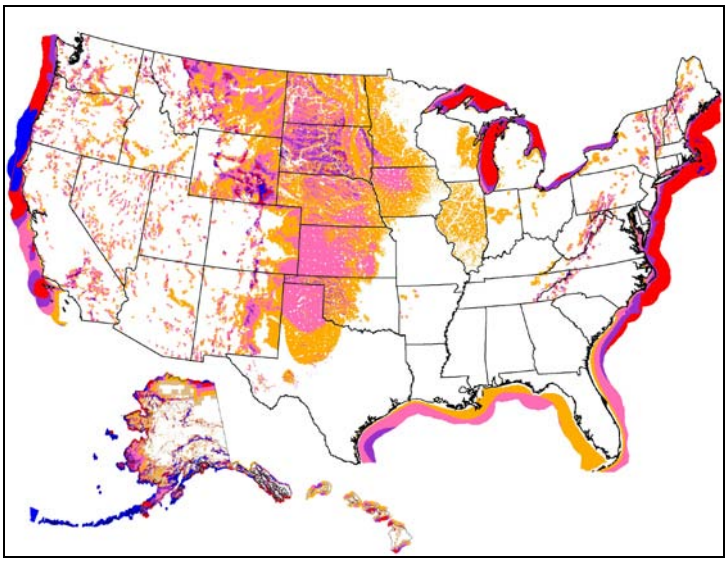

Figure C.1 United States Wind Power Resource Map (U.S. Department of Energy n.d.)

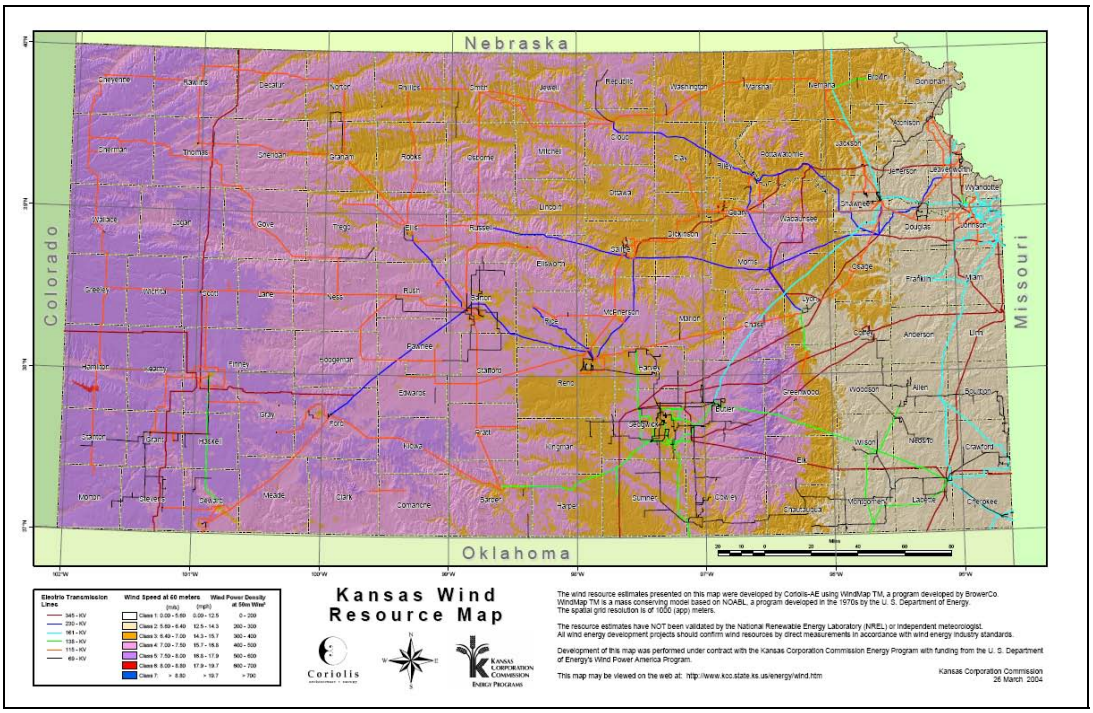

Figure C.2 Kansas Wind Power Resource Map (Kansas Corporation Commission, 2004)

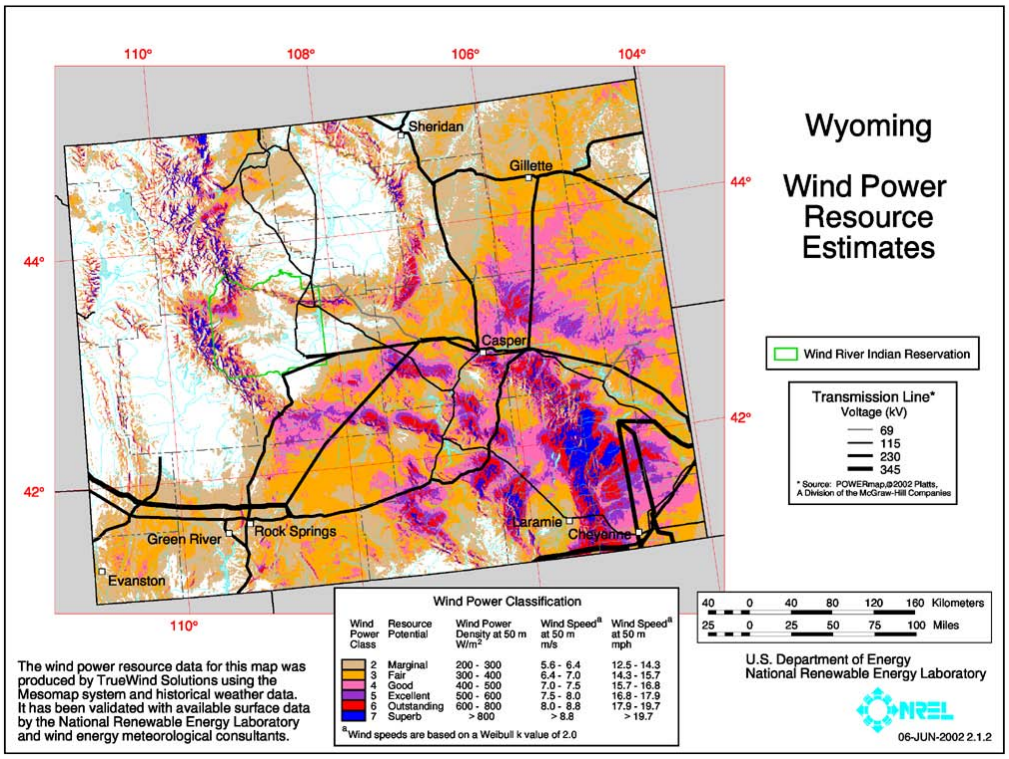

Figure C.3 Wyoming Power Resource Map (U.S. Department of Energy n.d.)

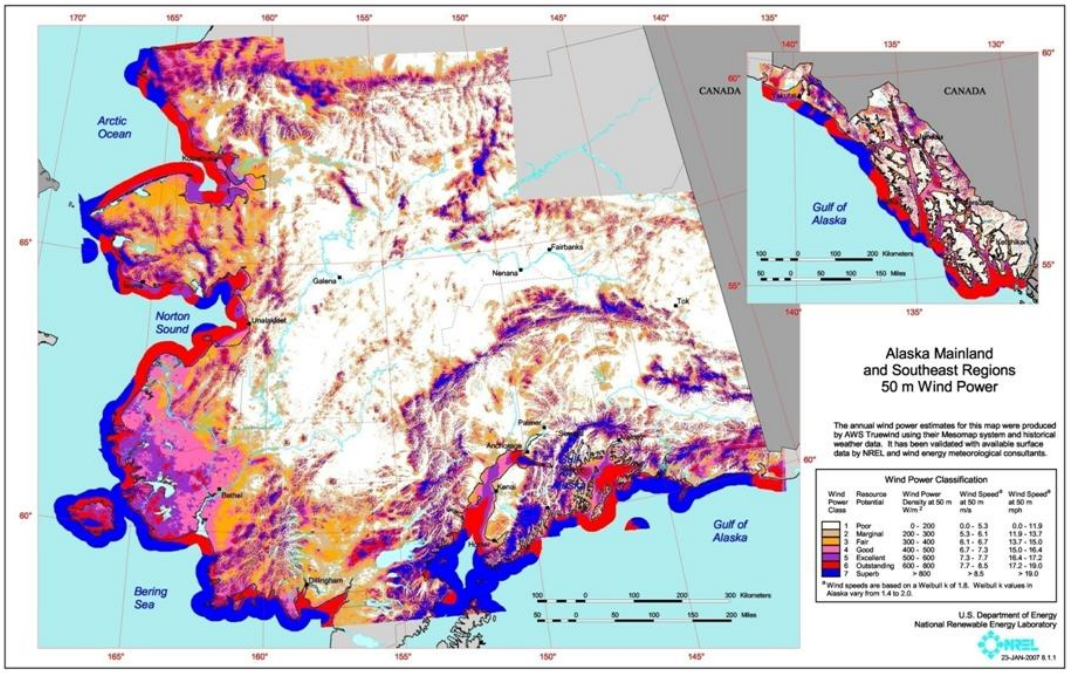

Figure C.4 Alaska Wind Power Resource Map (U.S. Department of Energy n.d.)

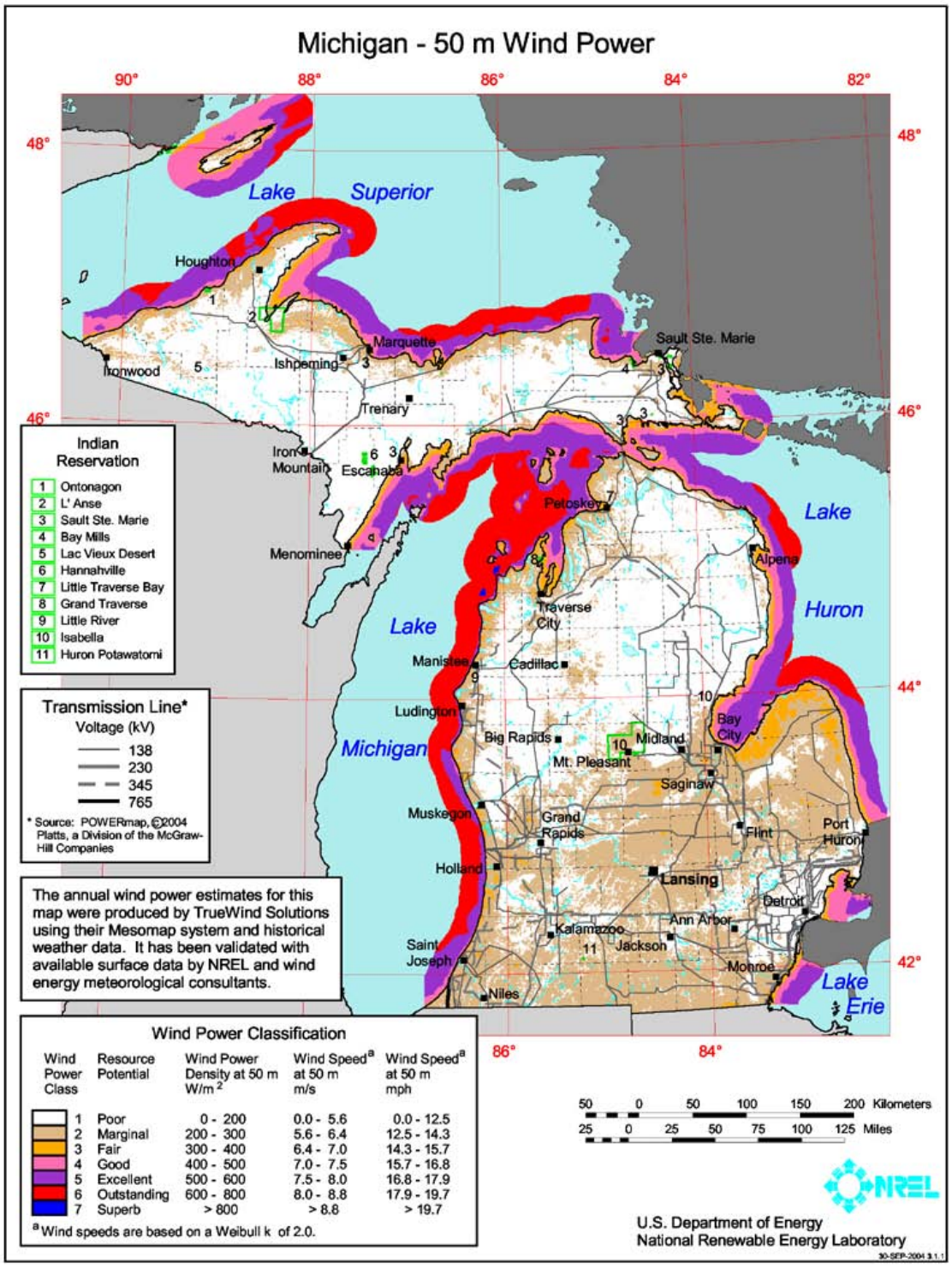

Figure C.5 Michigan Power Resource Map (U.S. Department of Energy n.d.)

APPENDIX D

This appendix provides the brief look at vortex shedding as a cause for fatigue cracking in high-mast luminaires. From the fatigue cracking data presented in Table 4.11 (Table D.1 reproduced below for convenience) the fatigue cracking occurs mostly in WPC 2 and 4. The wind velocity at 164 ft (50 m) for these two wind power classes are 13.4 mph and 16.5 mph respectively. When the wind velocities are adjusted to 120 feet (see Figure D.3) by Equation 6 they are 12.8 mph for WPC 2 and 15.8 mph for WPC 4 using an α of 0.143.

Table D.1 Wind Velocity of High-Mast Luminaires Based on WY Typical Pole

Wind Power Class	Average Diameter (in)	Wind Velocity at 164 ft (mph)	Wind Velocity at 120 ft (mph)
2	28.5 in	13.4	12.8
4	30 in	16.5	15.8

The critical wind velocity, velocity at which vortex shedding lock-in can occur, is then determined using Equations 11-2 and 11-3 of the Specifications (AASHTO 2001).

$$V_c = 0.68\frac{f_n d}{S_n}$$ **Equation 11-2**

$$V_c = 0.68\frac{f_n b}{S_n}$$ **Equation 11-3**

where:

V_c = critical wind velocity at which vortex shedding lock-in can occur (mph)
f_n = natural frequency of the structure (cps)
d = diameter of pole shaft for circular sections (ft)
b = flat-to-flat width of pole shaft for multi-sided sections (ft)
S_n = Strouhal number
= 0.18 (circular sections)
= 0.15 (multi-sided sections)
= 0.11 (rectangular sections)

Using the typical Wyoming high-mast luminaire as a design example (Figure D.3), the natural frequency of a typical structure is 0.53 cps (1st mode) and 2.04 cps (2nd mode). These were found by modeling the structure in SAP2000 and completing a modal analysis. Figure D.1 and Figure D.2 show the critical velocity of the structure with varying structure diameters or flat-to-flat widths. From these figures, it can be concluded that circular sections have lower lock-in velocities.

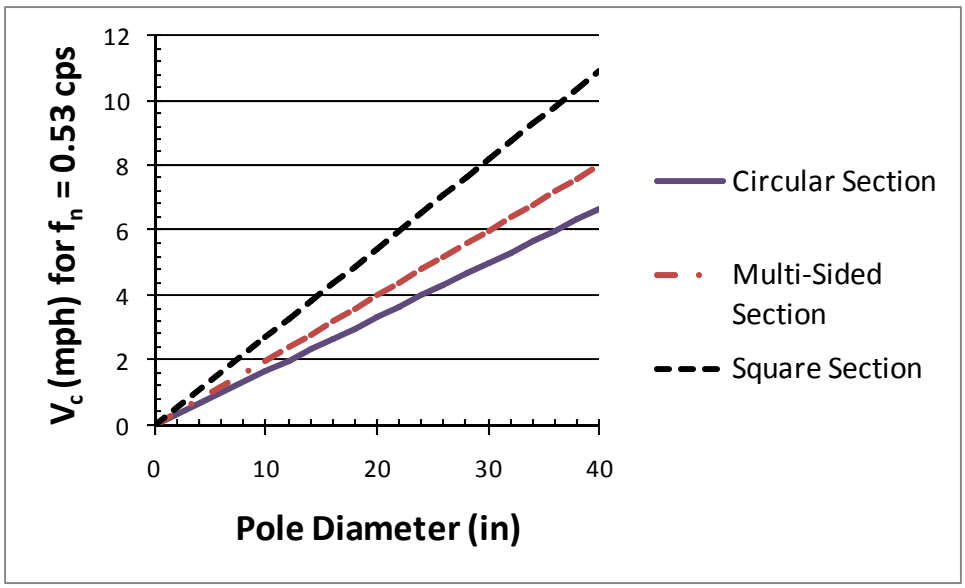

Figure D.1 Critical Velocities for Vortex Shedding Mode 1

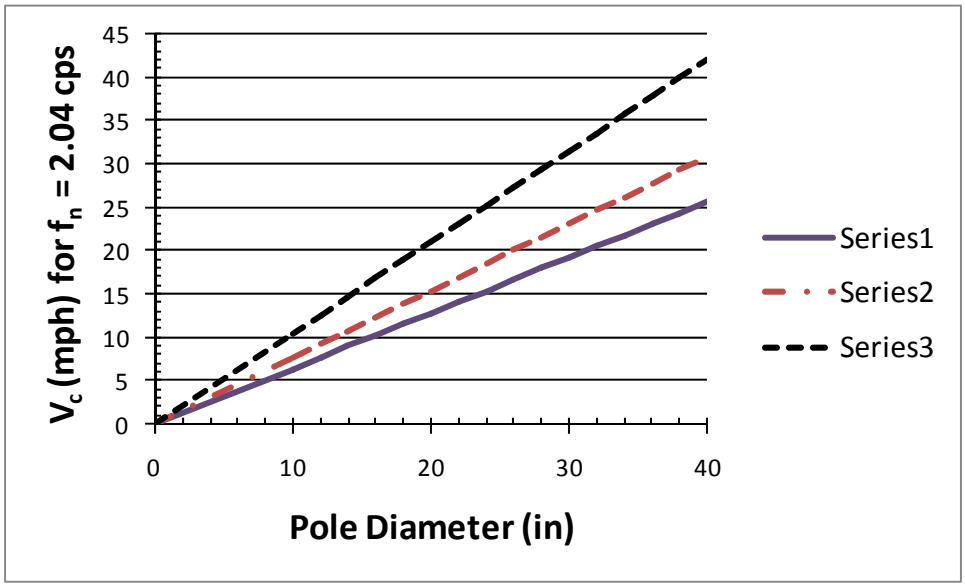

Figure D.2 Critical Velocities for Vortex Shedding Mode 2

The high-mast luminaires for this study come from Kansas. Using the Wyoming typical luminaire frequencies and the average diameter of the structures in WPC 2 (28.5 in) and WPC 4 (30 in), the critical velocities for these structures found by Equations 11-2 and 11-3 are:

	V_c given f_n = 0.53 cps (mph)			V_c given f_n = 2.04 cps (mph)		
d or b (in)	Circular	Multi-Sided	Square	Circular	Multi-Sided	Square
28.5	4.8	5.7	7.8	18.3	22.0	30.0
30	5.0	6.0	8.2	19.3	23.1	31.5

Table D.2 WPC Velocities and Related Vortex Shedding Critical Velocities (from Specifications)

Wind Power Class	Wind Velocity at 120 ft (mph)	Critical Velocity (mph) Mode 1	Critical Velocity (mph) Mode 2
2	12.8	4.8-7.8	18.3 - 30
4	15.8	5.0-8.2	19.3 – 31.5

Observable from Table D.2, the Wind Velocities and the Critical Velocities for Vortex Shedding do not coincide. This potentially rules out vortex shedding as a main form of fatigue cracking for WPC 2 and 4, the WPCs with the highest cracking percentage. However, a recent study by Phares, et al. (2007) showed that the critical vortex shedding frequency is controlled by mode 2 vibrations. In this study, they reported critical frequencies of 0.3 cps in mode 1, 1.3 cps for mode 2, 3.3 cps for mode 3 and 6.4 cps for mode 4 (Phares, et al. 2007, 57). Using their frequency for mode 2 and Equation 11-2 and 11-3, the resulting critical velocities for vortex shedding are:

	V_c (mph) given f_n = 1.3 cps		
d or b (in)	Circular	Multi-Sided	Square
28.5	11.7	14.0	19.1
30	12.3	14.7	20.1

Table D.3 WPC Velocities and Related Vortex Shedding Critical Velocities (from Phares, et al.)

Wind Power Class	Wind Velocity at 120 ft (mph)	Critical Velocity (mph) Mode 2
2	12.8	11.7-19.1
4	15.8	12.3-20.1

This values for the critical velocity of WPC 4 match up well with the multi-sided structure, and the critical velocity for WPC 2 compares closely with that of the circular cross section. Realistically each pole will have its own natural frequency, but the data provided by Phares, et al. suggests that for high-mast luminaires vortex shedding may be the leading cause of fatigue cracking. It also suggests that a predictive model based on the critical velocity of a mono-tube structure may prove extremely worthwhile in design for the fatigue life of high-mast luminaires.

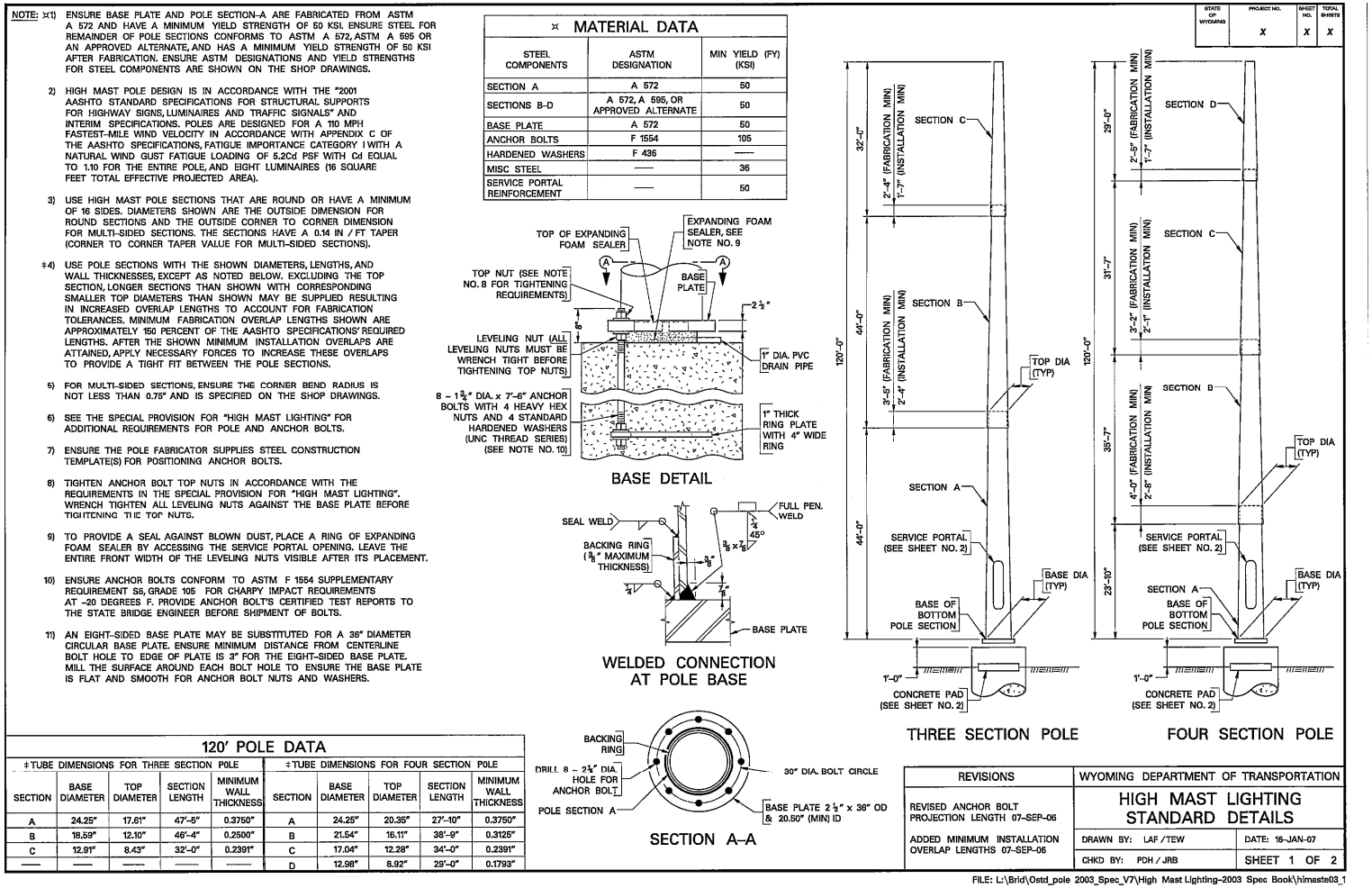

Figure D.3 Typical WYDOT Pole Plan Set